Further Development of Atmospheric Pressure, Self-Igniting Microplasma Devices (MPDs) for Elemental Analysis of Liquid Microsamples Using Atomic Emission Spectrometry (AES)

by

Scott Richard Weagant

A thesis

presented to the University of Waterloo

in fulfillment of the

thesis requirement for the degree of

Master of Science

in

Chemistry

Waterloo, Ontario, Canada, 2011

I hereby declare that I am the sole author of this thesis. This is a true copy of the thesis, including any required final revisions, as accepted by my examiners.

I understand that my thesis may be made electronically available to the public.

Abstract

The present elemental analysis workhorse worldwide is Inductively Coupled Plasma (ICP) Atomic Emission Spectrometry (AES) and Mass Spectrometry (MS). Due to the high power requirements, large gas consumption and the more obvious attribute, size, the ICP is tethered to the lab. Usually, samples must be collected, bottled, sometimes stabilized by acids and then shipped back to the lab for analysis (hours to days to weeks turnover rate). Due to the demand for a portable analyzer this thesis will focus on further development of microplasma devices (MPDs) for portable on-site analysis, in (near) real-time.

Mini-In-Torch Vapourization (mini-ITV) is the sample introduction method for MPDs which removes the need for sample preparation (further necessitates portability). Mini-ITV introduces the sample into the MPD via electrothermal vapourization of a dry (water-free) nano- to micro- volume sample. Pneumatic nebulization, the commercially available ICP sample introduction method would extinguish the microplasma.

Microplasma stability is the first issue addressed by confining the microplasma to a quartz tube ("wall-stabilized") in hopes of a more stable MPD background emission. Once stabilized MPD conditions were found key microplasma parameters were studied including MPD power, HVac frequency, operating mode, inter-electrode distance (IED) and observation location, in hopes of improved MPD analytical performance.

Microplasma excitation mechanism and maximum energy available in the microplasma for analyte are discussed. Some fundamental characteristics such as excitation temperature (T_{exc}) and changes in atom/ion population with variation in some of the key MPD parameters were also determined.

Acknowledgements

I would like to firstly thank Dr. V. Karanassios for accepting me in the group many years ago and for his abundance of knowledge in chemistry and everything else. If it were not for you, I would not have been accepted into graduate studies. Thank you for noticing my talent and not judging me based upon my undergraduate transcript. The research over the past few years has been delightful and quite interesting.

I would like to thank my wonderful girlfriend, Desiree, for the long talks of encouragement and stress relief throughout my graduate work. You have certainly made my life enjoyable over the past year and I hope that there are many more to come.

I would also like to thank my committee members for their time and efforts in helping me produce an end product that I can one day proudly display on a shelf in my place of employment.

I would also like to personally thank Dr. Bissonnette for allowing me to stay in the Chemistry undergraduate program many years ago when my marks were satisfactory and my interests/motivation were diminishing. I would have never thought of pursuing graduate studies in Chemistry at that point of my life and I thank you for keeping me determined.

Lastly, I would like to thank the Science Technical Shop in Physics, especially Hiruy Haile, for his machining expertise and contributions to the MPD project.

Table of Contents

List of Tables

List of Figures

List of Equations

List of Acronyms

A.U.	Arbitrary Units
ac	Alternating Current
AES	Atomic Emission Spectroscopy
B.P.	Boiling Point
CCD	Charge Coupled Device
CCP	Capacitively Coupled Plasma
DAQ	Data Acquisition
DBD	Dielectric Barrier Discharge
dc	Direct Current
D.L.	Detection Limit
EIE	Easily Ionizable Element
GC	Gas Chromatography
HCl	Hydrochloric Acid
HNO_3	Nitric Acid
HPLC	High Performance Liquid Chromatography
HVac	High Voltage Alternating Current
HVdc	High Voltage Direct Current
ICP	Inductively Coupled Plasma
I.D.	Inner Diameter
IED	Inter-Electrode Distance
ITV	In-Torch Vapourization
MCHD	Microhollow Cathode Discharge
mini-ITV	Miniature In-Torch Vapourization
MIP	Microwave-Induced Plasma
MPD	Microplasma Device
MSE	Microstructure Electrode Discharge
MTF	Mid-to-Front
NIST	National Institute of Standards and Technology
O.D.	Outer Diamter
PMT	Photomultiplier Tube
RF	Radio Frequency
RSD	Relative Standard Deviation
SCP	Stabilized Capacitive Plasma
SNR	Signal-to-Noise Ratio
Stdev	Standard Deviation
T_{exc}	Excitation Temperature
T_{rot}	Rotational Temperature
UV	Ultra Violet
VIS	Visible

Chapter 1
Introduction

1.0 Preface

The environment is affected by pollution from indigenous and exogenous factors and the need for environmental monitoring is vital. Environmental monitoring requires "a representative sample from a heterogeneous material."[1] For this, a series of samples are typically collected from an area (e.g. lake, soil, etc.) at various depths and locations. These representative samples must be shipped back to a lab for analysis. Sometimes analytical results can take hours, days, or even weeks to obtain. Would it not be expedient to eliminate this delay using a portable, battery operated elemental analyzer that would in essence bring the lab to the sample for rapid on-site analysis?

This project further influences the paradigm shift in classical analysis with the development of microplasma device (MPD) coupled to a portable spectrometer for analysis of liquid microsamples. This miniaturized system will not only have the ability to provide rapid on-site analysis (where the results are needed the most) but will also significantly reduce the carbon footprint of analysis. The MPD is used as atomization, ionization and excitation sources and a portable spectrometer captures the atomic emissions for microsamples introduced into the MPD to determine elemental composition. These low powered MPDs make use of a unique electrothermal sample introduction system, consisting of a small-size In-Torch Vapourization (mini-ITV) that is coupled to the MPD. These miniaturized plasmas have similar functional capabilities as their large scale atomic emission counterpart, such as the Inductively Coupled Plasma (ICP). Before introducing the widely used ICP, a brief overview of atomic spectroscopy is required to further appreciate and comprehend the mechanism of the ICP and MPD.

1.1 Atomic Spectroscopy

Atomic spectroscopy uses electromagnetic radiation to probe properties of atoms. When a gas phase atom is introduced into a plasma, an electron within the atom is promoted to a higher energy level, bringing the atom to an excited state. Atoms prefer to exist in their ground state causing this promoted electron to drop back to its original level, which is lower in energy. The energy loss from the electronic transition is released as a photon having energy,

$$E = h\nu \,, \qquad \textbf{(Equation 1.0)}$$

where h is Planck's constant (6.626×10^{-34} J • s) and v is frequency (Hz).
The emitted photon can then be detected, differentiated and quantified by a spectrometer coupled to a detector (Section 2.2).

To be analyzed by atomic spectroscopy, samples must be atomized, that is decomposed into gas phased atoms using for example a flame, furnace, or plasma. In the atomization step, the sample is introduced into the source (2000-6000 K) and decomposed into gaseous atoms. These gas phase atoms have the ability to absorb and emit electromagnetic radiation and each element has unique characteristic absorption and emission wavelengths.[1] Fig. 1.0 shows a block diagram of atom formation within an atomization and excitation source. Both ICPs and MPDs have sufficient energy to vapourize and atomize a sample and to excite or even ionize atoms. In addition, the ICP has sufficient energy to excite many ions and therefore ionic emissions along with atomic emissions are detected for ICP atomic emission spectrometry (ICP-AES) analysis. Because of the low power of the MPD, minimal ionic emissions are observed. As a result, the spectrum for the MPD is simplified significantly having fewer characteristic

emissions per element and this is in part what allows for applicability in the field using a small, portable spectrometer with relatively poorer resolution.

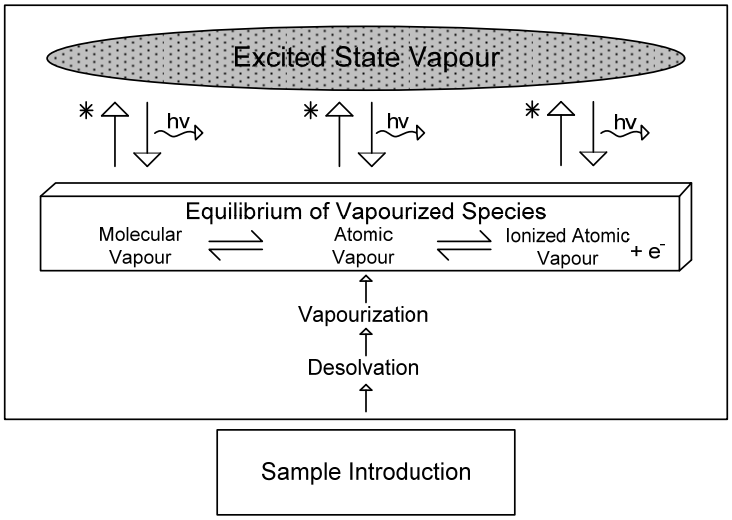

Figure 1.0: *Block diagram of atom formation (modified from [2]).*

1.2 Inductively Coupled Plasma (ICP)

Inductively coupled plasma atomic emission spectrometer (ICP-AES) was first introduced in the mid 1970's as an atomization, ionization and excitation source for atomic emission measurements. Later on in the mid 1980's, the ICP mass spectrometer (ICP-MS) was introduced. Today, ICP is widely used in labs as an elemental analyzer due to its sensitivity, reliability and applicability.

A plasma is a hot gas made up of neutrals, ions, and electrons. The ICP is an inert Argon (Ar) plasma confined within a quartz torch that consists of three concentric tubes forming central channel, and auxiliary and cooling channels. As illustrated in Fig. 1.1, an ICP requires 12-20 L of Ar per minute. As the name suggests, radio frequency (RF) is "inductively coupled" via a water cooled load coil located on the outside of the top of torch. This RF is provided by a RF generator that operates typically at frequencies of 27 and 40 MHz and powers of 1 to 2 kW. The inductive coupling of RF provides a circular

motion of electrons and ions. The plasma is initiated by a seed of electrons or a spark from the Tesla coil. The electrons are accelerated in the RF field and then collide with Ar neutral atoms causing ionization of Ar atoms. The ionization produces free electrons and Ar ions that can collide with more Ar neutral atoms thus causing further ionization of Ar atoms. Eventually, the plasma reaches an equilibrium and is self-sustaining. The ICP has the ability to vapourize, atomize, ionize and excite atoms, as well as ions, due to its high operating temperatures of 6000-10 000 K. ICP atomic emission spectrometry and ICP mass spectrometry are the most sensitive methods for elemental analysis with ICP-MS being a more sensitive method than ICP-AES. Both methods proved to be very useful for environmental monitoring and for analyses for example of samples of importance to industries such as mining, food and beverage.[3]

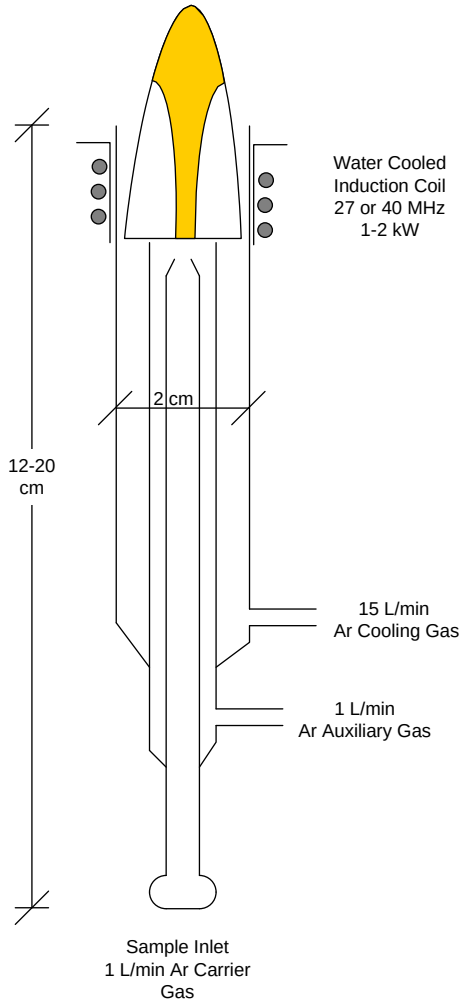

Figure 1.1: *Schematic of inductively coupled plasma (ICP) torch.*

1.3 Why Miniaturize?

Miniaturization of a plasma source will not only reduce the cost of analysis due to reduced power and gas consumption but it will also facilitate portability and on-site determinations. In a microplasma review, Karanassios showed in a calculation that the power density of the MPD can be similar to that of ICP (~0.1 W/mm^3). Also, (if required) MPDs can be made to have more power per unit volume than the ICP. This finding suggests "that microplasmas could be made to perform potentially equally as well

as their laboratory-scale counterparts".[4] Microplasmas do in fact provide useful analytical results and since joining the Karanassios research group in 2007, Weagant has yet to try a MPD configuration that has not successfully ignited.[5,6,7]

Because of the low gas flowrate of the MPD, e.g., 150-300 mL min^{-1}, various exotic noble gases (e.g., Kr, Xe and Ne) can be used as plasma gases. These gases have some desirable performance characteristics (e.g., He and Ne for halogens which can not be excited otherwise with Ar due to insufficient excitation energy). These gases are more expensive as compared to Ar and would be impossible to use for an ICP because the volume of gas per unit time required is large. He is an exception and has been used for halogen detection with an ICP.[3]

1.4 Microplasma Applications

There are various applications for microplasmas including medical (e.g., destruction of cancer cells)[8-9], dental (e.g., spray coating of teeth)[10], nanoparticle synthesis [11-12], nanosheets and nanoarchitectures,[12] green energy (e.g., fuel cell power)[13], etc. The microplasmas at interest for this thesis are for analytical applications.

1.5 Other Analytical Microplasma Research Groups

Many researchers are interested in microplasmas for analytical tools.[4,14-16] In order for something to be considered micro- it must have at least one dimension that is sub millimeter and/or millimeter size or be micro-fabricated. The various types of miniaturized plasmas include but are not limited to miniature inductively coupled plasmas (ICPs); capacitively coupled plasmas (CCPs); microwave-induced plasmas (MIPs); a dielectric barrier discharge (DBD); microhollow cathode discharge (MCHD) or microstructure electrode (MSE) discharges, other microglow discharges; microplasmas

formed in micrometer-diameter capillary tubes for gas chromatography (GC) or high-performance liquid chromatography (HPLC) applications, and a stabilized capacitive plasma (SCP) for GC applications. The power requirements, design and mechanism of plasma formation varied for the various types of microplasmas mentioned above but one major similarity that stood out is that most miniaturized plasmas required samples that were in gaseous form.[4] Our research group, with the convenience of mini-ITV as a sample introduction system, has the ability to analyze sample types other than just gaseous samples, e.g., liquids, slurries and solids. The removal of the water before introducing the microsample into the microplasma is what allows such low power operation (5-15 W) of the MPD.

1.6 Summary of Major Objectives

The purpose of this project is to address the stability of the microplasma background. Past planar MPD research had problems with the microplasma background emission changing when mini-ITV introduced samples into the MPD.[5,7] The MPD optical emission was monitored using a fibre optic based spectrometer. Part of the problem was associated with the microplasma channel being too wide and allowing for the microplasma to move out of the view of the fibre optic cable. This instability caused the need for rigourous normalization of the data (Section 3.0). For this project, a wall-stabilized tubular geometry will be used to confine the microplasma, leaving minimal room for the microplasma to move. This was expected to remove the need for normalization of data. There is also a series of variables that directly influence the background emission stability and the performance of the MPD. These variables include: inter-electrode distance (IED); operating frequency of the microplasma power supply;

microplasma power; geometry and gas type; electrode size, shape and material; and viewing location of microplasma emission. The effect these variables have on analytical performance characteristics was examined. Since MPDs can be made to have more power density than ICPs the question that needs to be answered is whether more power is beneficial? Will more power just add spectral complexity with the appearance of more spectral lines? Or will more power improve analytical performance? These are some of the questions addressed in this thesis.

Chapter 2

Instrumentation

2.0 Sample Introduction

Analytical samples can exist as solids, liquids, slurries and gases. In order to analyze a particular sample type, the sample must be first introduced via means that are compatible with the instrument be it a large size ICP or a small size MPD. Described below are two of the many sample introduction methods available today for ICPs.

2.0.1 Pneumatic Nebulization

On commercially available ICP instruments, the standard sample introduction system is pneumatic nebulization. The nebulizer creates a fine mist or aerosol of sample solution via a jet of high pressure gas. This mist then proceeds to a spray chamber which collects larger droplets on the chamber walls for waste allowing only the fine mist droplets to make it into the ICP torch.[3] This procedure works well for various applications but also has multiple drawbacks. Firstly, the sample being analyzed must be in solution which requires the additional step of acid digestion for solid samples and this additional step is time consuming and can lead to contamination of the sample. Secondly, when a sample is put into solution, the sample constituents are diluted. In addition, one does not always have a large sample size and dilution may cause the concentration of some elements to drop below their detection limits. Futhermore, the pneumatic nebulizer is only 1-5 % efficient and most of the sample solution is collected in a waste container (which requires waste disposal). Ideally, the sample introduction method should be able to handle various sample types, i.e., solids, slurries and liquids and should also minimize sample waste.

2.0.2 In-Torch Vapourization (ITV)

In-Torch Vapourization (ITV) developed in the Karanassios lab solves all of the problems associated with pneumatic nebulizers. ITV is a dry sample introduction method that is capable of handling solid, slurry, and liquid samples and is >95% efficient. Fig. 2.0 shows a schematic of a mini-ITV, which is a smaller version of ITV typically used with ICPs, having lower power requirements and lower gas flow rate. The mini-ITV system consists of a ceramic rod with a Rhenium (Re) coil at the end for holding the sample. A Re cup has also been used with larger size ITV as used for ICPS for solid samples but will not be discussed further because it was not used in this work. This Re coil filament is connected to wires that run through the entire ceramic support. The wires are connected to a direct current (dc) power supply. This Re sample holder is electrically heated by passing direct current through the filament. Rhenium was chosen for the coil material due to its relatively high melting point (3186°C) and for the fact that Re has no known ductile-to-brittle transition temperature. The ceramic support fits into a glass chamber and has a Teflon sleeve that also provides an air tight seal. The glass vapourization chamber has tangential flow of carrier gas and is designed to ensure that a centralized vortex draws the entire sample out of the vapourization chamber towards the MPD. The mini-ITV has an optimal flow rate of 200-300 mL/min for the size and design of the vapourization chamber. The support gas requires the addition of 3% hydrogen gas (H_2), which acts as an oxygen scavenger and prevents formation of Re oxides.[17-20] In order to introduce gaseous samples, the ceramic support and coil are simply removed and the chamber is capped at the back with a septum. Gaseous samples are injected through

the septum and into the chamber. There is no need for addition of H_2 to the plasma gas in this case because there is no Re to be oxidized.[6,22]

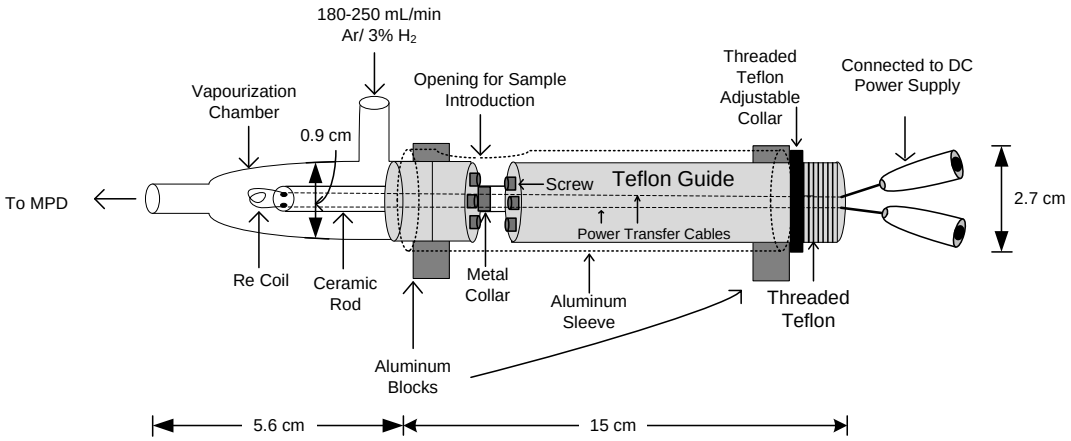

Figure 2.0: *Schematic of mini-In-Torch Vapourization (mini-ITV). (Illustration not to scale)*

How does one operate a mini-ITV sample introduction system? To introduce a sample, the ceramic rod is drawn back to the opening in the aluminum sleeve by pulling on the Teflon guide. Then using a micropipette (Eppendorf™) a liquid or slurry can be carefully aliquoted onto the coil. Typically, sample volumes are in the µL to nL range. This relatively large range of sample volumes demonstrates mini-ITV's programmable concentration ability. For example, if the sample is too dilute, one can simply increase the sample volume to bring the analyte of interest into the dynamic range of the instrument. After a sample has been deposited on the Re holder the Teflon guide is pushed back into the vapourization chamber forming an air tight seal with the vapourization chamber. A low power (~0.3 W) is applied to the Re holder to vapourize the water solvent in the sample and leave only a sample residue on the coil. Typically, drying times are 1-2 minutes on average depending on the sample volume. If the sample

contains organic or biological material then 1-2 W can be applied to char the sample. During the final vapourization step, higher power is applied to the coil (e.g., 20-100 W) to vapourize all of the analyte off the Re holder which is picked up by the vortex towards the MPD.[5-7, 17-20, 22]

The ITV sample introduction system has the ability to remove the water from the sample prior to sample vapourization. One reason the ICP requires so much thermal character and power is because a small fraction of that power is used solely for the removal of water. Even with such high powers (1-2 kW), too much water can extinguish the ICP. In Karanassios' microplasma review paper, a "back-of-the-envelope-type calculation" showed that the ICP requires at minimum 10 W to vapourize the water.[4] In an earlier paper by Olesik, a more rigorous calculation showed that it requires approximately 30 W for vaporization of μm size water droplets.[21] If the MPD had to remove water from the sample then it would no longer be a low power device.

2.0.3 Mini-ITV Operating Conditions

The vapourization power of mini-ITV varies from ~10-100 W (temperatures of <1000 to just under 3000 ºC, which approaches the melting temperature of Re) depending on the element of interest.[6] The vapourization event lasts for a fraction of a second at higher powers and up to 5 seconds for low powers. The longer vapourization time for lower powers allows one to slowly release the analyte but this only works for the more volatile elements. The "programmability" in vapourization temperatures of the various elements allows for on-coil selective thermal vapourization. This selective vapourization allows for separation of overlapping spectral emissions (if necessary) in the time domain and removal of highly concentrated matrix elements (e.g., Na in sea water sample).

Without the removal of potentially interfering matrix components, the detector would otherwise saturate and stray light could add unwanted errors to the analysis.

2.1 Microplasma Device (MPD)

The microplasma device (MPD) research in the Karanassios lab at the University of Waterloo has been in development for the past several years. Various geometries of MPDs have been tried and these previous results have guided the designs of next generation devices. Both high voltage direct current (HVdc) and high voltage alternating current (HVac) MPDs have been tested. The HVdc MPDs applied constant stress on of the electrodes because of the acceleration of ions due to the high voltage. This caused sputtering of the electrode material. Sputtering decreases the longevity of the device and adds unwanted emissions (from the electrode material) to the spectra. For the HVac MPD, the electrons and ions will feel a pull in both the forward and reverse directions because of the alternating electric field. The flow rate of the gas is what brings the ions and electrons from the inlet to the outlet. The electrodes of ac MPDs do not have emissions from the electrode material and because of this, all subsequent MPDs were powered with HVac.[19, 20, 22,]

A typical MPD consists of two electrodes, one electrode connected to high voltage alternating current (HVac) and one electrode connected to ground. It also has a channel, a groove or a tube where the plasma can form between the two electrodes. It also has and an inlet and outlet for the plasma gas (Fig. 2.1). A dc power supply feeds either constant voltage with variable current or constant current with variable voltage into the HVac power supply. The HVac power supply steps up the voltage to 3-10 kV and provides a sine wave at 40-80 kHz. The MPD typically requires 5-15 W of nominal dc

power and 100-500 mL min^{-1} of plasma gas. Mini-ITV is the sample introduction method that was used and is directly coupled to the MPD. The MPD optical emissions have been captured in the past using a monochromator, i.e., one wavelength at a time, and a portable polychromator spectrometer, i.e., multiple wavelengths from 200-850 nm (discussed in Section 2.2).

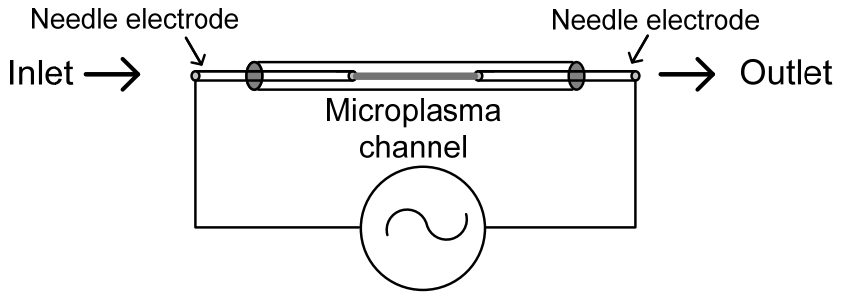

Figure 2.1: *Schematic of tubular MPD.*

2.1.1 Past Microplasma Device (MPD) Work

There are two main divisions of microplasma structures employed: planar geometry and tubular geometry. Initially, the planar geometry was chosen because of the desired future micro-fabrication on silicon wafers of an optimal planar MPD design. In Fig. 2.2, there is a schematic of the micro-machined planar MPD developed by Kara Johnson and Andrea T. Smith, past students of the research group. This is an example of one of the first generation MPD developed by the group. The microplasma channel was etched through the centre glass wafer using hydrofluoric acid. The top glass wafer contained two holes for the inlet and outlet. The bottom quartz wafer allowed for viewing the microplasma. Together, the top and bottom wafers confined the etched channel of the middle layer making a sandwich-like three layer design. As electrodes, Nickel (Ni) ribbon (among other materials) was used at both front and back end of the structure. The

total area of the chips used to fabricate the MPDs was 25 x 25 mm^2 with various channel dimensions (e.g., length of 5-20 mm, width of 1-5 mm and depth of 0.15-0.75 mm). This initial device proved to have impressive analytical performance with absolute detection limits of low pico- gram (pg) to nano- gram (ng) range using a PMT-based monochromator. A minor drawback was the somewhat poor precision of ~18%.[22] However this paved the way for future development of MPDs. The next generation needed to have not only the confined plasma channel but also inlet and outlet tubes parallel the channel to eliminate possible sample loss in the sharp corners.

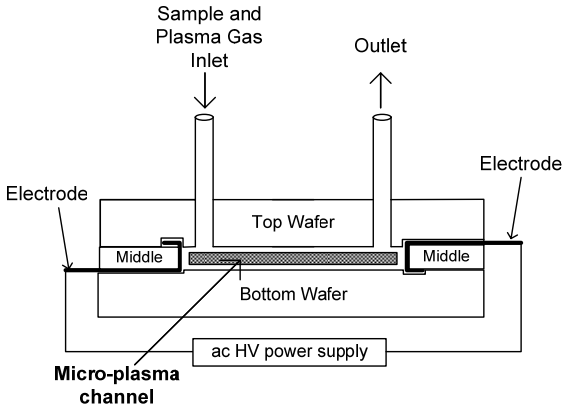

Figure 2.2: *Schematic of micro-machined planar MPD. Sandwich-type MPD with glass etched through middle glass wafer and quartz bottom wafer for far ultraviolet (UV) transmission and Nickel (Ni) ribbon as electrodes.*[22]

The next generation MPD was the tubular geometry (Fig. 2.1) because the tube acted as an air-tight confined channel that the plasma was able to fill entirely, having no kinks in the design from inlet to the plasma channel. This design consists of a quartz tube with an inner diameter of 1.3 mm or less and a stainless steel needle electrode in both ends. This requires a metal to quartz bond. This was done successfully in the past by a metal to glass and quartz or glass to metal bond. For convenience of being able to make new devices quickly and cheaply, cement or glue was chosen as a metal-to-quartz bonding agent. Although the glue worked when low MPD powers were used, once hotter

or more powerful plasma was created, the glue would begin to show up in the background spectra as carbon (C) atomic emission peaks, and sometimes would blacken the device leaving it unusable. Nonetheless, these tubular devices provided promising results that drove future MPD research.

Using the tubular MPD, Smith[19] measured performance characteristics of the plasma including excitation temperatures (T_{exc}) using Fe as a thermometric species (3600 K for Ar and 3200 K for He) and rotational temperature (T_{rot}) of He MPD (1180 K). Estimated detection limits for He/H_2 tubular MPD using a PMT-based system ranged from 3-1200 pg for 8 elements (Ba, Cd, Ca, Pb, Li, Na, Sr, and Zn). At this stage of the MPD development, one was still seeing "if it will work" and "how well will it work" using completely unoptimized MPDs. Smith showed applicability for MPDs as ion sources for mass spectrometry (MS) as well as field applicability for MPDs using a portable spectrometer. Devices began to work on every attempt, and would last from days to weeks, even months. Smith briefly used the CCD spectrometer for obtaining background spectral information of various MPD gases and excitation temperatures of Ar and He using Fe (from Ferrocene) as a thermometric species; no analytical data was obtained using the CCD spectrometer.[19]

Continuing with the tubular geometry MPD and using Ar/H_2 as the plasma gas, Hou[20] found optimized mini-ITV operating conditions (i.e., gas flowrate, Re coil insertion position within the vapourization chamber). This optimization was determined for a smaller mini-ITV system than the mini-ITV used in this thesis. The inter-electrode distance (IED) for the MPDs was varied 2-10 mm. The excitation temperature (T_{exc}) was determined using a 2-point line method for Ar and Ar/H_2 background emissions (3500 K

for Ar and 3000 K for Ar/H_2). Rotational temperature (T_{rot}) was also determined for Ar (1200 K) and Ar/H2 (1150 K). Using an 8 mm IED MPD, estimated detection limits for 8 elements (Cd, Li, Mg, Mn, Na, Pb Sr, and Zn) ranged from 0.05–18 pg using the optimal mini-ITV coil insertion position and gas flowrate determined for each element. These clearly demonstrate (among others) the benefits of mini-ITV optimization and paving the way for future MPD development.[20]

2.1.2 Planar MPDs on Plastic – Past Work by the Author

In the summer term of 2007, Weagant began research on MPDs. Both the undergraduate work term and the master's qualifying term research were done on a planar MPD fabricated out of Teflon and various other plastics. As mentioned earlier, planar geometry was chosen to facilitate possible future microfabrication of MPDs. Plastic was chosen because it was cheap, readily available and easily modified. A portable, fibre optic spectrometer Stellarnet© EPP 2000C (Stellarnet, Oldsmar, FL) with charge coupled device (CCD) detector was used to capture emissions.

Initially, a three-layer sandwich design (quartz-to-plastic-to-plastic) was used for the planar He/H_2 MPD design. The microplasma channel was cut out from the middle layer with a knife. The three pieces were held together by a clamp or a screw (Fig. 2.3). Sample introduction (via mini-ITV) was orthogonal (i.e., 90º) to the MPD and He/3% H_2 was used as the carrier gas and the plasma gas. Throughout, a pinkish colour $_{He/H2}$ was used. In fact, since the beginning of MPD research, the brightest possible pinkish MPD was always used.[5,19,20] The philosophy was that what is good for the microplasma background, i.e., He (or Ar), H_2 and other impurities, must be good for the analyte. The planar He/H_2 MPD had estimated detection limits ranging from 1.5 to 350 ng using the

CCD spectrometer.[5] Instability of microplasma background emission was a key concern. Part of this instability was due to the fact that the He/H_2 MPD had the plasma channel width too large in comparison with the microplasma dimensions (4.9 mm channel and 0.700 mm microplasma). The channel was made wide in order to prevent the plastic from melting but the width used was larger than needed. Future planar MPD designs had a smaller channel width.

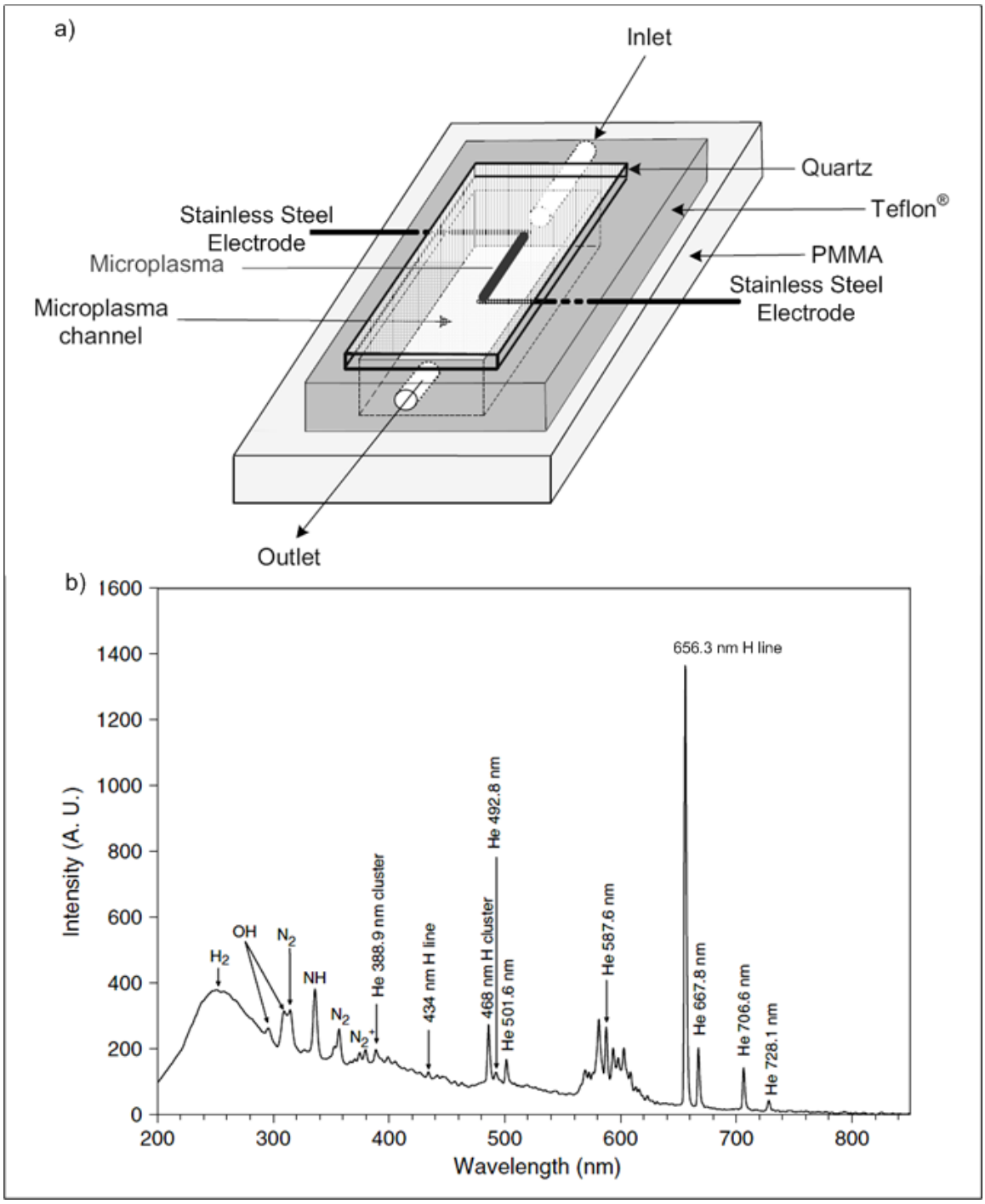

Figure 2.3: a) *Schematic of planar He/H_2 MPD three-layer sandwich design and b) 2-d (intensity vs. wavelength) plot of He/H_2 MPD background spectrum (modified from* [5]*).*

The He/H_2 MPD would provide a stable background when the appropriate conditions were used. However, when mini-ITV reached higher vapourization powers

(temperatures), the plasma would move as the hot gas from the mini-ITV came into contact with the microplasma. As the plasma shifted, the background and the analyte signal intensity would decrease since the plasma was moving out of the view of the fibre optic cable. Spectral regions with larger background intensities, e.g., the hump from 200-400 nm caused by H_2 and air peaks due to air entrainment would be affected more than weaker background intensities. The mini-ITV event would only last for less than a second and then the background would return to its original levels. Because of this instability, some signal processing was required, e.g., normalization of background. The high points of "the hump" at 252 nm as well as up to three other background spectral features (Fig. 2.3b) were employed as an "internal standard" to normalize the episodes containing analyte signal and background to an appropriate background episode. The normalization would bring the background spectral features to equivalent intensities for proper background correction. All of the analyte signals required some degree of normalization, i.e., 1 to 4 point normalization, with this device.[5]

This configuration of planar MPD went through multiple design changes. One flaw initially was that the outlet was too small and pressure built up in the back. To avoid the back pressure and fluctuations of the microplasma background emission, the outlet needed to be a larger diameter than the inlet. Also, the microplasma channel width needed to be reduced for better confinement of the microplasma. Another flaw was air entrainment through the top plate and through the outlet of the MPD. Addition of air (molecular gases) into the Ar/H_2 MPD causes a crackling sound and also adds spectral lines to the background emission spectrum. To address this problem, a more airtight way of incorporating the top quartz plate into a Teflon structure was developed by the Student

Technical Services (STS) machine shop at the University of Waterloo which reduced unwanted spectral features (e.g., OH, N_2 and NH peaks) from 300-400 nm.

A new planar MPD design (Fig. 2.4) reduced the three-layer MPD to a two-layer design (i.e., quartz and Teflon) with stainless steel sewing needles (1.02 mm diameter) as electrodes, an inlet and outlet and a quartz plate on top of the channel. In order to minimize fluctuation in background emission, a MPD with smaller channel width was chosen. For example, channel width was reduced to 3.2 mm (compared to 4.9 mm used previously with the He/H_2 MPD). In addition, the mini-ITV was made to be co-linear with the MPD as well as Ar/H_2 rather than He/H_2 uses as the microplasma gas. The ease of modification of the plastic allowed for inter-electrode distance (IED) to easily be adjusted by simply adding another hole for one of the electrodes. As the inter-electrode distance increased, so did the power being drawn from the dc power supply and this also increased the temperature of the MPD.

With the Ar/H_2 planar MPD, two modes of plasma were clearly visually observed. One mode of operation gave the MPD background emission a pinkish colour, the other a bluish colour. In contrast to the work done with the He/H_2 MPD in which an MPD with a pinkish colour background emission was used,[5] work done with an Ar/H_2 MPD involved a microplasma with a bluish colour emission. Stable operating conditions were obtained when a 12 mm inter-electrode distance (IED), 8.0V and 0.50A (4 W of power), and a sine wave frequency of 70.7 kHz were used. The estimated detection limits for the 9 elements tested ranged from 5-650 pg using the CCD spectrometer. This is over an order of magnitude improvement for some elements. Some of the improvements were possibly

due to use of mini-ITV that was co-linear with the MPD, with no sharp corners for potential sample loss. Another reason for the improvement

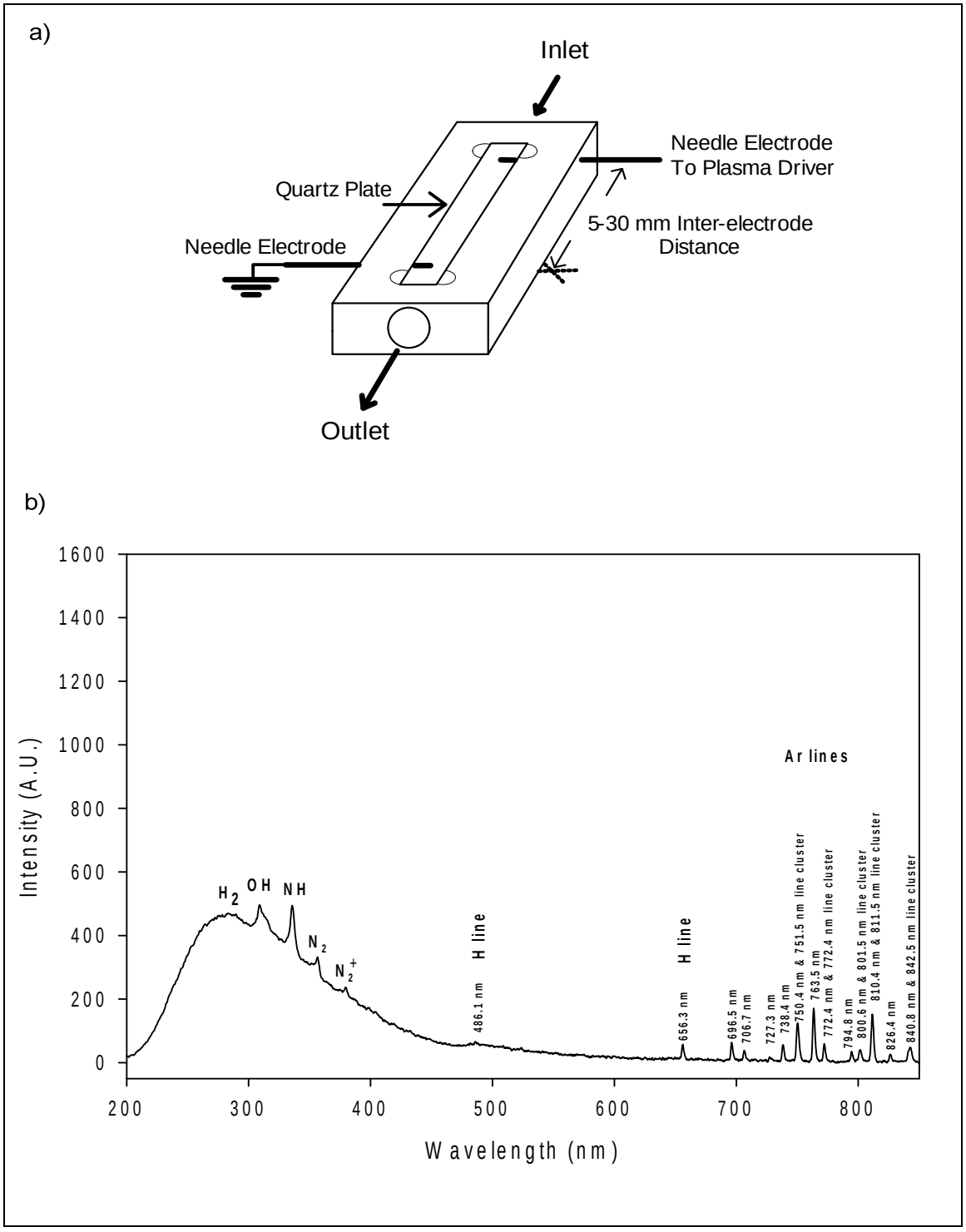

Figure 2.4: *a) Schematic of planar Ar/H_2 MPD two-layer design and b) 2-d (intensity vs. wavelength) plot of Ar/H_2 MPD background spectrum (modified from [7]).*

was due to the increased stability of the bluish background spectrum. In fact, the need for normalization was reduced to 30% of samples run, normally requiring a 1-point normalization at 280 nm. This represents a large improvement over the He/H_2 MPD, for which tedious normalization of 1-4 points were needed for 100% of the samples analyzed.[7] Such improvements in bluish MPD background stability will be discussed in more detail in Chapter 3.

2.1.3 Normalization of MPD Data

Normalization of the MPD data was necessary to bring the background spectra of the various episodes (or spectral scans) to equivalent levels. An example of a non-normalized versus a normalized analyte signal for Cd (3 ng) is shown in Fig. 2.5. This is an example of a 1-point normalization made at 280.77 nm for all of the episodes containing signal. Since the channel width is ~4.5x the size of the microplasma, it leaves room for the microplasma to move out of the view of the fiber optic cable. Fig. 2.5a) shows the 3-d (intensity vs. wavelength vs. time) raw data for Cd (3 ng) and the dip in the background is labeled with arrows. The dip in the background is even more evident when the raw data is super-imposed in a 2-d (intensity vs. time) plot (Fig. 2.5b). The normalization applied at 280.77 nm brings the background spectral episodes to the same intensities and this can be seen in the normalized 3-d raw data plot (Fig. 2.5c). The improvement is even more evident in the super-imposed 2-d normalized raw data plot (Fig. 2.5d). The background subtracted normalized 3-d plot demonstrates a flat background correction (Fig. 2.5e). The labeled Cd 2-d spectrum (Fig. 2.5f) was obtained by summing only the spectral episodes that contained Cd signals in Fig 2.5e.

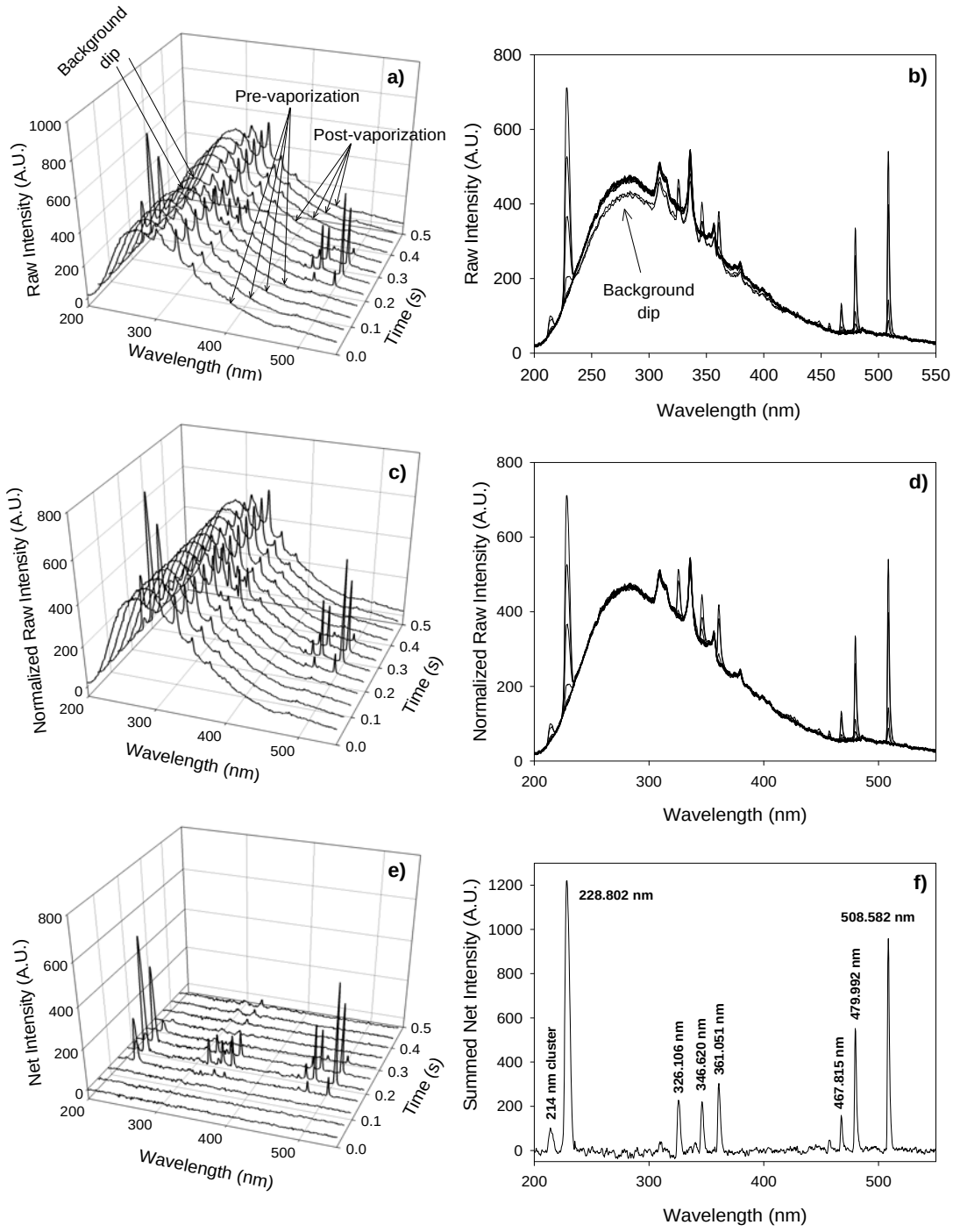

Figure 2.5: *An example of a non-normalized versus normalized Cd (1 ppm, 3 µL) signal obtained using the planar Ar/H_2 MPD coupled to a CCD spectrometer. a) 3-d (intensity vs. wavelength vs. time) raw signal, b) super-imposed 2-d (intensity vs. wavelength) raw signals, c) normalized 3-d raw signal, d) super-imposed normalized 2-d raw signals, e) normalized 3-d net signal, and f) 2-d summed net Cd signal.*[7]

The normalization was only necessary (most often) for the more volatile elements (e.g., Cd, Pb) because the more volatile elements leave the coil rapidly and the dip in the background would occur shortly after the mini-ITV was turned on. Since the dip would come and go before the episodes with medium to low volatility analytes, the background instability had little to no effect on the signals from analytes having medium to low volatility.[7]

2.1.4 Tubular Ar/H_2 Microplasma Device (MPD) - Current Work

To reduce or eliminate fluctuations in MPD background emission, a tubular geometry (i.e., a wall-stabilized) MPD was used. Similar to the planar devices and depending on operating conditions, a pinkish and a bluish colour background spectrum was visually observed emanating from the MPD. Fig. 2.6 compares the background spectral features of the pinkish and bluish microplasma modes. The pinkish mode has a more complex background emission spectrum in comparison to the bluish mode. In Fig. 2.7, colour photographs of both the a) pinkish and c) bluish MPDs are shown, along with their respective waveforms (b& d). The bluish MPD maintained the sine waveform output from the HVac power supply. The pinkish MPD had a distorted waveform with numerous spikes (zero crossings) which caused the frequency counter to read frequencies beyond the output of the HVac power supply.

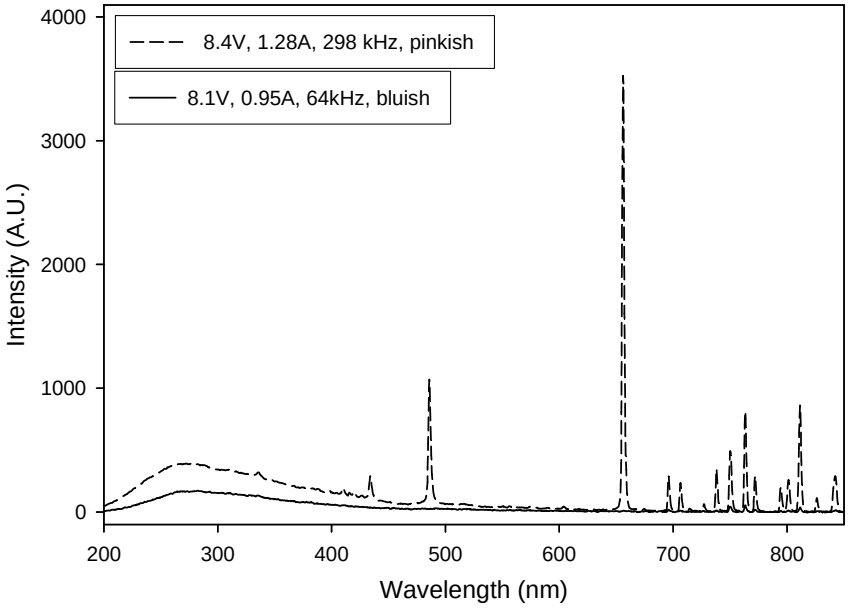

Figure 2.6: *Comparison of pinkish colour and bluish colour tubular 30 mm IED MPD background spectra from 200-850 nm (acquired using portable CCD spectrometer).*

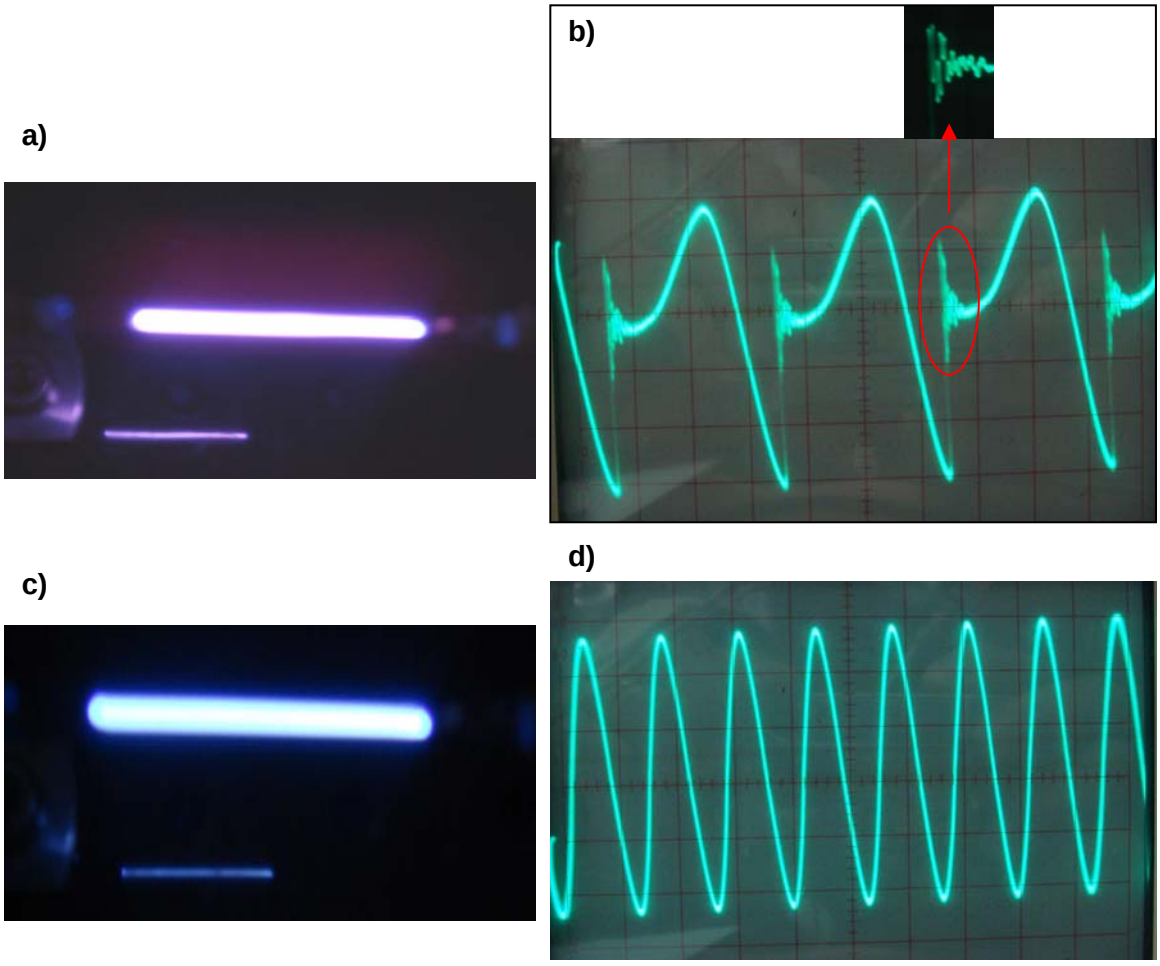

Figure 2.7: *Photograph of a) pinkish colour tubular geometry MPD and b) the distorted waveform as well as c) bluish colour tubular geometry MPD and d) the sine waveform.*

2.1.5 MPD Battery Operation

Since the MPDs only require 5-15 W to operate, it has been shown in the past and confirmed in the present that MPDs can operate either from a 18 V Dewalt® or from a 14.4 V Makita® rechargeable drill battery.[7,19, 22,] Vander Wilp showed with a smaller mini-ITV, which had a smaller diameter coil and smaller volume vapourization chamber, that mini-ITV can be operated by a 14.4 V Makita ® drill battery.[23] For this thesis, I will use the wall outlet powered digital dc power supply for both mini-ITV and MPD operation as a result of the convenience of not having to recharge any batteries. Since battery operation has already been demonstrated, this project will focus on further development of MPDs and not on battery operation.

2.1.6 Microplasma Device (MPD) and Mini-ITV Instrumentation

For the MPDs used for the entire thesis, a tubular geometry was used. Gauge 18 (1.27 mm O.D. and 0.838 mm I.D.) stainless steel hypodermic syringe needles (Becton Dickinson and Co., Franklin Lakes, NJ) with partially dulled tips are glued (5 minute epoxy, LePage) into either end of ~1.3 mm I.D. quartz tubing (LaSalle Scientific, Guelph, ON), to form an airtight seal. The inter-electrode distance (IED) of the MPD is 30 mm unless otherwise noted. The operation of the MPD requires dc power and such power was obtained using Xantrex ® XPL 18-3 regulated dc power supply (0-18.0 V, 0-3.00 A, Xantrex Technology Inc., Burnaby, BC). The dc is delivered to an ac plasma generator which converts the dc to ac and steps up the voltage to 3-10 kV. The HVac plasma generator or driver being used is the PVM12 which is a high voltage ac (HVac) power supply (model PVM12, Information Unlimited, Amherst, NH). The mini-ITV is powered by a Xantrex ® XHR 20-30 dc power supply (0-20 V, 0-30A). An oscilloscope

(20 MHz, Model 2125, BK Precision, Yorba Linda, CA) is used to monitor the waveform generated by the ac plasma driver. A frequency counter (BK Test Bench 388A, BK Precision) allows the HVac frequency to be monitored and reproduced. Standard solutions were signal element ICP-grade solutions stabilized in HCl or HNO_3 from High Purity Standards (Charleston, USA) and those stabilized in HNO_3 from SPC Science (Quebec, Canada). The standards were diluted with distilled water (18 MΩ) to appropriate concentrations.

2.1.7 Microplasma Device (MPD) Warm-up

In the past, planar MPDs were run for 20-30 seconds before starting the data acquisition during introduction of the sample. This was done in order to warm up the device and ensure a fairly constant background signal. The warm-up time of 20-30 seconds was chosen arbitrarily in the past but is 20-30 seconds long enough to obtain a constant background?

In order to address this question a 30 mm inter-electrode distance (IED) bluish MPD was monitored for 120 s at the Ag prominent emission line (328.07 nm) using a monochromator. This spectral line falls on a higher point of the H_2 hump from 200-400 nm (Fig. 2.4) and will give an indication of the time required to warm up the device. Fig. 2.8 shows data taken at 100 Hz (total of 120 s) for a low power bluish MPD (8.26 W). This figure clearly demonstrates that in order to have an MPD with reproducible background emission (at this particular wavelength, plasma conditions, instrumentation, etc.) the MPD must be warmed up for roughly 60 s. Using this new information and extending the warm-up time to incorporate different conditions and IEDs, all of the data in this thesis were acquired using a MPD warm-up time of 80 s, unless noted otherwise,

prior to data acquisition (DAQ). This was done in order to enhance the precision of the MPD.

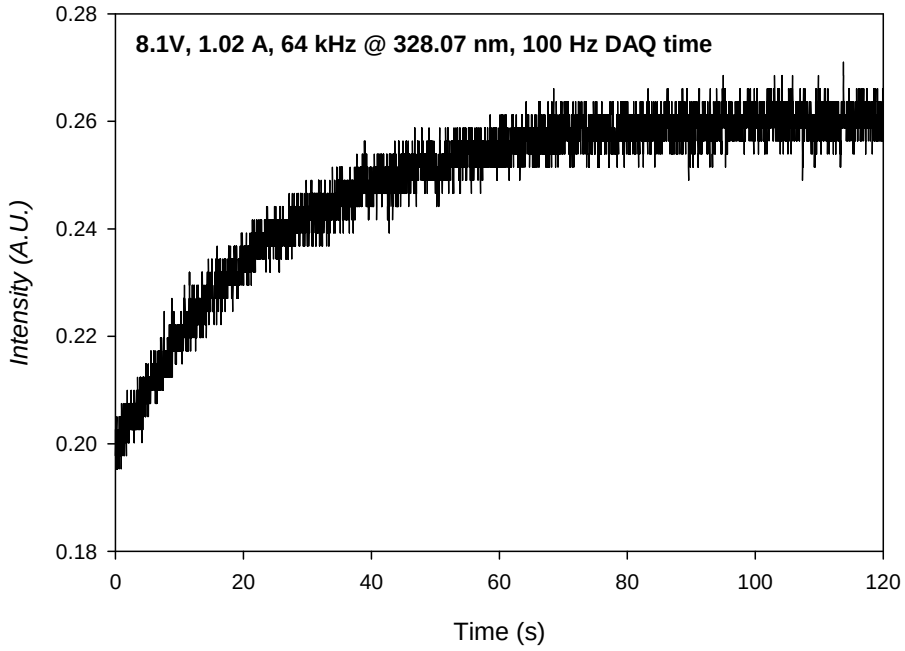

Figure 2.8: *Bluish MPD background emission at 328.1 nm for 120 s at 100 Hz data acquisition (DAQ) time demonstrating MPD warm-up time.*

2.2 PMT-based Monochromator and CCD Spectrometer

The majority of experiments described in this thesis used a portable polychromator equipped with a charge coupled device (CCD) detector because of the large wavelength coverage and the useful information that can be obtained from viewing such a spectral range. A monochromator with photomultiplier tube (PMT) detector was also used for determining the limiting precision of the MPD. It was also to show the estimated detection limit improvements when using the more sensitive PMT detector as compared to the CCD detector.

2.2.1 Mini-ITV Transient Signal

The mini-ITV vapourization event produces a transient signal that lasts from 100 ms to a few seconds depending on the vapourization power. The spectrometer used to record the transient signal is a Heath monochromator with a PMT detector at it's exit slit (Fig. 2.9a). Data was acquired at a rate of 100 Hz, which is fast enough to capture the entire transient signal generated from a microsample introduced via mini-ITV (Fig. 2.9b).

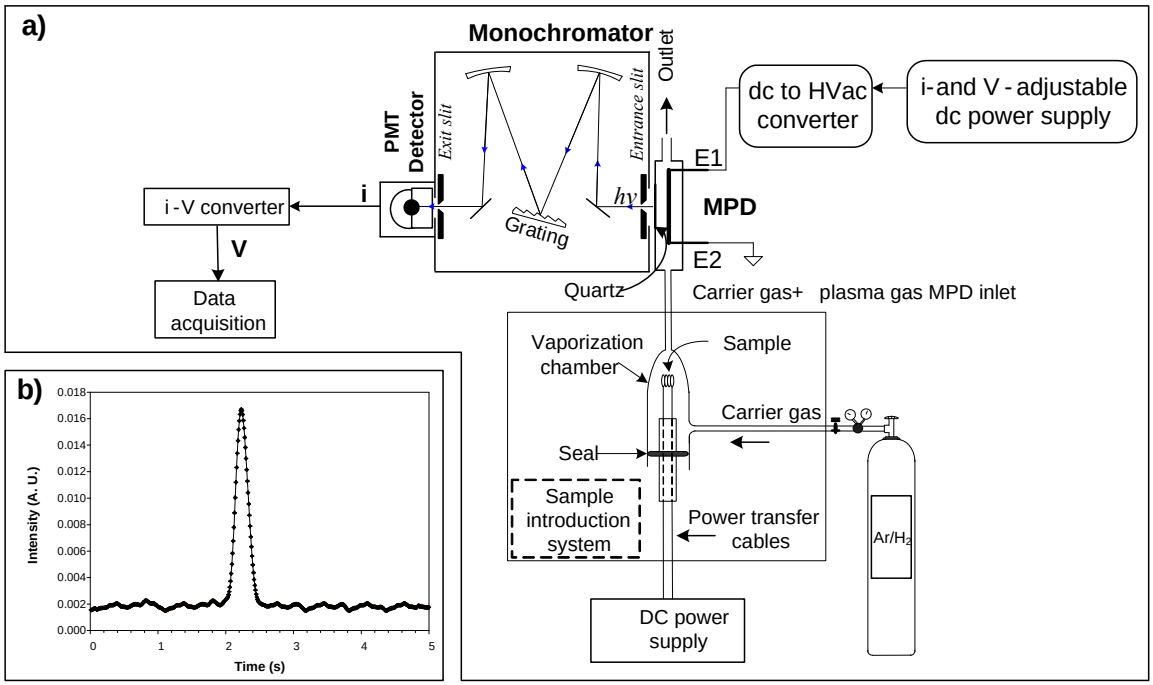

Figure 2.9: *a) Schematic of MPD with PMT-based monochromator (microplasma is formed between E1 and E2) and b) example transient signal.* [7]

2.2.2 Monochromator with Photomultiplier Tube (PMT)

The monochromator is used for monitoring of a single channel (wavelength) at a time. The Heath monochromator is a scanning Czerney-Turner spectrometer comprised of an entrance and exit slit, mirrors and a grating (Fig. 2.9a). Scanning monochromator simply means that the monochromator is capable of scanning a spectral range (depending

upon the spectral response of the PMT detector) but only one wavelength at a time. The monochromator has a 0.35 m focal length, an adjustable entrance and exit slit (200 μm slit is used unless otherwise noted), and a grating with 1200 grooves mm^{-1}. Photons are guided through the monochromator's exit slit to the PMT (Model R928, 180-900 nm spectral response, -800 V, Hamamatsu Photonics, Japan). Photons impringing on photoemissive cathode are converted to electrons and multiplied by the dynode chain of the PMT with a gain of 10^5 to 10^6 electrons. This current output at the anode of the PMT is then amplified and converted to voltage (Stanford Research Systems Low-Noise Current Preamplifier Model SR570, Sunnyvale, CA). This voltage is read by the computer using custom Labview software (National Instruments, Austin, TX).[24]

2.2.3 Portable Polychromator with Charge Coupled Device (CCD)

The portable StellarNet© EPP2000C spectrometer (Stellarnet, Oldsmar, FL) uses an integrating 2048 pixel CCD detector that covers the spectral range of 200-850 nm simultaneously. This allows the user to monitor a wavelength range and not just at one wavelength. The CCD detector is an integrating detector that can integrate the signal for as short as 4 ms or as long as 1000 ms. The light travels through a fibre optic cable (0.3 m, 600 μm) and into the spectrometer through a 25 μm entrance slit. A flat field concave grating then guides the light to the CCD detector for quantification, as schematically shown in Fig. 2.10. This USB- or battery-operated spectrometer is small in size, 44 x 94 x 150 mm, and can be easily transported into the field. The small size means that the resolution suffers (~0.5-1 nm resolution) since the focal length of the spectrometer is one of the factors contributing to resolution. Due to the simplicity of the

analyte emission spectra that the MPD produces, (with on average 1-5 spectral lines per element) the relatively poor resolution spectrometer is of no major concern.[25]

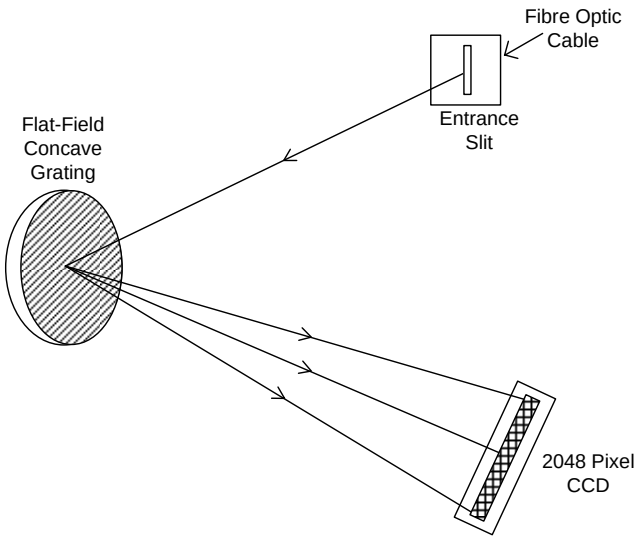

Figure 2.10: *Schematic of Stellarnet © EPP2000C concave grating CCD spectrometer.*

Using the Stellarnet SpectraWiz software that comes with the spectrometer, there is a function called "episodic data capture." This allows one to capture data that contain individual spectra or episodes, i.e., a snapshot of the complete spectrum from 200-850 nm, for a set increment of time (e.g., integration time of 4-1000 ms). For example, the majority of data has been taken using 15 ms integration time and 16 ms for data transfer (31 ms total per episode). Then the detector refreshes for another set increment of time before taking the next spectrum or episode. This 16ms data transfer delay between readings results loss in analyte signal and the need for a faster detector is evident.

In essence, one is losing half of the transient signal to data transfer. Although compromised resolution and analyte emission loss are unwanted characteristics of the CCD polychromator, the ability to record the entire background spectrum simultaneously allows one to study microplasma conditions and monitor any disturbances or changes in the MPD background. For example, if the mini-ITV is loosely connected to the MPD or

air-tight seal is lost, the peaks caused by the air entrainment will show up in the background spectrum and this will alert the user that something is wrong with the setup. In the case of the PMT system, this is more difficult to detect. For example, one is "in the dark" for everything except the one wavelength of interest being monitored so unless the selected wavelength is in a plasma background region affected by air entrainment, the user will not notice any change in MPD operating conditions.

Fig. 2.11, a) shows an example of 3-d plot (intensity vs. wavelength vs. time) for raw Zn data (10 ppm, 3μL) obtained using episodic data capture for a bluish tubular MPD. A background spectrum (i.e., one free of analyte signal) from pre- or post-vapourization is selected and then subtracted from every spectral episode to give the background correction spectra in b). Then the background corrected episodes containing analyte signal are summed up to give the traditional 2-d net intensity vs. wavelength graph shown in c).

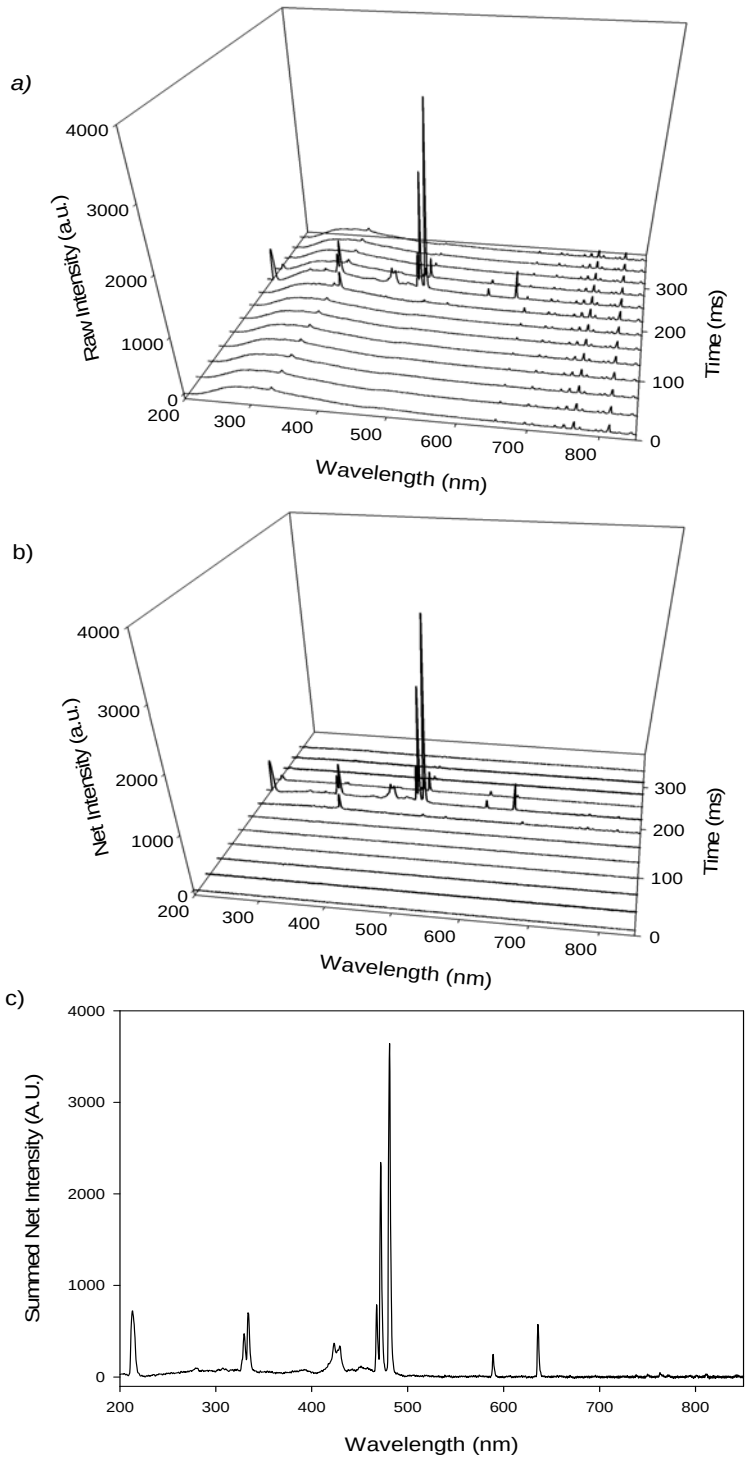

Figure 2.11: *Zn signal (10 ppm, 3µL) for tubular MPD with 50 mm inter-electrode distance (IED) in 3-d (intensity vs. wavelength vs. time) plot for a) raw data, b) background corrected signal, and c) 2-d (intensity vs. wavelength) summed net Zn signal plot.*

2.2.4 Fibre Optic Cable Diameter and Length

The CCD spectrometer has the ability to adjust it's resolution simply by adjusting fibre optic cable diameter (and length). The work done with the He/H_2 MPD was carried out using a fibre optic cable with a length of 2 m and a diameter of 600 μm, simply because that is what was sold with the spectrometer. After purchasing fibre optic cables with various diameters, i.e., 600 and 1000 μm, and various lengths, i.e., 0.3 and 2 m, it became apparent that changing the diameter and the length of the fibre optic cable changed the intensity and the resolution of the emission lines generated from a Hg lamp (also available from Stellarnet). The effect caused by the change in cable diameter is shown in Fig. 2.12. The larger diameter cable provided a non-even increase in intensity but with poorer resolution. The increased diameter is the conceptual equivalent of increasing the slit height for a fixed slit width. It is well known that increasing the slit height for a fixed slit width, will cause spilling of light into adjacent pixels (or space) and this results in poorer resolution and broadening of the emission peak.[2] Fig. 2.13 shows what happens when the length of the fibre optic cable is varied. The shorter length provided increased intensity but with (apparent) poorer resolution. For all of the experiments requiring the CCD spectrometer a 600 μm diameter and 0.3 m long fibre optic cable was used to take advantage of mid-range light throughput and resolution.

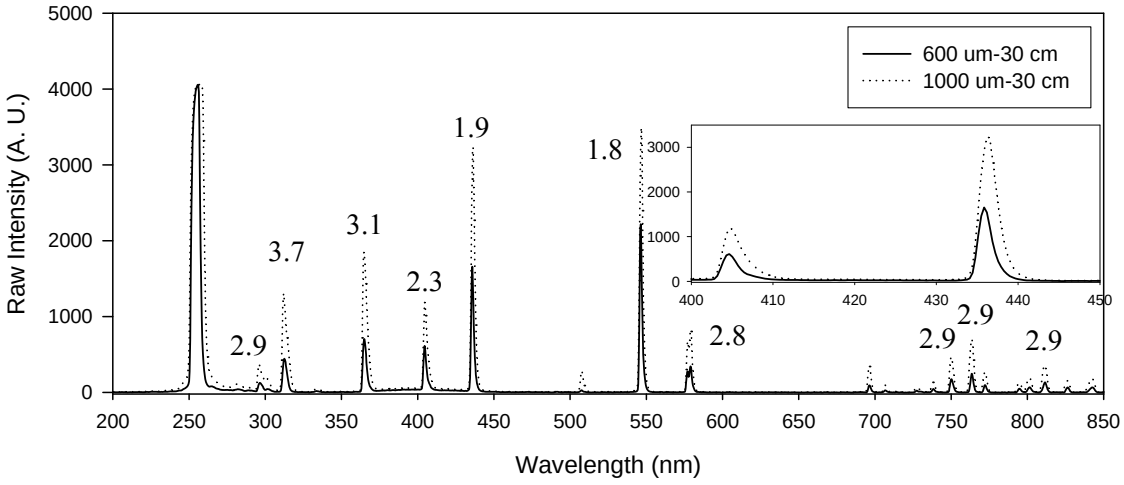

Figure 2.12: *The effect of fibre optic cable diameter using a Hg lamp source.*

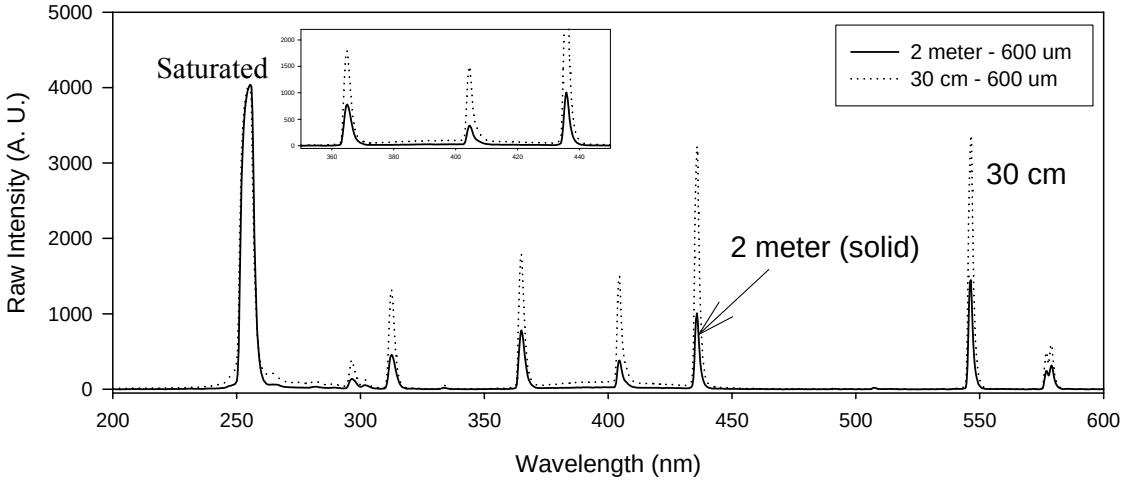

Figure 2.13: *The effect of fibre optic cable length using a Hg lamp source.*

Chapter 3

Microplasma Stability

3.0 Tubular Microplasma Stability

A key issue that arose in previous work using planar MPDs was the plasma background stability. Confinement of the microplasma with a tube (i.e., a wall-stabilized MPD) was thought to improve the stability of the background emission since the microplasma has less distance to shift or move (1.3 mm I.D. quartz tube and 0.600-0.800 μm microplasma). This reason alone was the motivation for switching to the tubular Ar/H_2 MPD. With a more stable plasma background emission, one would be able to further characterize the MPD with ease. Given that a tubular geometry will reduce the distance that the plasma can shift, one must still investigate whether such a geometry will produce more stable background emission spectra. Also, does the mode of the plasma, i.e., bluish or pinkish influence the stability of the MPD background emission spectra?

3.1 Pinkish Tubular Microplasma Device (MPD)

All three lengths of inter-electrode distance (IED) tested, i.e., 10, 30 and 50 mm, were able to form the pinkish plasma but reproducing the frequency, power and background emission levels and spectral lines was very difficult. Sometimes the 80 s MPD warm-up time did not stabilize the pinkish MPD. A problem associated with having to run the pinkish MPD for prolonged periods of time is the generation of heat. As the MPD electrodes heat up, the glue that binds the electrode and quartz glass begins to melt. The pinkish MPD is more "thermal" in character than the bluish plasma and gets hot to the touch. Overall, the pinkish MPDs had a much shorter lifetime than the bluish MPDs.

The pinkish plasma has a complex background spectrum with Ar atomic emissions in 600-850 nm region, hydrogen lines at 434, 468 and 656.2 nm (ascending order of line intensity) and H_2 hump from 200-400 nm (Fig. 3.0). The background spectral features are dependent on the microplasma operating conditions. The pinkish mode (for a given frequency) will occur when the dc power supply operates in variable current and controlled voltage mode. The plasma switches into the bluish mode as soon as the current becomes controlled (the dc power supply can be either voltage or current controlled but not both simultaneously). The almost-saturated 656.2 nm H line is what gives the plasma the pinkish colour.

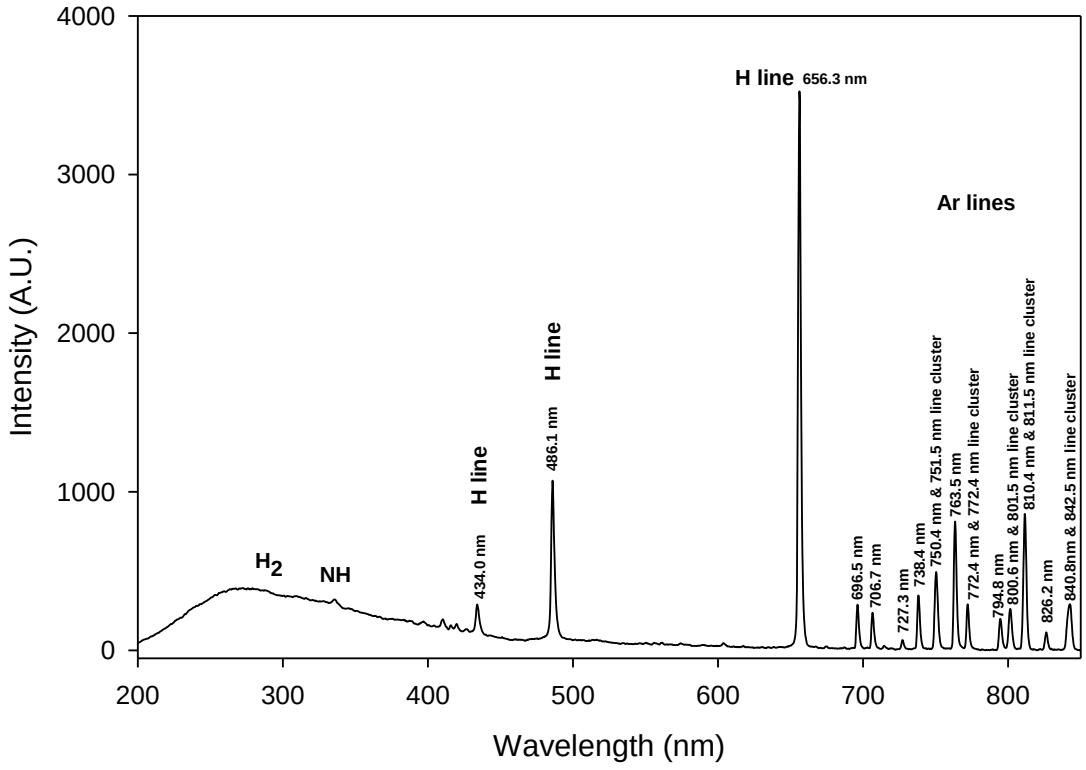

Figure 3.0: *Labeled pinkish Ar/H_2 tubular 30 mm IED MPD background spectrum from 200-850 nm.*

Operating conditions with stable background spectra were found for various pinkish MPDs but as soon as the mini-ITV introduced the hot gas containing the dried microsample, (as would be expected during sample vapourization) the plasma background spectra changed. This lead to poor background correction as demonstrated in Fig. 3.2 (b-c). In Fig. 3.2a), the raw data for a Ca (1 ppm, 3 µL) and Li (100 ppb, 3 µL) signal is shown for a relatively low mini-ITV vapourization power (20 W). It is impossible to see the fluctuation of the hump from 200-400 nm in Fig. 3.2a) but fluctuation is clear in the background corrected Ca signal in Fig. 3.2b). The H lines increase as the mini-ITV heats up and this shows up in background corrected spectra in Fig. 3.2 (b-c). Fortuitously, the Ca 422.67 nm line is almost baseline resolved and the Li 670.78 nm line is baseline resolved but a number of elements would not avoid the affect of the background change. These large fluctuations of the 656.2 H line and other spectral features introduced the need for signal processing (i.e., normalization), which is what this study was trying to remove altogether. Like the planar He/H_2 MPD[5], the fluctuations are non-linear across the wavelength axis and would require rigorous 2-4 point normalization. The confinement within the tube limits microplasma movement to ~200-300 µm on either side. In this case, the fluctuations are in the positive direction suggesting that within the pinkish mode some emission lines are sensitive to the heat introduced by the mini-ITV (i.e., the H_2 hump, the H lines and Ar lines).

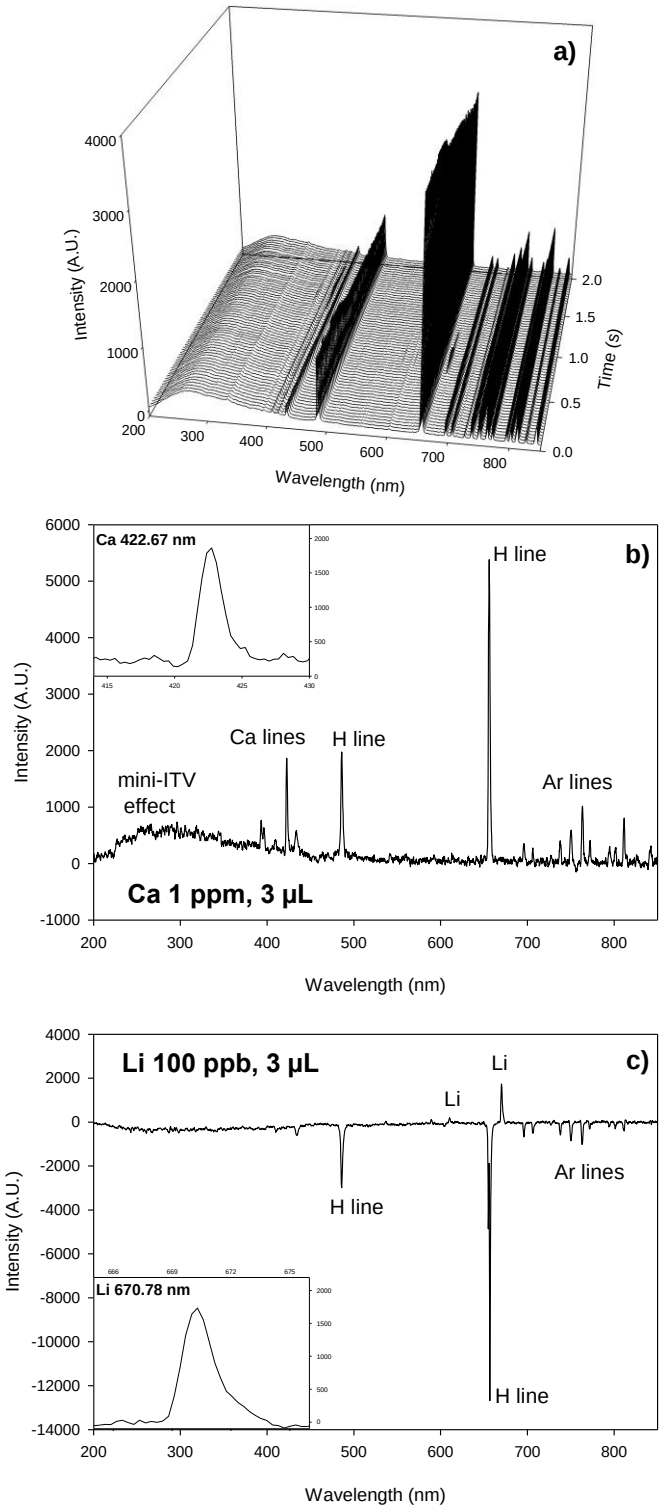

Figure 3.1: *Example of tubular pinkish MPD background instability when Ca (1 ppm, 3 µL) and Li (100 ppb, 3 µL) dried microsample is introduced via mini-ITV. a) Raw 3-d (intensity vs. wavelength vs. time) plot and background corrected 2-d (intensity vs. wavelength) plots for b) summed net Ca signal and c) summed net Li signal.*

3.2 Bluish Tubular Microplasma Device (MPD)

The wall-stabilized, tubular geometry MPD does exactly as thought with the bluish mode, that is, it confines the microplasma to the tube which in turn, improves the stability of the background spectra. This was observed for a variety of powers and inter-electrode distances (30, 50 mm IEDs). If there was a background disturbance caused by mini-ITV, it was minimal, primarily within a few episodes ahead of the analyte signals. The 10 mm IED MPD could not form bluish plasma (for this particular plasma frequency generator, geometry, tube diameter, electrode diameter and material, etc.). The tubular bluish MPD background emission (Fig. 3.2) is very similar to that of the planar bluish MPD.[7] The intensity of the background varied with IED, power and observation location.

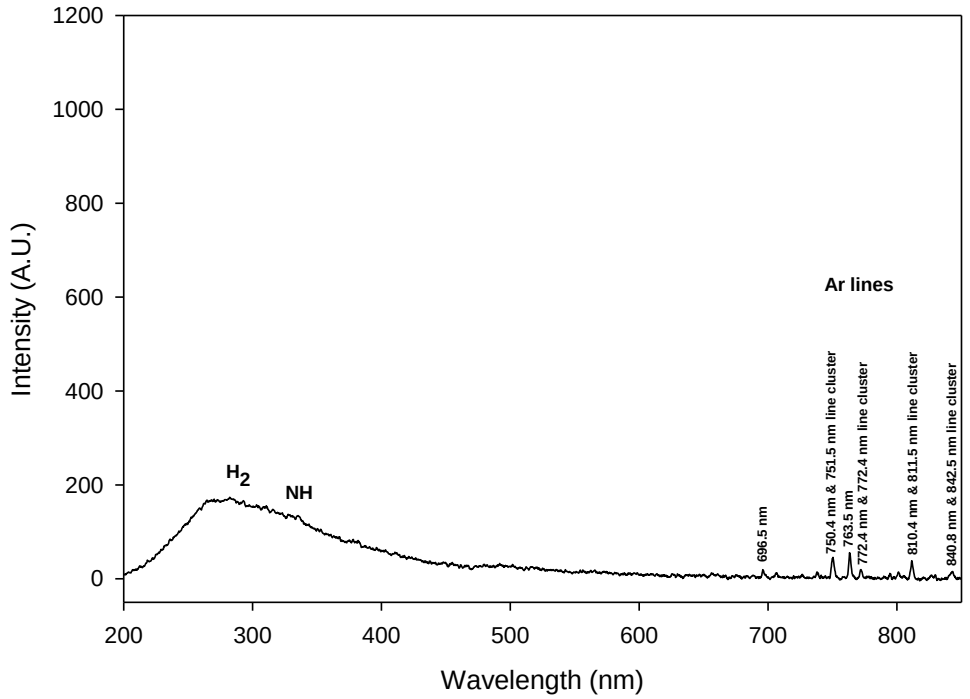

Figure 3.2: *Labeled bluish Ar/H_2 tubular 30 mm IED MPD background spectrum from 200-850 nm.*

The tubular bluish MPD can operate for minutes at a constant background (once the initial "thermal" equilibrium has been reached) without heating up sufficiently to melt the glue but it has been noted that with an increase in power and IED, the temperature of the bluish MPD would become hot to the touch. Overall, due to the stability and simplicity of the bluish MPD background spectrum there was never a need for normalization of any of the data in this thesis (0% compared to 30% for planar Ar/H_2 MPD[7] and 100% for He/H_2 MPD[5]).

An example of this background stability is demonstrated in Fig. 3.3 using Cu (1 ppm, 3 µL) at medium to high mini-ITV power (~60 W). In Fig. 3.3a), superimposed 2-d (intensity vs. wavelength) plots are shown for 23 spectral episodes. In this case, 3 spectral episodes contain raw analyte signals (e.g., Cu), 10 episodes contain pre-vapourization background emission and 10 episodes contain post-vapourization background emission. Minor fluctuations in the spectral hump observed around 280 nm (Fig. 3.3a) occurred before the Cu signal appeared but background correction was not affected and baseline resolved peaks were obtained (Fig. 3.3b).

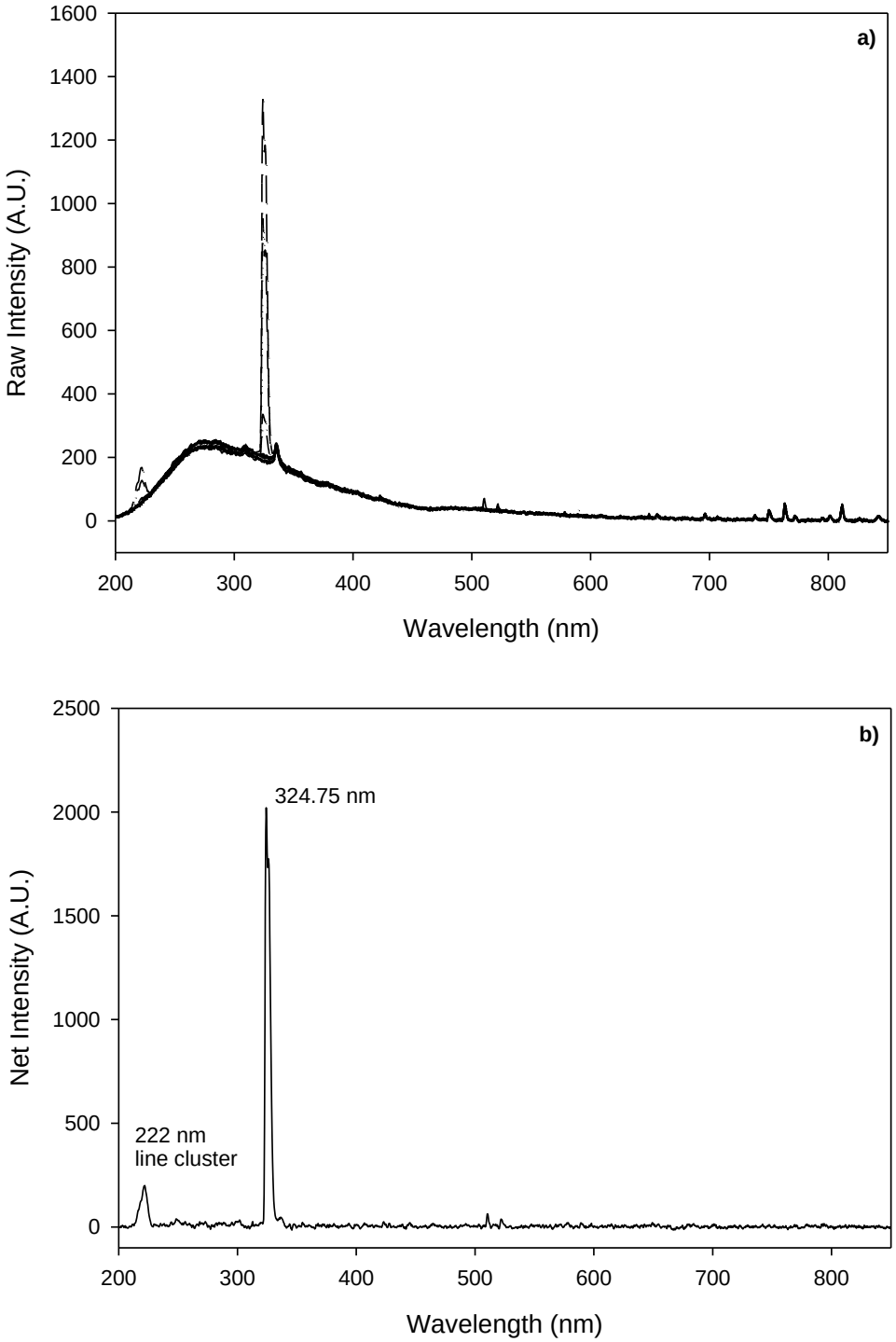

Figure 3.3: *Example demonstrating the stability of tubular bluish MPD using Cu (1 ppm, 3 µL) with mini-ITV at higher vapourization power (~60 W), a) super-imposed 2-d (intensity vs. wavelength) plots for 23 spectral episodes containing Cu raw signals (3 episodes) and background emission spectra (10 episodes pre-vapourization and 10 episodes post-vapourizaiton) and b) 2-d plot of summed net Cu signal.*

The bluish MPD can be tuned to have more power by increasing the current limit and/or adjusting the voltage or frequency. Once the dc power supply switches from current control to voltage control, the microplasma switches from bluish colour to pinkish colour instantly (for the bluish frequencies tested in this thesis). As the bluish MPD increases in power and becomes more hot to the touch and pinkish-like, the lifetime of the device decreases as well as the stability of the background emission.

To further test for background emission instabilities of the higher power bluish MPD the PMT-based system was used (Fig. 3.4). In a), Fe (1 ppm, 3 µL) is introduced into the MPD at increasing vapourization powers (temperatures). As the vapourization power surpassed ~60 W (for the particular MPD conditions), a second peak began to appear in the analyte emission signal acquired at 248.8 nm. In Fig. 3.4b), a coil blank with mini-ITV turned on for about 0.5 s at the highest vapourization power demonstrates that an artifact occurs at this wavelength. The next coil blank with mini-ITV left on for about 5 s (i.e., the duration of signal acquisition) shows the increase in the background levels to the same height of the previous blank but with the background never returning to the original level. Finally, the third figure in this sequence shows the Fe (1 ppm, 3 µL) with mini-ITV left on. This series of figures clearly demonstrates that the hump from 200-400 nm changes with increasing mini-ITV power/temperature, as seen with the pinkish MPD, reconfirming that the H_2 hump is sensitive to the heat from mini-ITV. From these data (Fig. 3.4) it can also be concluded that using maximum mini-ITV vapourization power is not always beneficial.

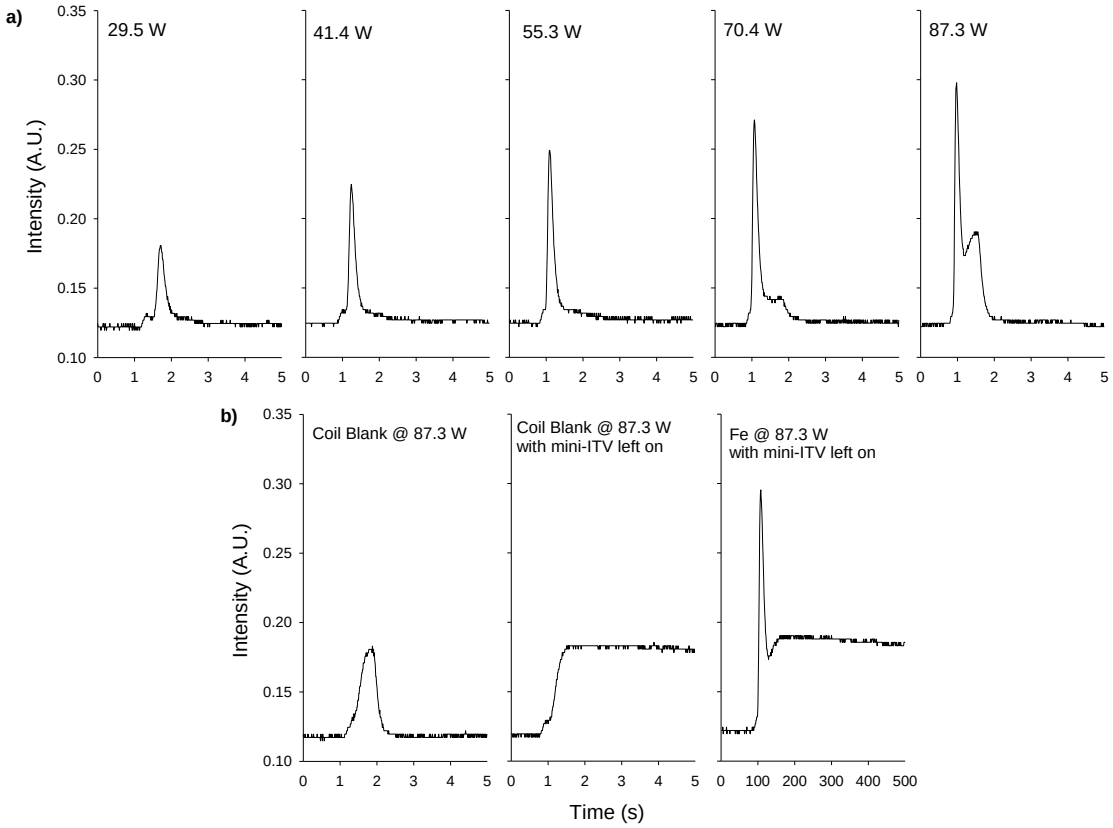

Figure 3.4: *PMT signals acquired at 248.8 nm demonstrating a) the effect of mini-ITV power on Fe (1 ppm, 3 µL) signal and higher power bluish MPD background. b) To confirm that Fe was not responsible for both peaks observed at higher mini-ITV vapourization powers, coil blanks at 87.3 W with mini-ITV turned on briefly (<0.5 s) and mini-ITV left on for about 5 s were tested as well as Fe (1 ppm, 3 µL) signal with mini-ITV left on for about 5 s.*

In summary, using a rule-of-thumb from the past that states that "the higher the mini-ITV vapourization power the higher the signal peak height" one would expect an increase in signal-to-noise ratio (SNR) with increasing mini-ITV power and an improvement in the detection limit. This rule is only beneficial for elements in wavelength range unaffected when using high vapourization power by mini-ITV. For example, the improvement in SNR in the Fe signal obtained when vapouring an Fe containing microsample at 55.3 W is marginal as compared to the improvement obtained

when vapourizing the same amount of Fe containing sample at 87.3 W (Fig. 3.4a). It is noteworthy that ~90 W is the maximum vapourization power that can be applied to this mini-ITV coil and that SNR is related to the detection limit. Getting back to the signal shown in Fig. 3.4a, as vapourizing power is increased from 55.3 W to 87.3 W background correction gets progressively more complicated. Clearly, the slight improvement in SNR is outweighed by complicated background correction.

Mini-ITV coil blank signals (i.e., those obtained without pipetting a sample or water on the coil) were obtained as shown in Fig. 3.4b. As vapourization power increased (e.g., 87.3 W), a peak signal appeared. In this case the 87.3 W vapourization power was applied to the coil for about 0.5 s. Since nothing was placed on the coil and the coil was not retracted from the vapourization chamber (as would be required to pipette a microsample), is this signal due to spectral interference vapourizing from the coil, or from the ceramic or from the vapourization chamber?

To address these questions, a coil blank was run one more time at 87.3 W, but with mini-ITV left on for about 5 s. Interestingly, the peak disappeared and was replaced by a constant-intensity signal (e.g., between 2-5 s in the middle frame of Fig. 3.4b). Furthermore, the constant intensity signal had the same intensity as the maximum intensity of the peak signal obtained when 87.3 W of power was applied to mini-ITV for only 0.5 s. This experiment was replicated several times yielding similar results. Thus, spectral interference was ruled-out because had it been interference from material vapourizing from the coil, the ceramic or the chamber the intensity levels would change the more times the experiment was run. In fact, the post-vapourization intensity levels were the same as those observed when running a coil blank (Fig. 3.4b, middle frame and

right-frame). Furthermore, peak height of the Fe signal observed when applying 87.3 W for 5 s (right-most frame, Fig. 3.4b) was statistically the same (right-most frame, Fig. 3.4a) when applying 87.3 W for only 0.5 s. Thus, based on these results spectral interference was ruled-out.

From these results, it can also be concluded that for MPDs operated as described in this thesis, using the maximum vapourization power is not always beneficial, at least from the SNR and background correction points of view. From these results, it can also be speculated that as vapourization power increases (e.g., to 87.3 W), the temperature of the mini-ITV carrier-gas entering the microplasma becomes a significant fraction of T_{gas} inside the microplasma channel. In the future, it would be interesting to examine this possibility.

3.3 Bluish Tubular Microplasma Device (MPD) Limiting Precision

The bluish MPD has reproducible background emission levels from one run to the next but will the same be true for analyte signals? What is the limiting precision of the MPD for background and analyte signals? The limiting precision of the MPD was tested using the monochromator/PMT system (Fig. 3.5) because data can be acquired faster than the CCD spectrometer. Since the majority of work for this thesis has been carried out using the CCD polychromator (which has poorer precision due to the known fact that over half of the transient mini-ITV signal is being lost due to data transfer delays), the limiting precision of the CCD polychromator must also be determined.

The limiting precision of the PMT was determined by running 10 separate runs of Ag (1.5 ng) at 328.07 nm on the Heath monochromator. In Fig. 3.5, the raw data for these 10 runs is shown. This figure demonstrates that the background and peak height do

not change significantly from run to run. In Table 3.0, the precision of the background, net peak height and net peak area is calculated. The limiting precision of the device was determined to be 2.7, 4.5 and 4.0 % for the bluish MPD background, net peak height and net peak area, respectively. Note that in these precision values there is an added error from the Eppendorf© pipette (certified to < 3% error). Also, the peak heights are 0.5 % worse than peak areas since peak height depend on the placement of the microsample on the coil and the rate at which the coil heats up. Since the data acquisition (DAQ) time is sufficiently fast and no data are lost (as with the CCD spectrometer), peak areas will account for the entire microsample introduced into the MPD, and thus should have better precision.

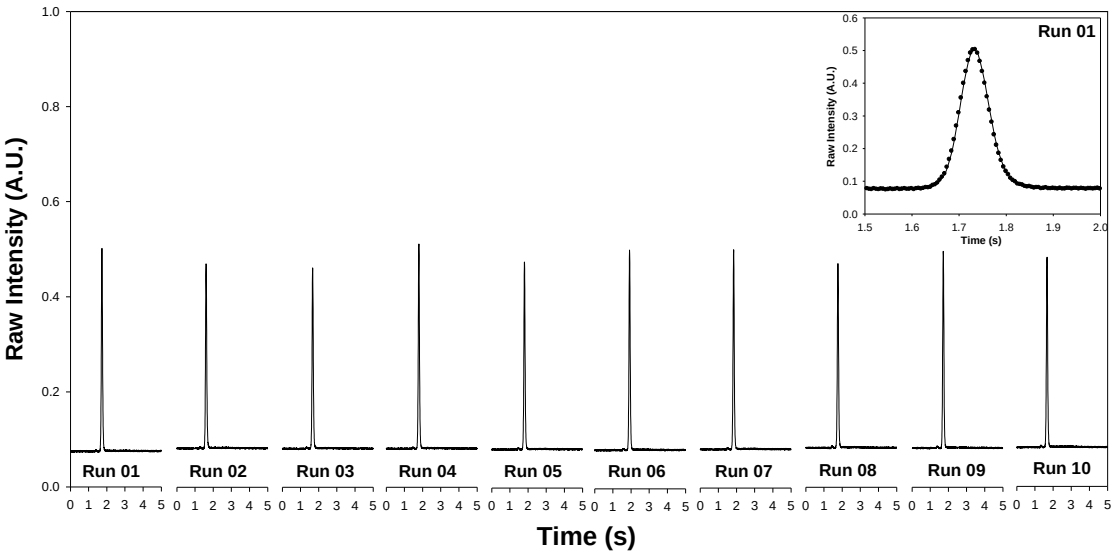

Figure 3.5: *PMT raw signals for 10 individual consecutive runs of Ag (500 ppb, 3 µL) at 328.07nm demonstrating the limiting precision of the MPD with a PMT-based system.*

Table 3.0: *Average, standard deviation and relative standard deviation for PMT signals from run 1-10 of Ag (500 ppb, 3 µL) at 328.07 nm.*

Run #	Raw Signal	Average Background	Net Peak Height (A.U.)	Net Peak Area (A.U.)
1	0.5017	0.0754	0.4263	6.689
2	0.47	0.0821	0.3878	6.338
3	0.4612	0.0814	0.3798	6.119
4	0.5118	0.0815	0.4303	6.885
5	0.4752	0.0813	0.3939	6.356
6	0.502	0.0816	0.4205	6.807
7	0.501	0.0816	0.4195	6.750
8	0.4704	0.0833	0.3868	6.252
9	0.4958	0.0827	0.4131	6.630
10	0.4817	0.0826	0.3991	6.488
Average	0.4871	0.0813	0.4057	6.531
Stdev	0.0174	0.0022	0.0183	0.258
%RSD	**3.57**	**2.71**	**4.52**	**3.96**

The limiting precision of the CCD polychromator was determined by using 25 individual runs of Ag (500 ppb, 3µL) and monitoring the peak height and the peak area of the 328.07 nm Ag emission line. The average background was determined by averaging background intensities at 282 nm for all episodes. The results for the 25 Ag runs are shown in Table 3.1. The relative standard deviation (RSD) for the background is 1.4 % and the RSD of the net peak height and area is ~17.5 %. The precision is therefore 3-4x poorer than the PMT system. In order to improve RSD, a faster detector is required with shorter data transfer delays. Since this suggestion does not lie within the scope of this project, 3-4 replicates will be run for each sample where statistical confidence is required.

Table 3.1: *CCD polychromator limiting precision for the background, net peak height and net peak area (328.07 nm) for 25 individual Ag (500 ppb, 3 µL) runs.*

Run #	Average Background (A.U.)	Net Peak Height (A.U.)	Net Peak Area (A.U.)
1	213.74	1562	12872
2	214.94	1811	14753
3	216.56	1537	12985
4	216.21	2002	16521
5	219.03	1995	16120
6	212.23	1275	10339
7	212.75	1673	13106
8	215.50	1784	14583
9	215.38	1722	14118
10	216.56	1566	12861
11	215.38	1361	11119
12	218.73	1442	12141
13	218.86	1158	9464
14	218.52	1547	12610
15	216.50	1582	13345
16	215.46	1288	10278
17	215.95	1190	9626
18	219.49	1865	15206
19	222.56	1560	12527
20	222.96	1109	9120
21	218.82	1188	9810
22	219.95	1421	11456
23	221.78	2006	16411
24	222.01	1882	14944
25	221.44	1574	12953
Average	**217.65**	**1564**	**12770.72**
Stdev	**3.05**	**274.00**	**2224.29**
% RSD	**1.40**	**17.52**	**17.42**

3.4 Conclusions

The stability of microplasma background emission when introducing dried microsamples via mini-ITV has been a key issue since the beginning of the MPD research using the CCD spectrometer. With past students, the monochromator was mostly used for acquiring data. Since the entrance slit on the monochromator is less than or equal to 200 µm, any minor movement of a 600-900 µm microplasma would not affect the analytical signals. With the CCD spectrometer, the diameter of the fibre optic cable

is 600 μm and since the microplasma is 700-900 μm in diameter, any instability will show up in the spectrum. Confining the plasma to a tube provided even more stability than the planar MPD geometry with a relatively wider channel.[5,7] The bluish mode of plasma also increased the stability of the plasma. With increasing MPD power, the bluish mode shifts towards the pinkish mode and the microplasma becomes more unstable, especially in the vicinity of the broad Hydrogen signal spanning 200-400 nm. Hydrogen lines are sensitive to the heated gas from mini-ITV, especially when the MPD is operated in pinkish mode. As the vapourization power (or coil temperature) increases and using higher power bluish MPD, so does the Hydrogen hump instability.

Chapter 4

Analytical Performance of the Microplasma Device (MPD)

4.0 Overview

Emission of the microplasma device (MPD) background has been shown to change depending on the region of the plasma that is viewed between the electrodes (observation location), frequency, power and whether a pinkish or bluish mode is used. Furthermore, it has been shown that the Li signal intensity varies with MPD power at a fixed observation location.[7] And, it has also been visually observed that with high concentrations of Na (> 5-10 ppm), as one increased the power of the MPD (i.e., by increasing the voltage, current or both and/or by increasing the IED), the yellow emission (588.995 and 589.592 nm) would only occur at the front part of the microplasma (with front defined as the part of the microplasma closest to the mini-ITV outlet). At lower MPD powers, the entire channel would fill with yellow colour.[6] What is happening to the Na signal?

Although electrical power has been shown to affect the analytical performance, it is not known whether other parameters (mentioned above) that affect the plasma background emission will also affect the analytical performance of the MPD. In the past, the philosophy was that the brighter a pinkish plasma was the better and more intense analyte signals of the MPD would be.[5,19, 20, 22] Does the pinkish MPD have better analytical performance than the bluish? Does more power mean improved signal intensity?

This chapter will focus on the analytical performance of the tubular MPD by demonstrating the effect of observation location of 4 elements, having different volatilities and covering a wide wavelength range. In particular, inter-electrode distances

(IEDs) and the MPD operating modes (i.e., pinkish and bluish); the effect of MPD power and operating mode on fixed observation locations; and estimated detection limits of 16 elements will be determined using both the CCD spectrometer and the more sensitive monochromator system with PMT.

4.1 Observation Location of the Microplasma Device (MPD)

Observation location can be compared to viewing location for the ICP torch. The analyzable elements by ICP have different signal response (or intensities) depending on the viewing distance above the load coil of the ICP torch. Analyte residence time, i.e., the amount of time that analyte interacts with (or resides) in the plasma, is one factor responsible for this variability in viewing locations. Another factor is the excitation and ionization energy of the element. Easily ionization elements (EIEs) such as group I metals, i.e., Na, Li, K, require a region that is far above the torch (~20 cm). The prominent lines for the EIEs are atomic lines, not ionic lines because most ionic lines for these elements have excitation energies that are higher than the ICP can provide. Thus, EIEs must be viewed in a "colder" region where population of atoms is higher. Commercially available ICP systems have the default viewing height set to a compromised position that allows for analysis of a wide variety of periodic elements at the cost of analytical performance.[3]

Other plasma researchers have also noted an observation height dependence for signal intensities.[3, 26, 27] In past work with the planar MPD, the fibre optic cable was fixed arbitrarily in the centre of the microplasma (i.e., middle distance between the two electrodes) due to the stability at this particular location.[5-7] Is this the best observation

location for all elements? What happens to the observation location as the IED and consequently power changes?

An observation location study maps the emissions of 3µL samples of Ca (1 ppm), Li (100 ppb), Ag (1 ppm) and Zn (1 ppm) at four locations, i.e., front, mid-to-front, middle and back with three inter-electrode distances (IEDs), i.e., 10, 30 and 50 mm was undertaken. Bluish and pinkish modes will be used for 30 and 50 mm IED and only pinkish mode will be used for 10 mm (unable to form the bluish mode at this IED with the current setup). Dried microsamples of the standard solutions were introduced into the MPD using fixed mini-ITV vapourization power of 20 W (4.0 V, 5.0 A). These elements were chosen due to their wide spectral range coverage (213-670 nm) and variable excitation energies of the emission lines (1.8-5.8 eV). In Table 4.0, the operating conditions for this study are listed. The most prominent line of each element was used, i.e., Ca (422.67 nm), Li (670.78 nm), Ag (328.07 nm) and Zn (213.86 nm).

Table 4.0: *Observation location study conditions including inter-electrode distance (IED), voltage, current, frequency, power density and mode.**due to distorted waveform*

Inter-electrode Distance (mm)	MPD Operating Conditions					
	Voltage (V)	Current (A)	Frequency (KHz)	Nominal Power (W)	Power Density (W/mm^3)	Mode
10	8.4	0.63	****670.0**	5.3	0.6738	Pink
30	8.1	1.10	64.1	8.9	0.3782	Blue
30	8.4	1.35	****280.0**	11.3	0.4813	Pink
50	8.3	1.83	61.4	15.2	0.3868	Blue
50	11.0	1.93	****300.0**	21.2	0.5406	Pink

In Fig. 4.1 and 4.2, it is clearly evident that the MPD behaves similarly to that of the ICP, that is, the optimum observation location changes depending on the element of

interest. In fact, observation locations are not only element dependent but also dependent on IED, MPD power and operating mode. This power dependence for observation height (location) has also been observed with an ICP and other analytical plasma sources.[3,26,27]

General trends from Fig. 4.1 and 4.2 show that of the 4 elements and 5 MPDs, the maximum emission does not appear at the front or the back electrode. The only exception is Zn, with 30 mm IED bluish MPD. Residence time in the microplasma is likely to explain why the maximum emissions do not occur at the front and back observation locations. At the front, the analytes do not interact with the plasma long enough. At the back, it is likely that the analytes reside too long in the microplasma, losing atomic population to ions. As the power density increases within a fixed IED, the device becomes hotter to the touch and likely, analytes will require less residence time to obtain similar net intensities.

An inter-comparison of all the MPDs tested is only possible at the front viewing location. For example, looking just at the front observation location for the MPDs tested, Ca and Li have their maximum net intensity with the 50 mm IED pinkish MPD (Fig. 4.1 and 4.2). This suggests that more MPD power density for Ca and Li is better at this particular viewing location (power density dependence of these 4 elements will be looked into in the next section). Beyond that, other observation locations can only be compared within the same IED, i.e., mid-to-front location for 10, 30 and 50 mm IED is 2.5, 7.5 and 12.5 mm from the front electrode, respectively.

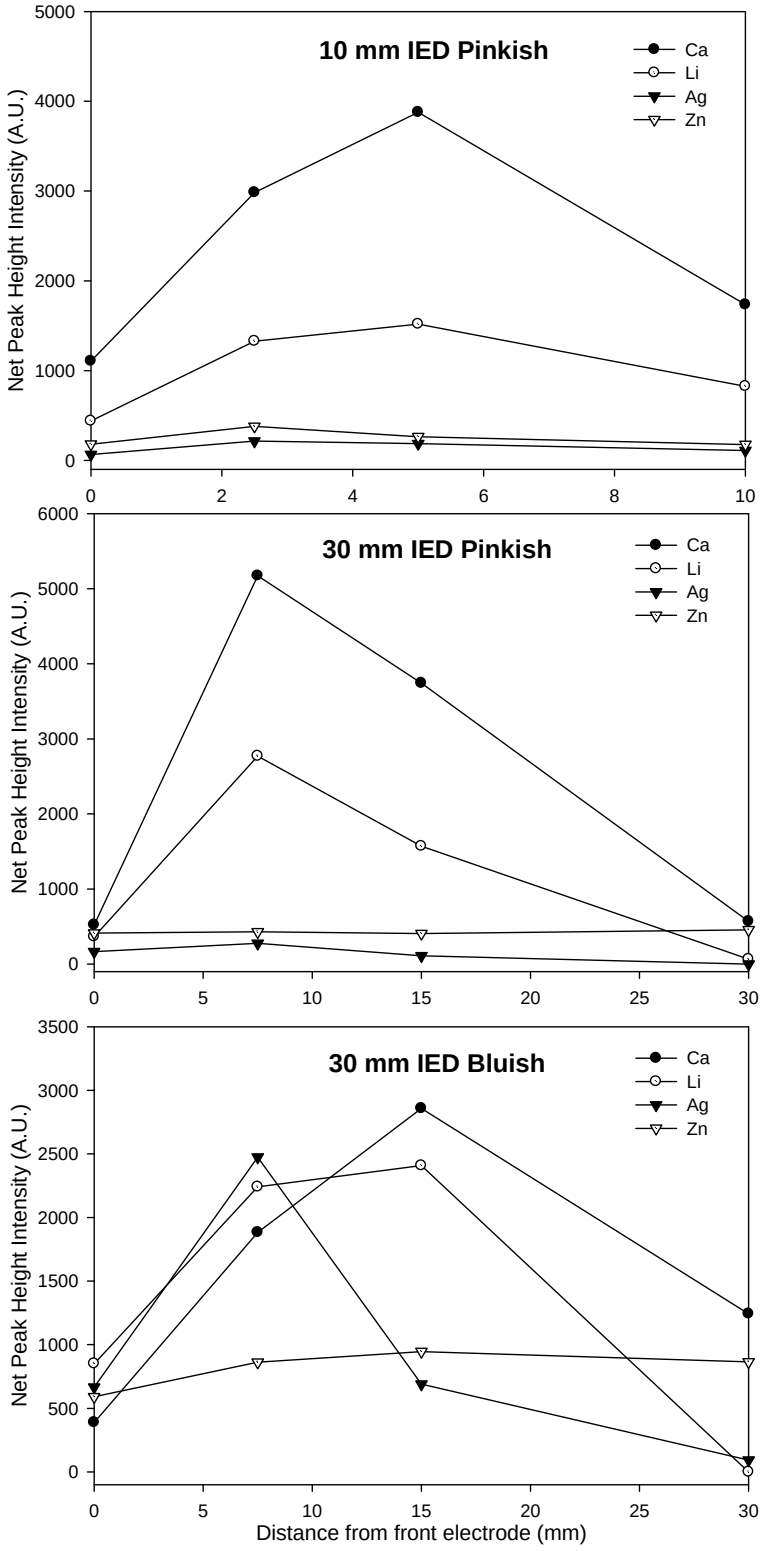

Figure 4.1: *Emission profiles for 3 µL of Ca (1 ppm), Li (100 ppb), Ag (1 ppm), and Zn (1 ppm) at front, mid-to-front, middle and back observation locations for 10 and 30 mm IED pinkish MPD and 30 mm IED bluish MPD.*

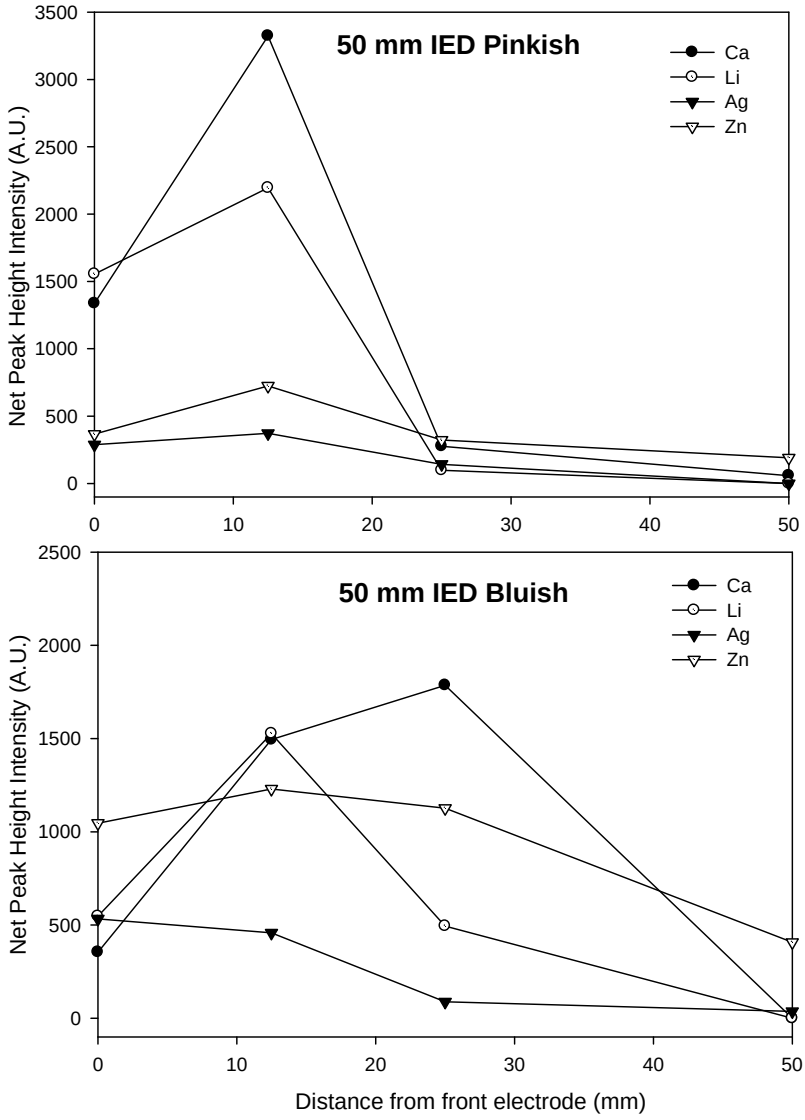

Figure 4.2: *Emission profiles for 3 µL of Ca (1 ppm), Li (100 ppb), Ag (1 ppm), and Zn (1 ppm) at front, mid-to-front, middle and back locations for 50 IED pinkish and bluish MPD.*

Now focusing on Ca and 30 mm IED MPDs (Fig. 4.1), one can see that higher power density of the pinkish MPD provides the more intense Ca signal. It can also be noted that the maximum emission for Ca comes out at mid-to-front location for the pinkish MPD and middle location for the bluish MPD. In the last chapter, the pinkish MPD is referred to as being more "thermal" than the bluish MPD. It appears that Ca requires less residence time in the more powerful and "thermal" pinkish MPD and had maximum net signal intensity at mid-to-front location. With the "softer" bluish 30 mm IED MPD, the maximum net Ca signal intensity was observed at middle location. This similar trend is seen with Ca and 50 mm IED MPDs (Fig. 4.2).

The last comment on the general trend of Fig. 4.1 and 4.2 suggests that observation location can be an "a good signal or no signal at all" situation depending on the element and MPD conditions. For example, by viewing the "wrong" location, one could conclude that a sample being analyzed did not contain the element of interest, which may not necessarily be the case. This clearly demonstrates the importance of observation location.

4.2 Microplasma Device (MPD) Power Study

From the analyte emission mapping study, it was shown that the pinkish MPD can provide very intense signals for some elements, e.g., Ca. As mentioned in Chapter 3 (Sec. 3.1), the pinkish MPDs had unstable background emission spectra and operating conditions. What if the bluish MPD could be tuned to higher powers to get the benefits of higher signal intensities (for elements like Ca) but still have the more stable and less intense emission background? The power of the MPD (within a given frequency) can be increased by either increasing the IED, the nominal dc power or both. There is a turning

point in the mode from bluish to pinkish as the current is allowed to increase to a point where the dc power supply automatically switches from current controlled to voltage controlled.

The purpose of the power study is to find operating conditions at mid-to-front and middle locations that provide increase signal intensities for Ca, Li, Ag, and Zn. Once again these four elements were chosen due to their spectral range coverage. The results from the power study will be used as a guide to obtain an indication of the preferential MPD power of 12 other elements, i.e., Ba, Cd, Cu, Eu, Fe, K, Na, Mn, Mg, Pb, Rb and Sr. From the mapping study, 3 of the 4 elements tested have maximum net signal emission when using the 30 mm IED MPDs. Zinc was the only element that has the maximum emission with bluish 50 mm IED but the second best emission for Zn was obtained using the bluish 30 mm IED MPD (~20% less). For these reasons, the power study will use a 30 mm IED MPD. Since front and back observation locations do not show net analyte emissions for any of the 4 elements tested at this IED, this study will only look at mid-to-front and middle observation locations (7.5 and 15 mm from front electrode, respectively).

The operating conditions used are listed in Table 4.1. Four electrical powers that generated microplasmas with bluish colour background emissions were tested. For three of the four microplasmas, the same HVac frequency was used (64.0 kHz). For the fourth microplasma, the maximum possible power that can used to sustain a microplasma with stable, bluish colour background emission was employed. To do so, the HVac frequency was changed to 56.6 kHz. Only one microplasma with stable pinkish colour background emission could be established (Table 4.1) and therefore, only one was tested. Once

again, the dried microsamples of Ca (3 ng), Li (300 pg), Ag (3 ng) and Zn (3 ng) standard solutions were introduced into the MPD at a fixed mini-ITV vapourization power of 20 W.

Table 4.1: *MPD operating conditions for power study including voltage, current, frequency, nominal dc power, nominal power density and mode.*
***due to distorted waveform*

MPD Operating Conditions					
Voltage (V)	**Current (A)**	**Frequency (kHz)**	**Nominal Power (W)**	**Power Density (W/mm^3)**	**Mode**
8.1	0.95	64.0	7.695	0.3261	Bluish
8.1	1.15	64.0	9.315	0.3947	Bluish
8.2	1.33	64.0	10.906	0.4621	Bluish
9.5	1.26	56.6	11.97	0.5072	Bluish
8.4	1.28	****298**	10.752	0.4556	Pinkish

Figures 4.3 and 4.4 show the effect of power, frequency and bluish and pinkish operating mode on Ca, Li, Ag, and Zn signals at mid-to-front (Fig. 4.3) and middle observation locations (Fig 4.4). Data acquired for pinkish MPD shown encircled in Fig. 4.3 suggests that for the experimental conditions used, it is not advantageous to use an MPD with pinkish colour background emission. In fact, not only is the background unstable (which adds the need for signal processing) but also the net intensity is less (for the elements tested, observation location, operating conditions used in this thesis, etc.).

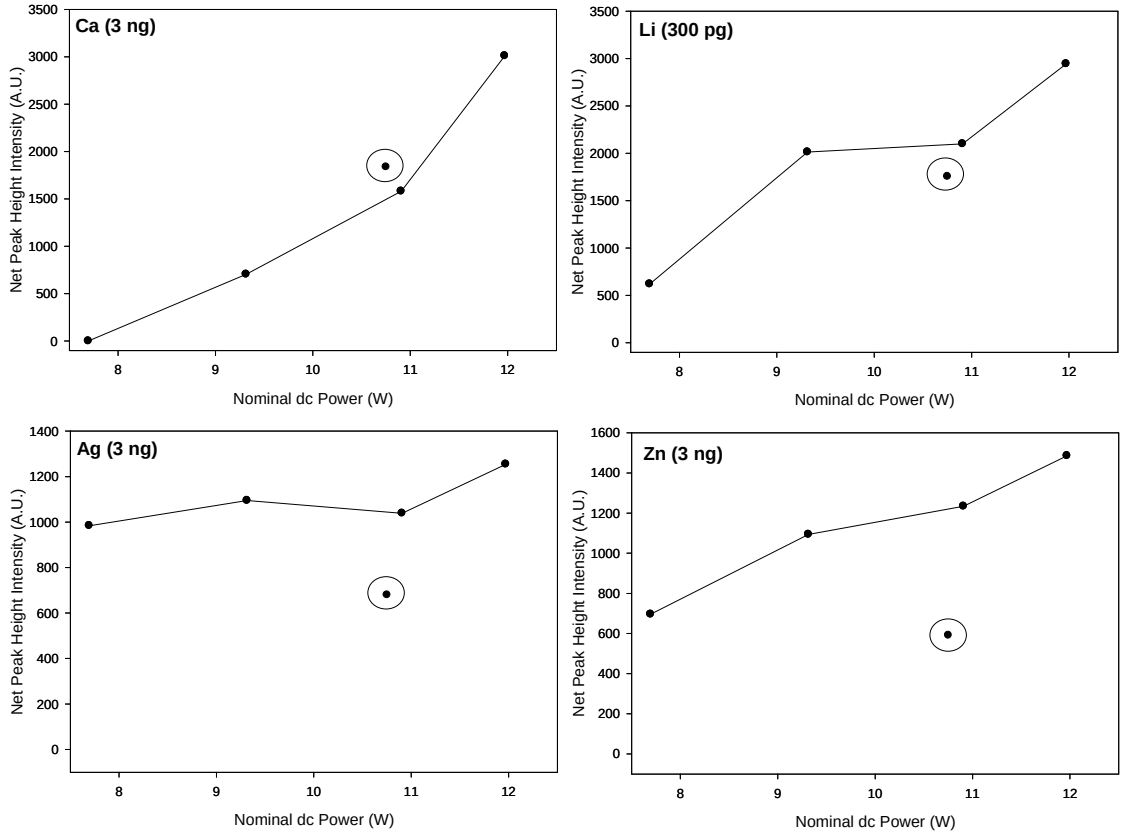

Figure 4.3: *The effect of power on 3 µL of Ca (1 ppm), Li (100 ppb), Ag (1 ppm) and Zn (1 ppm) signals at the mid-to-front observation location for 30 mm IED MPD. Five microplasma powers were used. Four of them generated bluish colour background emissions and the fifth (data shown encircled) generated a microplasma with pinkish colour emission.*

As mentioned in the Chapter 3 (Sec. 3.2.), the highest power bluish colour MPD was starting to approach the limit of the current control to voltage control turnover point where bluish colour MPD switches to pinkish colour MPD. At the mid-to-front observation location (Fig. 4.3), the highest power bluish colour MPD provided analyte signals with the best intensities for the 30 mm IED for all four elements. For example, Ca and Li signal intensities increased by a factor of two in going from a higher power bluish colour MPD operating at 64.0 kHz (10.906 W in Table 4.1) to the highest power, bluish colour MPD operating at 56.6 kHz (11.97 W in Table 4.1). In addition, increases

in net signal intensity were also observed for Ag and Zn. In this case, net signal intensities increased by a modest 20-25 % when bluish colour MPD power increased from 10.906 W (Table 4.1) to the maximum used in this thesis of 11.97 W (Table 4.1). Interestingly enough, Ca when using highest power bluish colour MPD had the 422.67 nm (I) line become the second prominent line next to the 393.37 nm (II) line, suggesting that MPD power also affects atom-to-ion net intensity ratios (discussed in the next chapter, MPD Characterization).

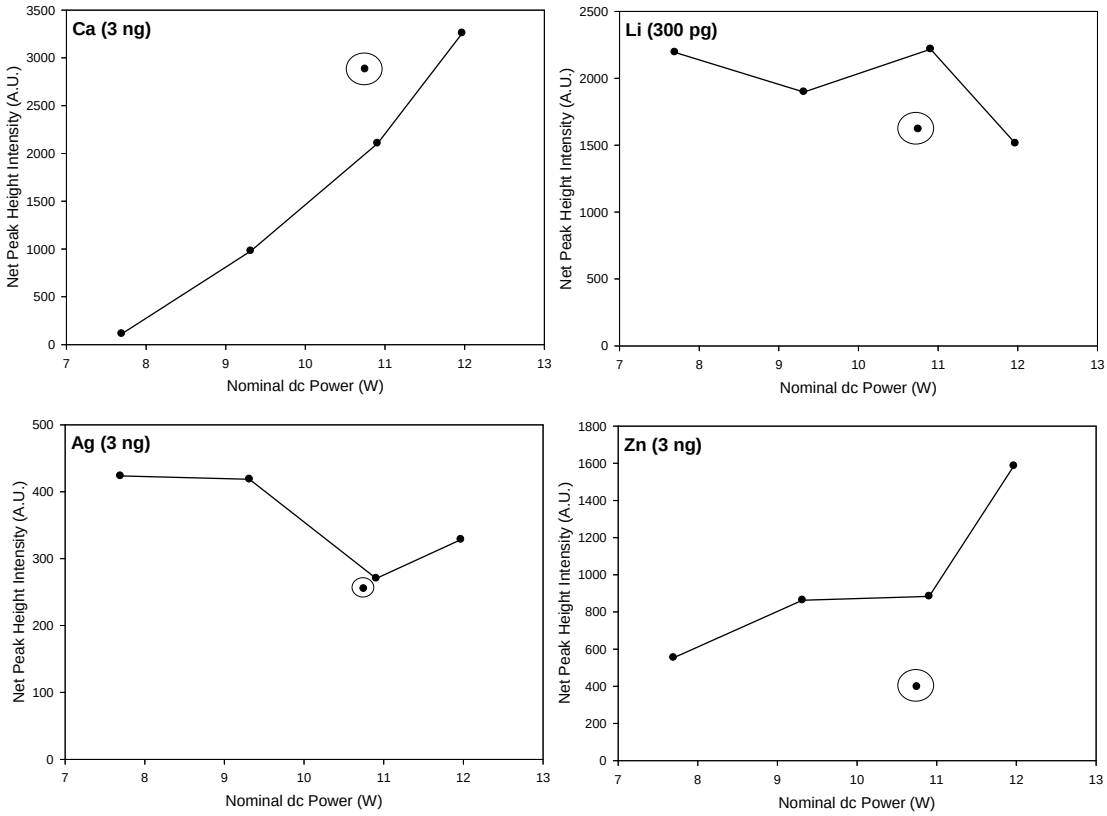

Figure 4.4: *The effect of power on 3 µL of Ca (1 ppm), Li (100 ppb), Ag (1 ppm) and Zn (1 ppm) signals at the middle observation location for 30 mm IED MPD. Five microplasma powers were used. Four of them generated bluish colour background emissions and the fifth (data shown encircled) generated a microplasma with pinkish colour emission.*

At the middle observation location (Fig. 4.4), the highest power is not always the best power. For example, Ca net intensity improves by ~10% as compared to mid-to-front observation location (Fig. 4.3) and the pinkish colour MPD and has comparable signal intensity to high power bluish colour MPD. Zinc also improves by 10% as compared to mid-to-front observation location (Fig. 4.3). In contrast, Li and Ag, decrease in intensity with increasing power (Fig. 4.4).

The observations described above were also confirmed visually by running 3 μL of concentrated Na solution (e.g., 1 ppm to as much as 100 ppm). Depending on IED and applied MPD power (at a given HVac frequency), a yellow colour emission was clearly seen above the bluish colour MPD background when the Na sample was introduced into the MPD. Depending on operating conditions (primarily MPD power and IED), yellow emission from Na at different parts of the microplasma was observed. Only two extreme cases will be described. In one case observed when low power was applied to a bluish colour MPD, Na yellow emission filled the entire microplasma from electrode to electrode. In the other case observed when high power was applied to a bluish colour MPD, Na yellow emission was observed only close to the entrance of the MPD. When intermediate powers were applied to a bluish colour MPD, the location of the maximum Na yellow emission varied between the two electrodes that were used to form the microplasma. In many respects, these visual observations confirm the spectroscopic measurements described above (e.g., the data shown in Figs. 4.3 and 4.4).

Spectroscopically, these decreases in signal intensity were likely due to atomic population loss to ions. In summary, this power study clearly illustrates that observation location, MPD power, HVac frequency and operating mode are intertwining variables

that affect the analytical performance of the MPD. As mentioned in the introduction, similar results have been observed in large scale ICPs, in particular, for observation height above the load coil.

4.3 Microplasma Device (MPD) Estimated Detection Limits

4.31 Estimated Detection Limits with CCD Polychromator

Estimated detection limits E.D.L.s (3 σ) where obtained by setting the standard deviation of the background noise to 1σ (i.e., signal-to-noise ratio (SNR) of 3). The SNR can be improved by either increasing the signal, or by decreasing the background noise or both.[24]

Using the information gained from the power study for Ca, Li, Ag and Zn, two MPD powers will be used to estimate the detection limits of 16 elements (i.e., Ag, Ba, Ca, Cd, Cu, Eu, Fe, K, Li, Mg, Mn, Na, Pb, Rb, Sr, Zn) from a tubular 30 mm IED bluish colour MPD using the CCD polychromator. The observation location will be fixed at the mid-to-front location (i.e., 7.5 mm from the front electrode located next to the outlet of the vapourization chamber).

The MPD power and observation location studies described above were used for selection of "optimum" MPD power level and observation location. Specifically, a medium power (9.315 W, 64.0 kHz) bluish colour MPD and a higher power (11.682 W, 56.6 kHz) bluish colour MPD were selected and used. Although an higher power bluish colour MPD gave the most intense analyte emission as compared to the other four powers tested (at mid-to-front observation location), some elements such as Ag and Zn, did not improve that much when MPD power increased. In addition to MPD power, mini-ITV vapourization power also plays a key role in SNR (and as a consequence in detection

limits). For example, in general, detection limits improve when analyte signals become taller and sharper. In turn, taller and sharper analyte signals can be obtained when vapourization power is increased, for instance to about 75-90 W (it is worth repeating that about 90 W is the maximum power that can be applied to this coil). But, as vapourization power increases and signals become narrower, fewer spectral episodes are collected by the CCD spectrometer. Out of the 12 other elements that were tested, it is possible that the medium power or "softer" microplasma will provide better SNR, especially in the 200-400 nm region.

In Table 4.2, estimated detection limits of 16 elements (Ag, Ba, Ca, Cd, Cu, Eu, Fe, K, Li, Mg, Mn, Na, Pb, Rb, Sr, Zn) for medium and high power bluish colour MPDs are listed. Some elements perform relatively the same (within 1-3x) at both powers (e.g., Ag, Pb, Mn, K, Cu, Na, Zn, Cd, Rb, Mg, Li). Other elements requiring higher vapourization temperatures require a higher power bluish colour MPD (Ca, Sr, Fe, Eu, Ba). There is up to 10x improvement in estimated detection limit for these elements when using higher power bluish colour MPD versus medium power bluish colour MPD. Figure 4.5 shows Fe and Eu example signals for medium power (9.315 W) and high power (11.682 W) bluish colour MPD for the same concentration (1 ppm, 3 μL). This further illustrates how crucial MPD power is for some elements.

Table 4.2: *Estimated detection limits with 30 mm IED bluish colour MPD at medium power (9.315 W) and higher power (11.682 W). The data was acquired at mid-to-front observation location with the CCD spectrometer.*

Element	9.315 W Estimated Detection Limit (pg)	11.682 W Estimated Detection Limit (pg)
Na	5	5
Cd	70	55
Li	15	5
Rb	120	85
Sr	600	195
Zn	125	95
Ca	235	40
Cu	35	60
K	35	35
Mg	90	35
Mn	25	35
Pb	170	195
Ag	20	30
Fe	275	40
Eu	1100	120
Ba	3500	310

Examples of net signals used for the estimated detection limit calculations of each element are shown in Figs. 4.6 to 4.21. These were acquired using a 30 mm IED bluish colour MPD at medium power (9.315 W, 64.0 kHz) and higher power (11.682 W, 56.6 kHz). Unlike the ICP, which has very complex analyte spectra,[3] all of the elements tested thus far by the MPD have relatively simple spectra. The most complex spectra of the 16 elements are for Eu and Fe. Although not all of the spectral lines are baseline resolved for Eu and Fe, there still is a variety of useable lines.

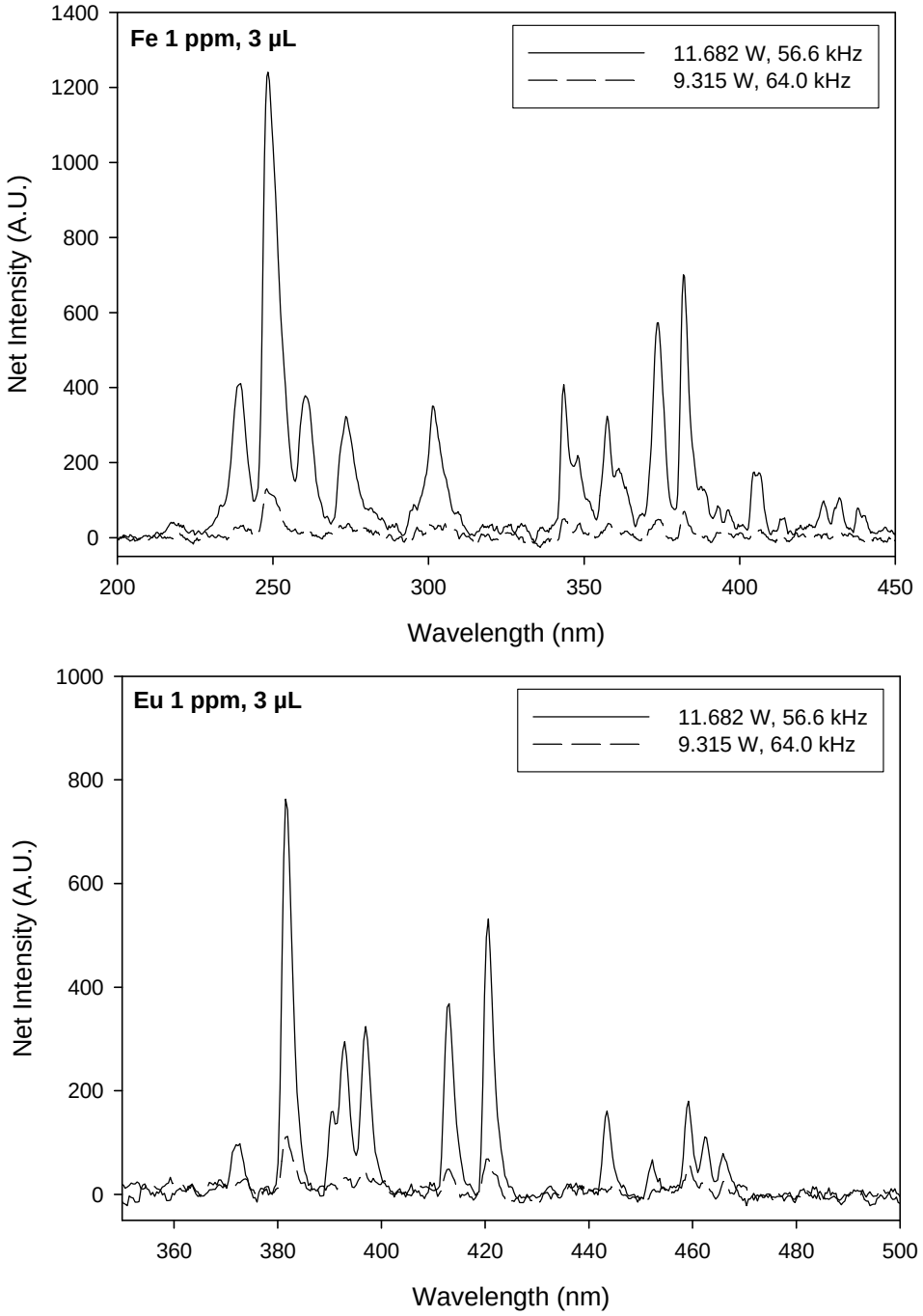

Figure 4.5: *Comparison of Fe and Eu signals (1 ppm, 3 µL) with med power (9.315 W) and high power (11.682 W) bluish colour MPD at mid-to-front observation location.*

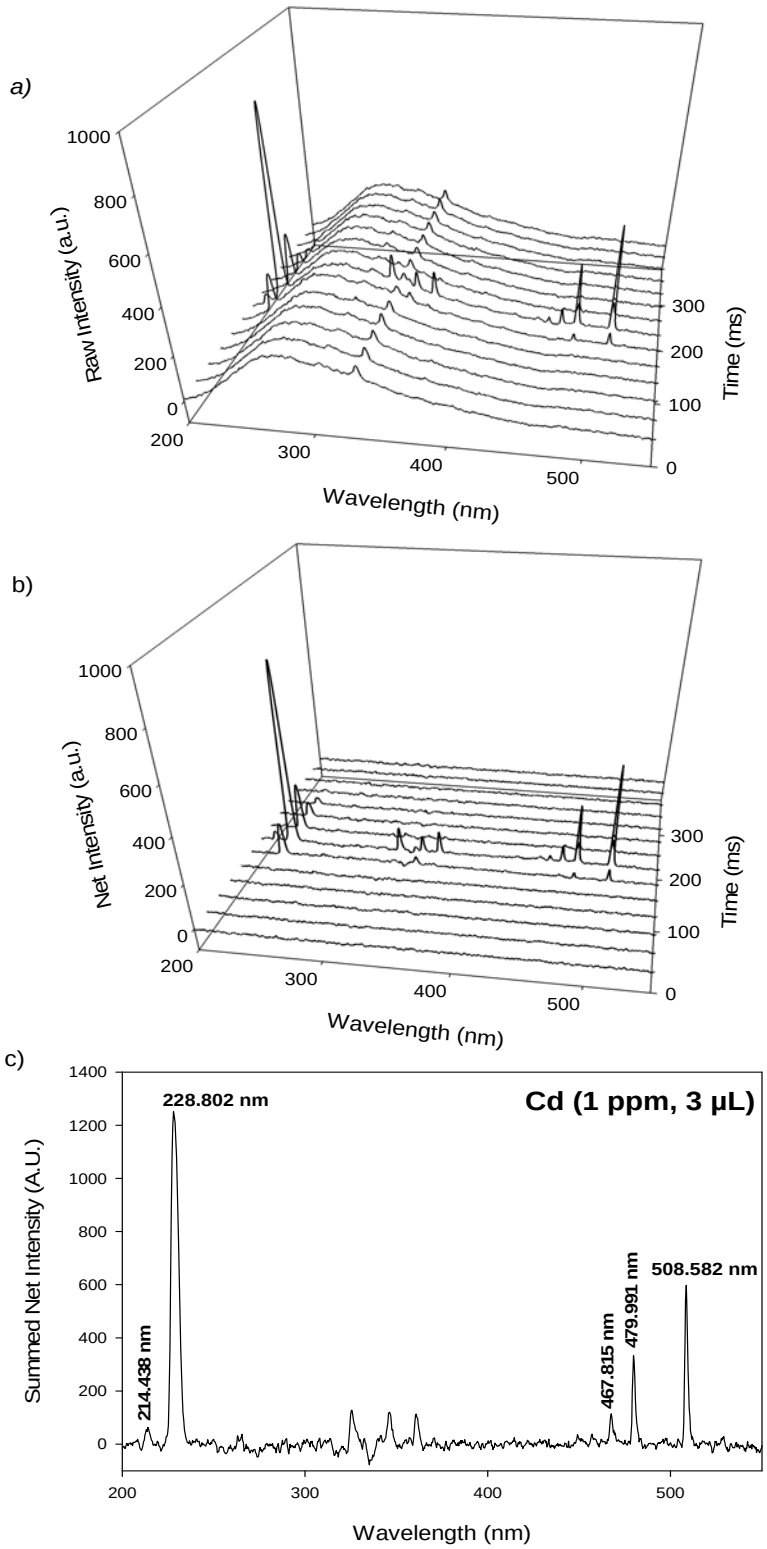

Figure 4.6: *Bluish colour MPD signal for Cd (1 ppm, 3 µL) captured with the CCD spectrometer. 3-d (intensity vs. wavelength vs. time) plots for a) raw data and b) background corrected data. And c), 2-d (intensity vs. wavelength) plot of summed net Cd signal.*

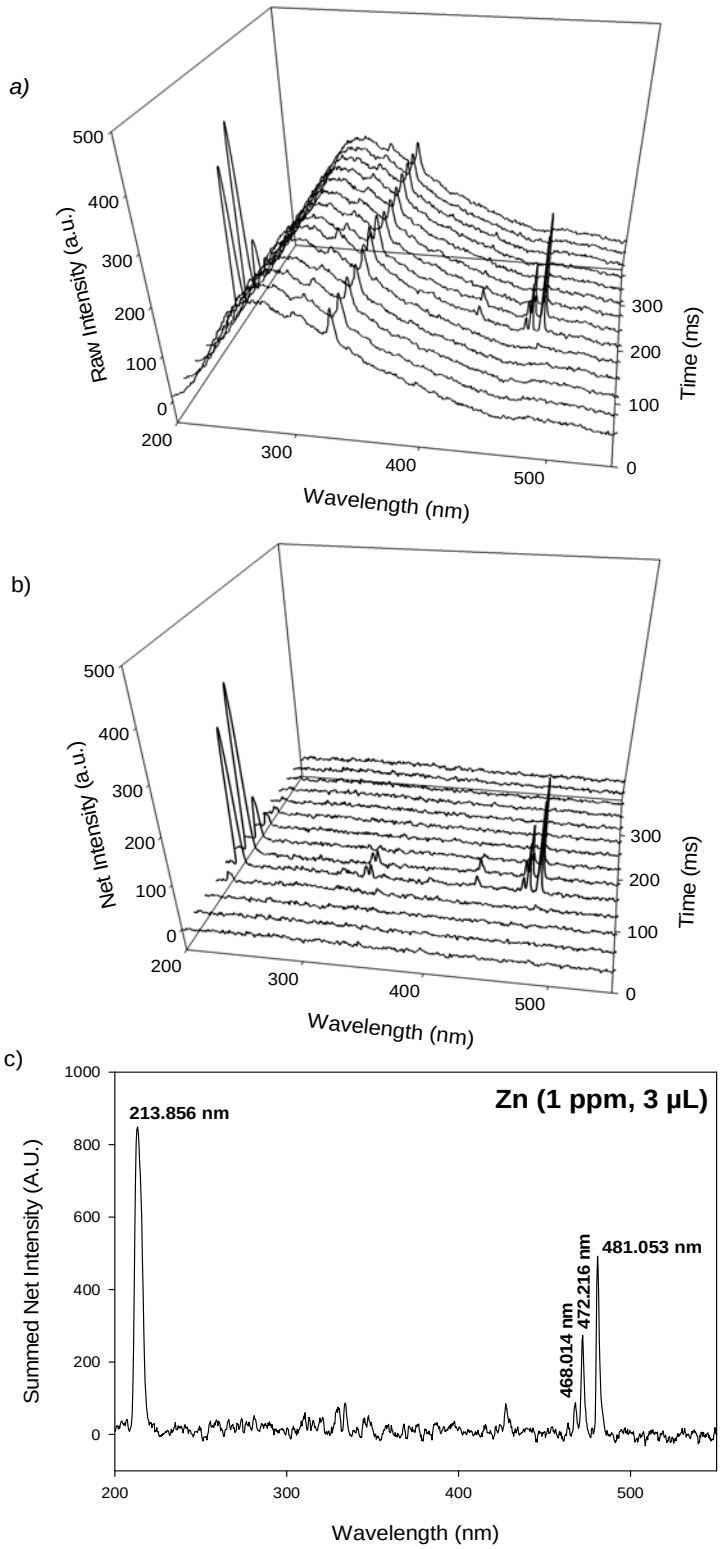

Figure 4.7: *Bluish colour MPD signal for Zn (1 ppm, 3 µL) captured with the CCD spectrometer. 3-d (intensity vs. wavelength vs. time) plots for a) raw data and b) background corrected data. And c), 2-d (intensity vs. wavelength) plot of summed net Zn signal.*

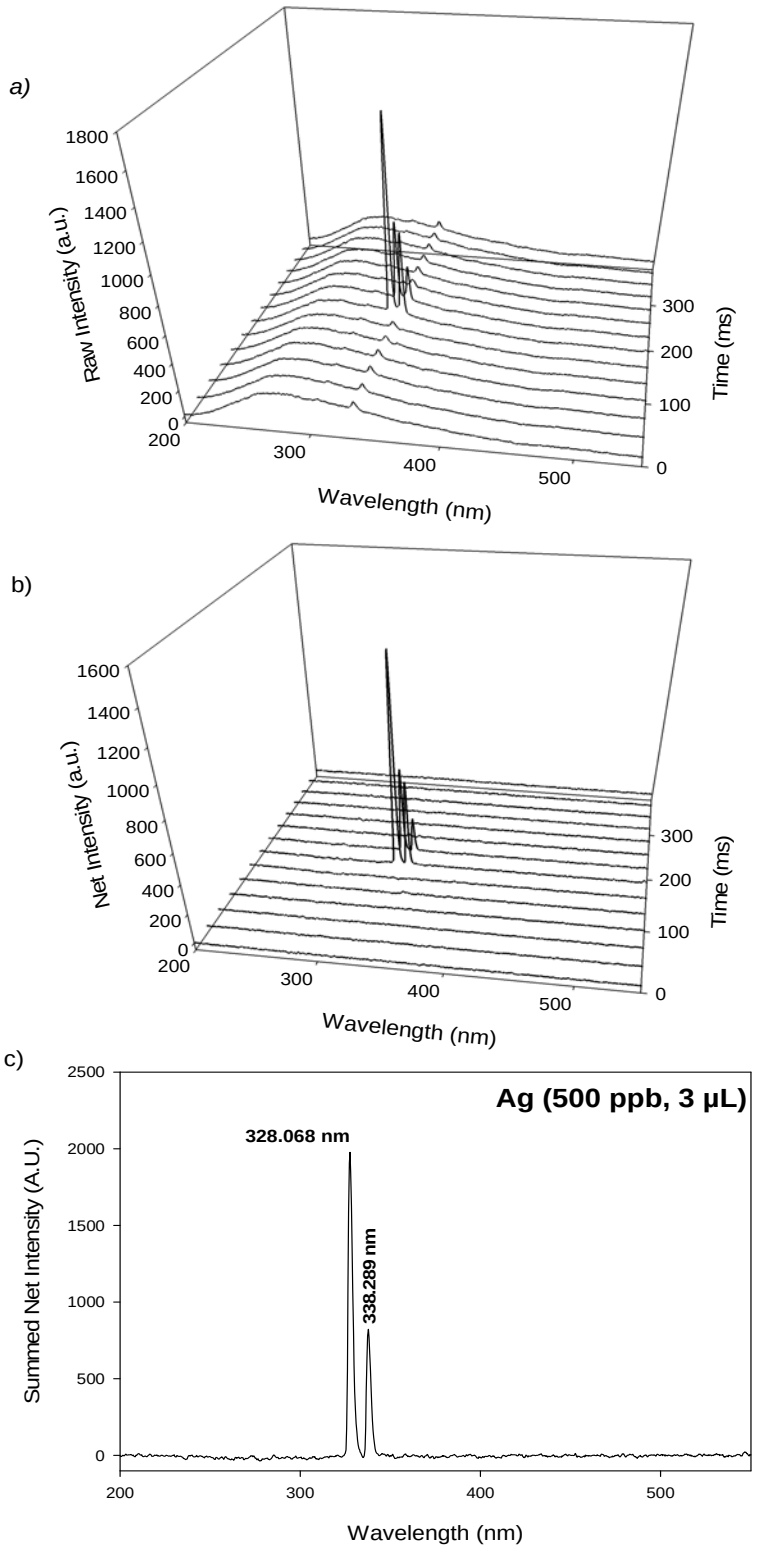

Figure 4.8: *Bluish colour MPD signal for Ag (500 ppb, 3 µL) captured with the CCD spectrometer. 3-d (intensity vs. wavelength vs. time) plots for a) raw data and b) background corrected data. And c), 2-d (intensity vs. wavelength) plot of summed net Ag signal.*

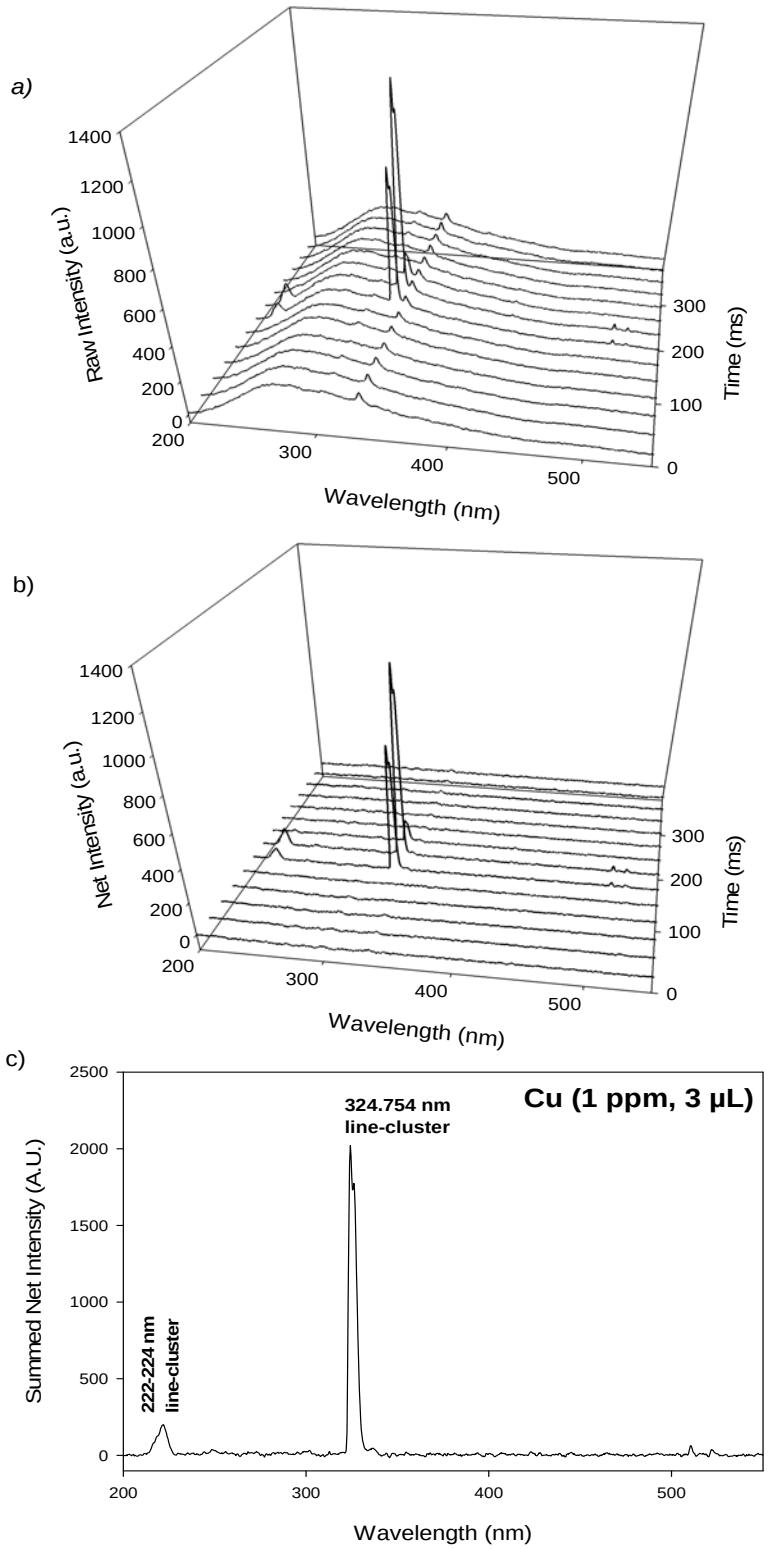

Figure 4.9: *Bluish colour MPD signal for Cu (1 ppm, 3 µL) captured with the CCD spectrometer. 3-d (intensity vs. wavelength vs. time) plots for a) raw data and b) background corrected data. And c), 2-d (intensity vs. wavelength) plot of summed net Cu signal.*

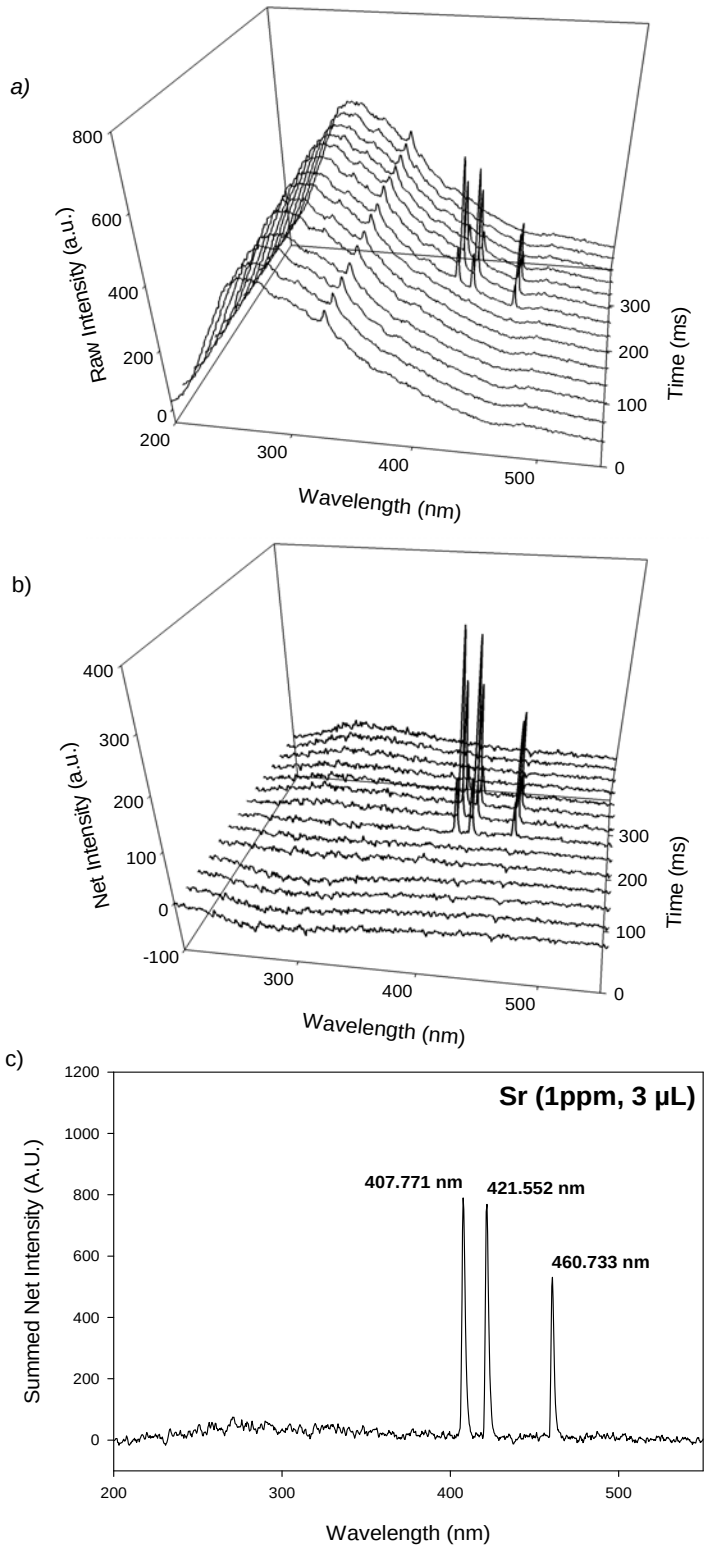

Figure 4.10: *Bluish colour MPD signal for Sr (1 ppm, 3 µL) captured with the CCD spectrometer. 3-d (intensity vs. wavelength vs. time) plots for a) raw data and b) background corrected data. And c), 2-d (intensity vs. wavelength) plot of summed net Sr signal.*

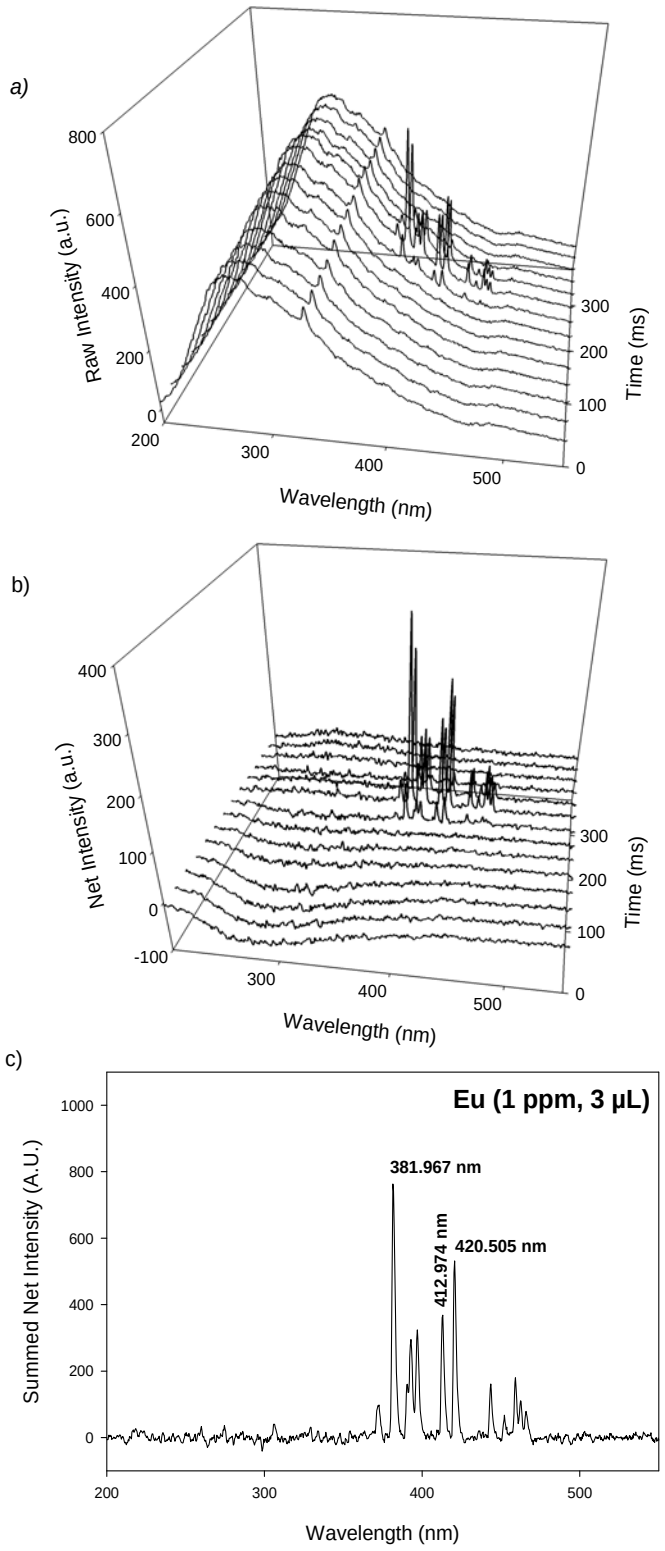

Figure 4.11: *Bluish colour MPD signal for Eu (1 ppm, 3 µL) captured with the CCD spectrometer. 3-d (intensity vs. wavelength vs. time) plots for a) raw data and b) background corrected data. And c), 2-d (intensity vs. wavelength) plot of summed net Eu signal.*

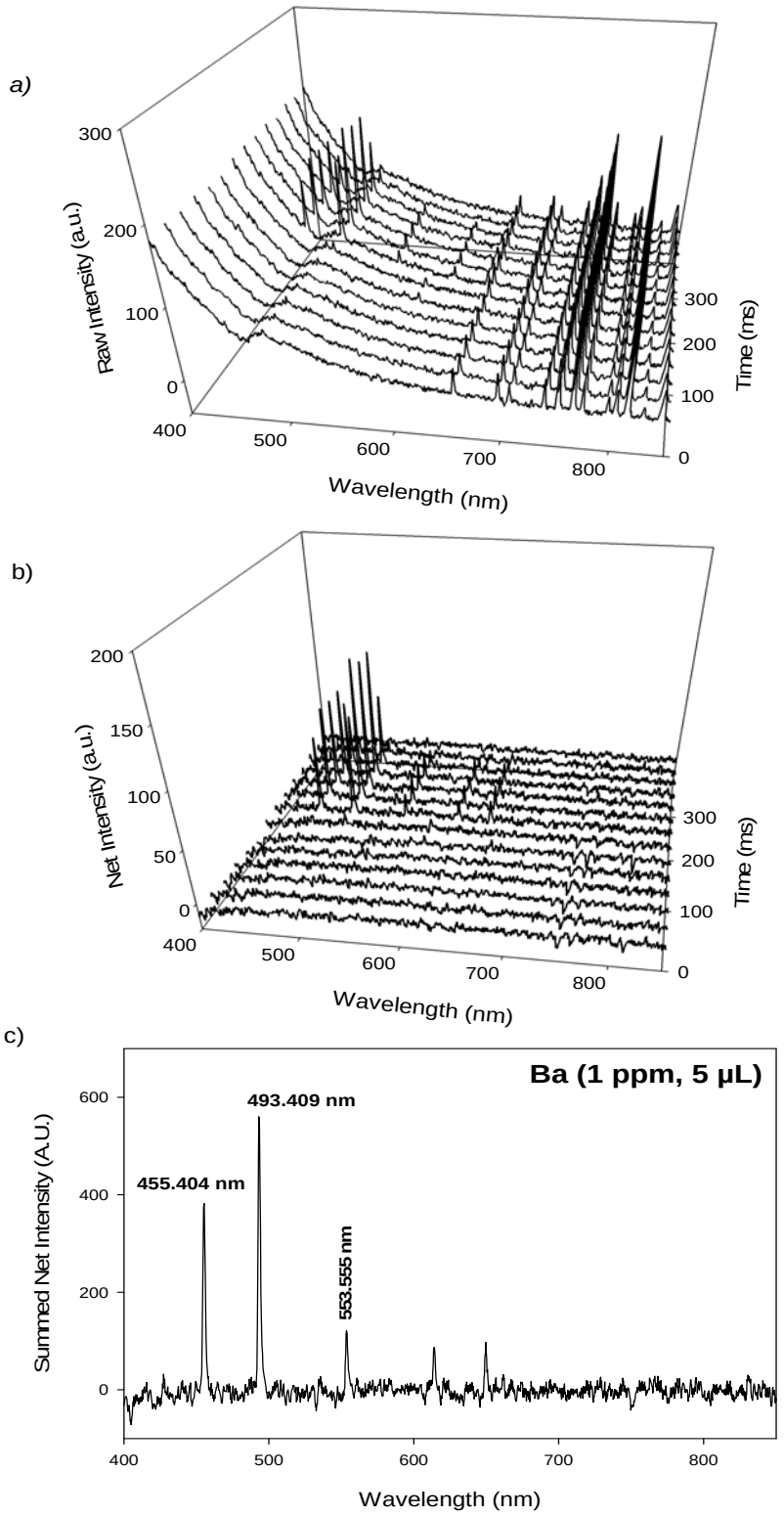

Figure 4.12: *Bluish colour MPD signal for Ba (1 ppm, 5 µL) captured with the CCD spectrometer. 3-d (intensity vs. wavelength vs. time) plots for a) raw data and b) background corrected data. And c), 2-d (intensity vs. wavelength) plot of summed net Ba signal.*

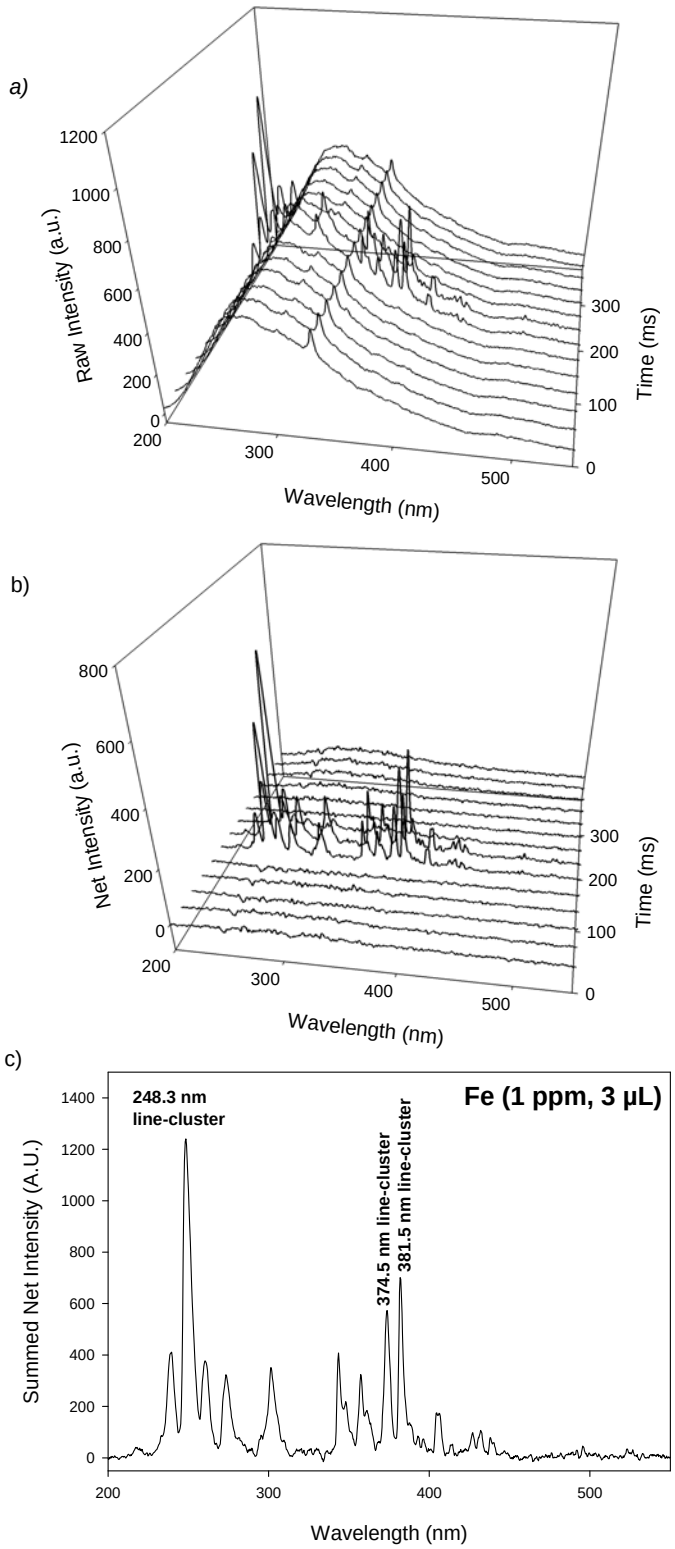

Figure 4.13: *Bluish colour MPD signal for Fe (1 ppm, 3 µL) captured with the CCD spectrometer. 3-d (intensity vs. wavelength vs. time) plots for a) raw data and b) background corrected data. And c), 2-d (intensity vs. wavelength) plot of summed net Fe signal.*

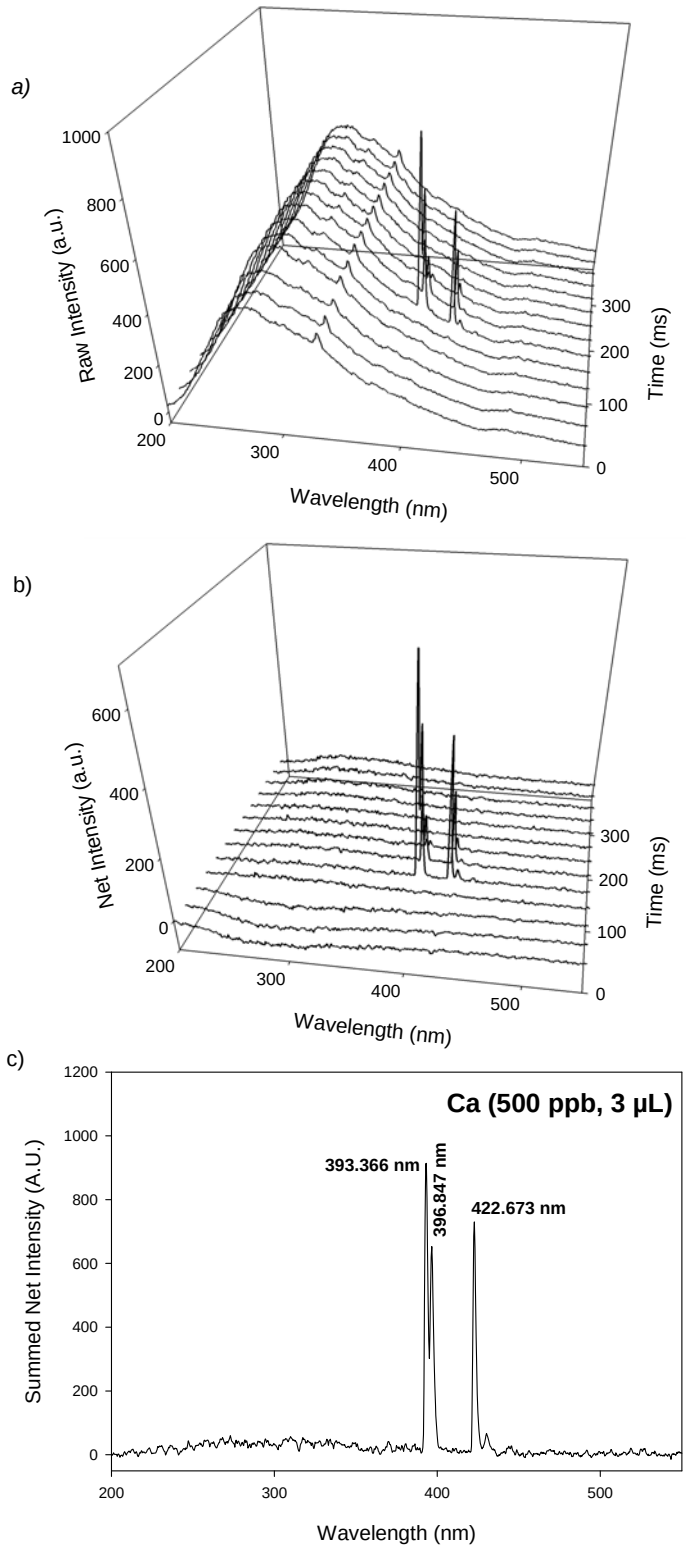

Figure 4.14: *Bluish colour MPD signal for Ca (500 ppb, 3 µL) captured with the CCD spectrometer. 3-d (intensity vs. wavelength vs. time) plots for a) raw data and b) background corrected data. And c), 2-d (intensity vs. wavelength) plot of summed net Ca signal.*

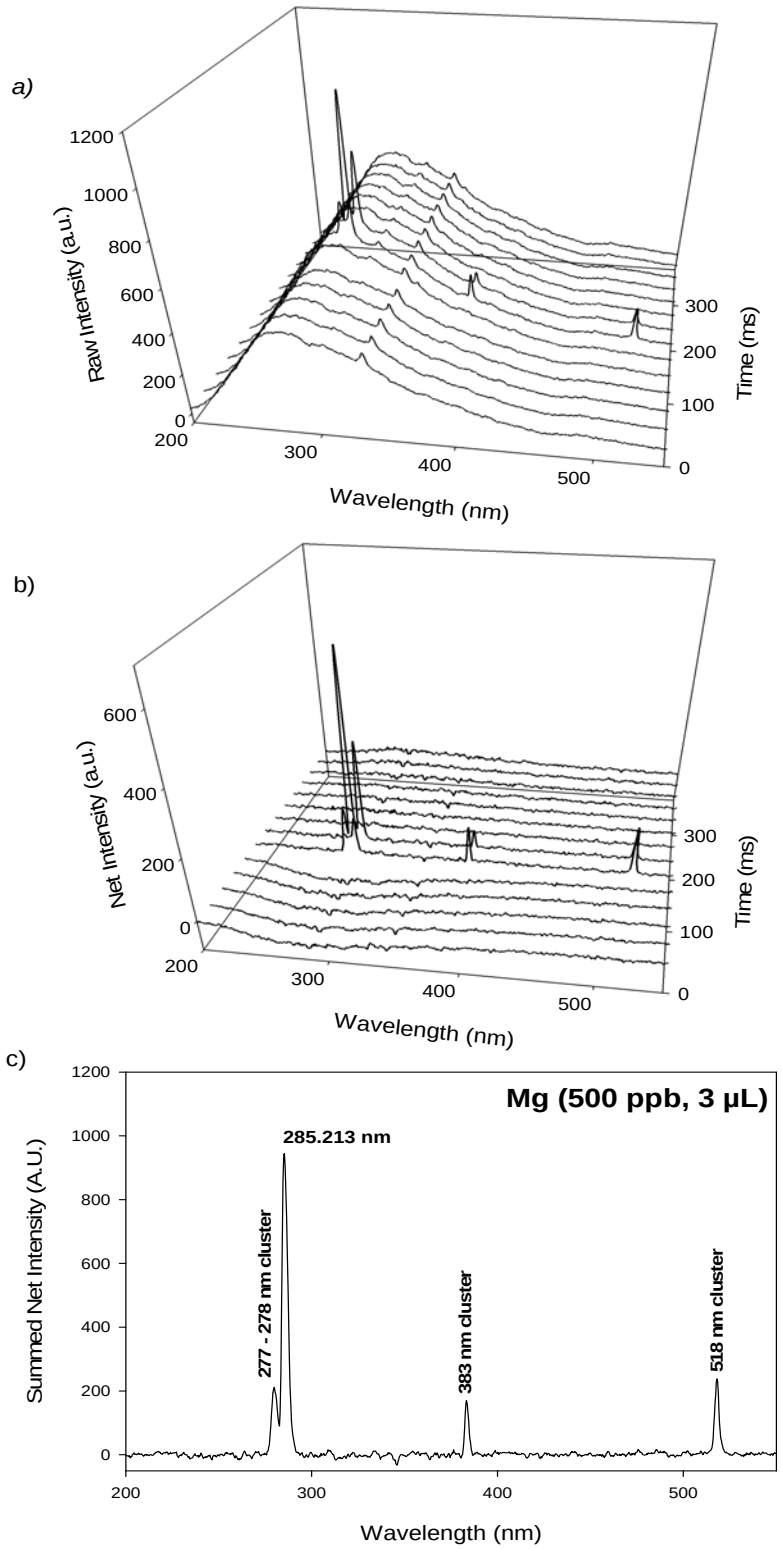

Figure 4.15: *Bluish colour MPD signal for Mg (500 ppb, 3 µL) captured with the CCD spectrometer. 3-d (intensity vs. wavelength vs. time) plots for a) raw data and b) background corrected data. And c), 2-d (intensity vs. wavelength) plot of summed net Mg signal.*

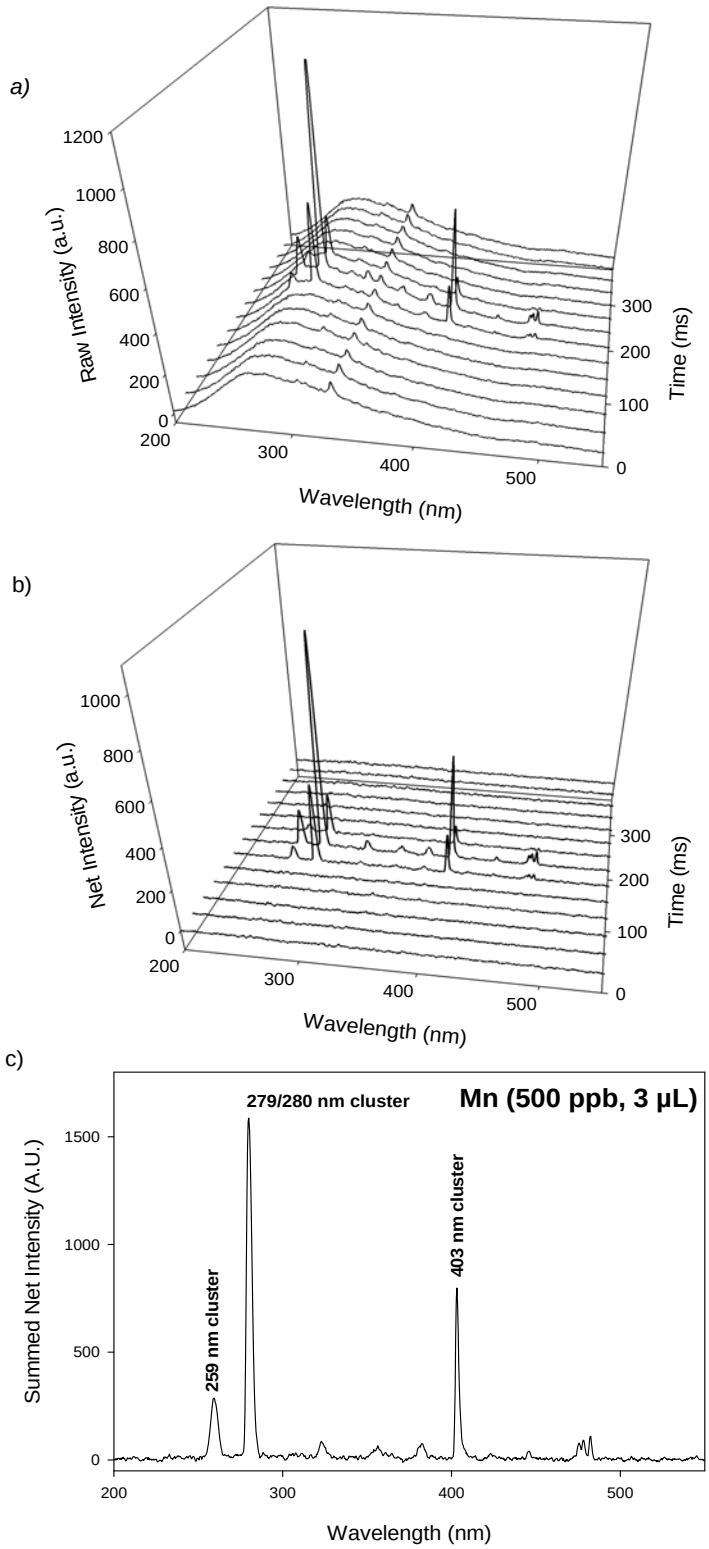

Figure 4.16: *Bluish colour MPD signal for Mn (500 ppb, 3 µL) captured with the CCD spectrometer. 3-d (intensity vs. wavelength vs. time) plots for a) raw data and b) background corrected data. And c), 2-d (intensity vs. wavelength) plot of summed net Mn signal.*

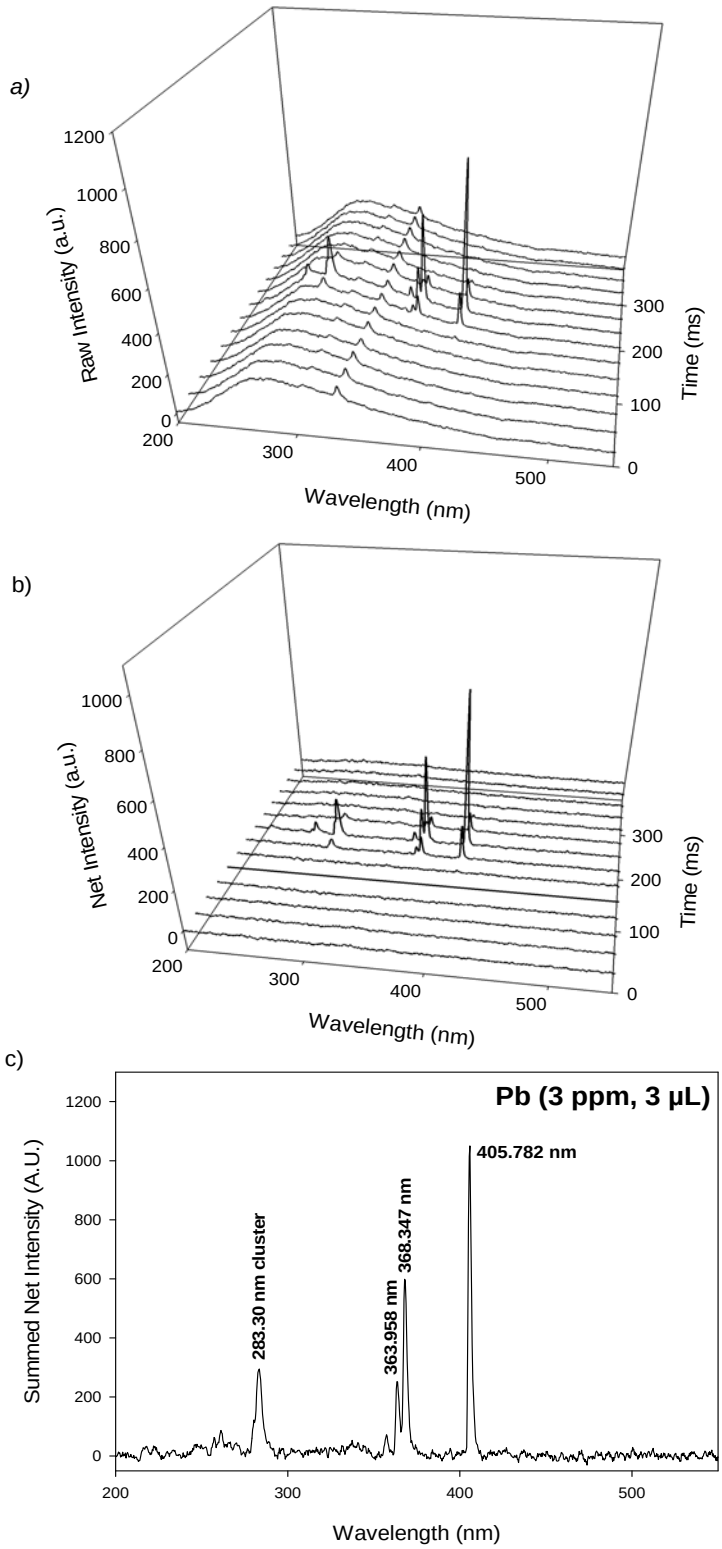

Figure 4.17: *Bluish colour MPD signal for Pb (3 ppm, 3 µL) captured with the CCD spectrometer. 3-d (intensity vs. wavelength vs. time) plots for a) raw data and b) background corrected data. And c), 2-d (intensity vs. wavelength) plot of summed net Pb signal.*

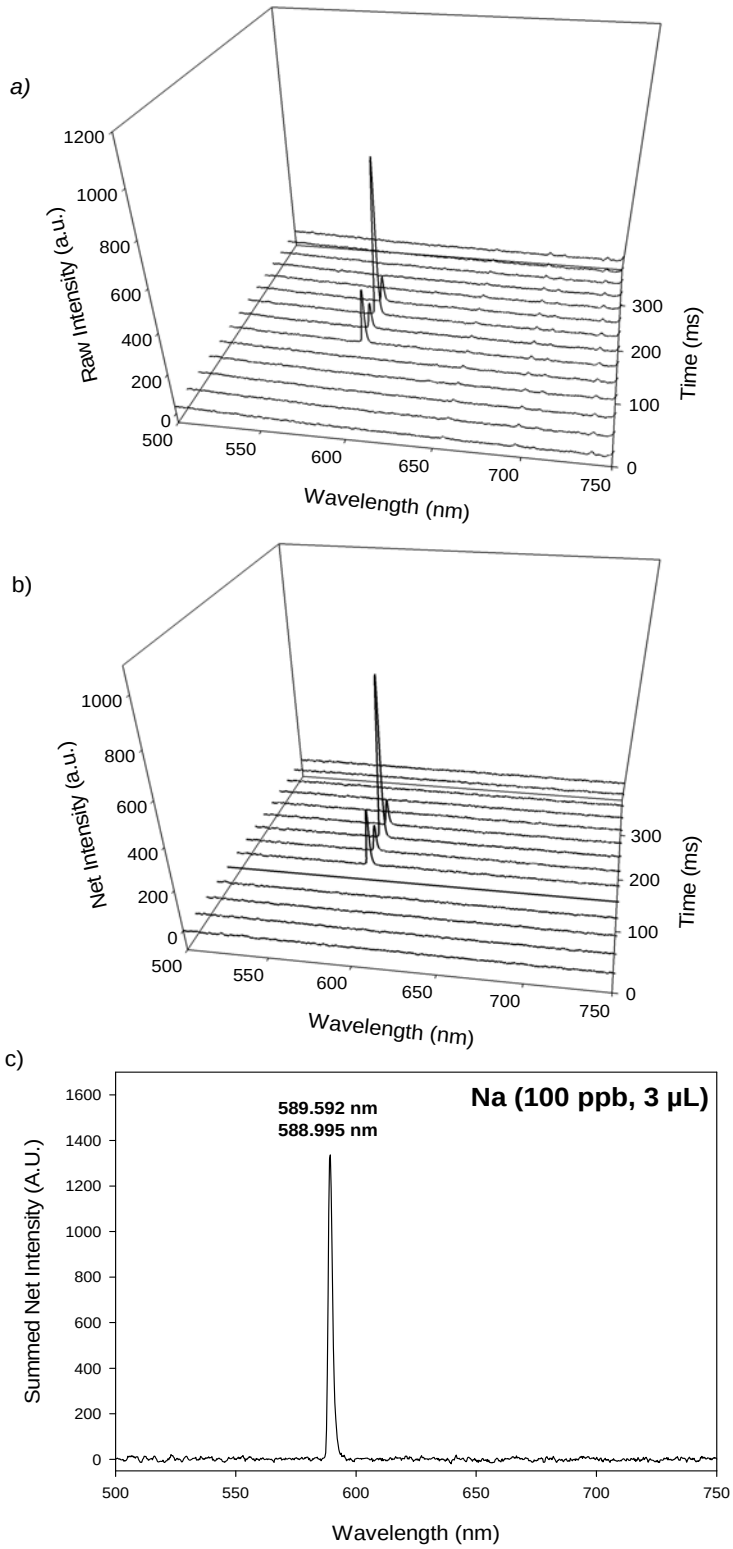

Figure 4.18: *Bluish colour MPD signal for Na (100 ppb, 3 µL) captured with the CCD spectrometer. 3-d (intensity vs. wavelength vs. time) plots for a) raw data and b) background corrected data. And c), 2-d (intensity vs. wavelength) plot of summed net Na signal.*

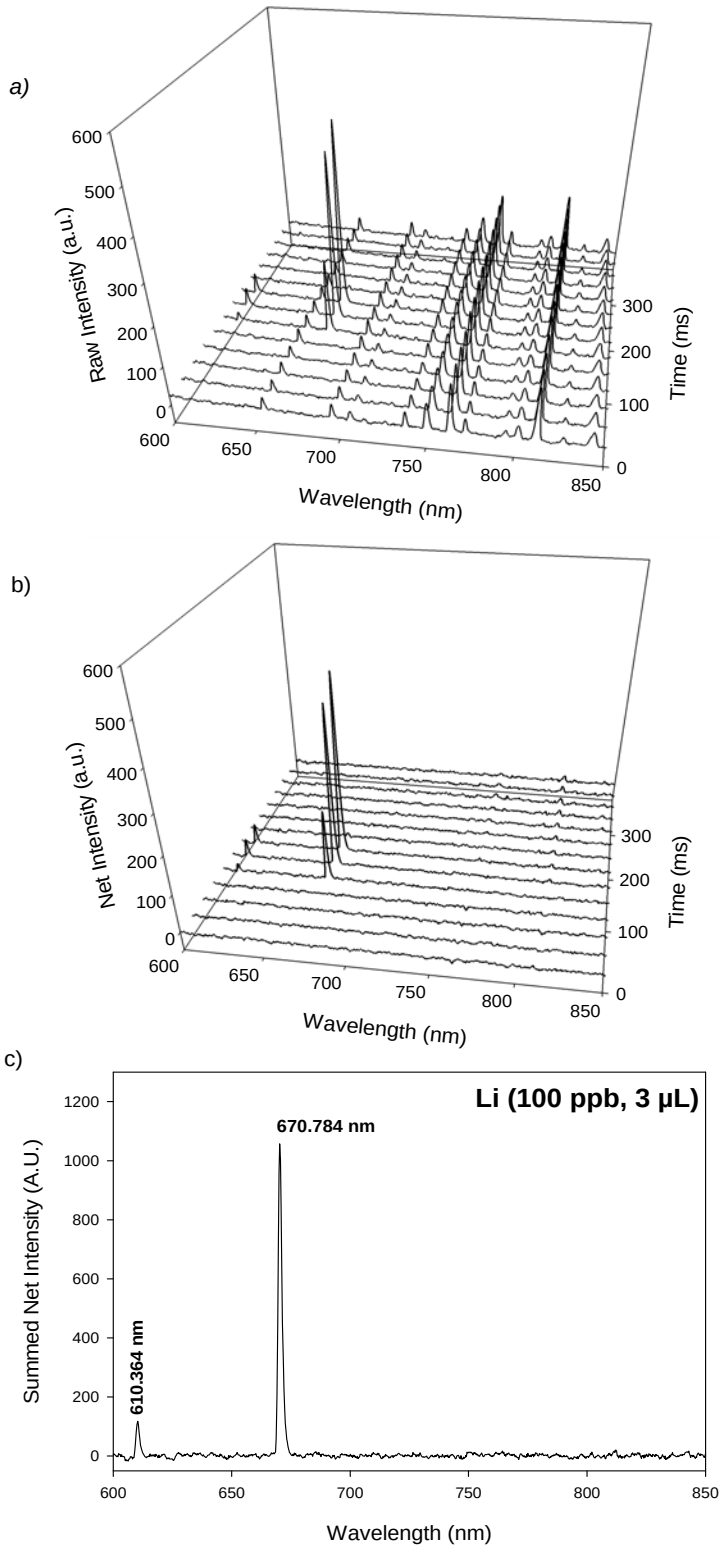

Figure 4.19: *Bluish colour MPD signal for Li (100 ppb, 3 µL) captured with the CCD spectrometer. 3-d (intensity vs. wavelength vs. time) plots for a) raw data and b) background corrected data. And c), 2-d (intensity vs. wavelength) plot of summed net Li signal.*

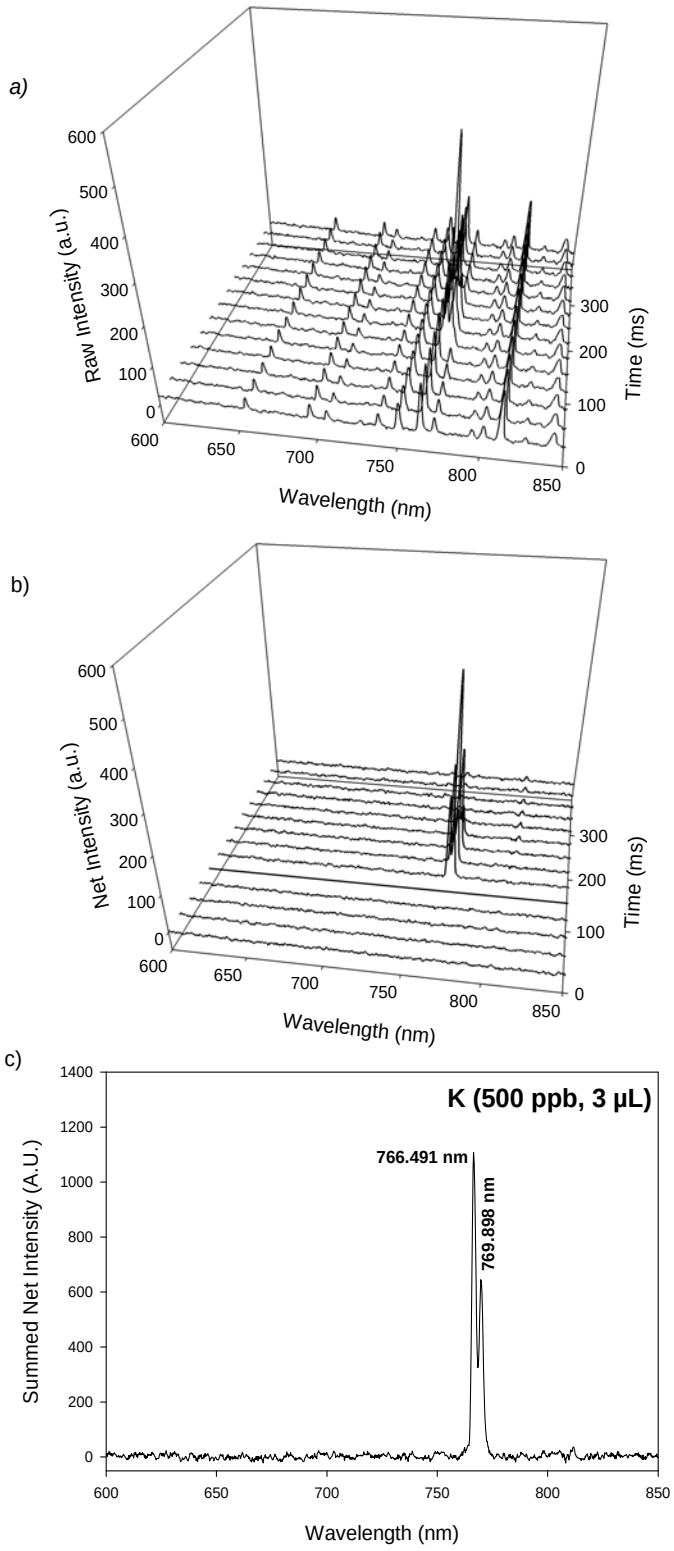

Figure 4.20: *Bluish colour MPD signal for K (500 ppb, 3 µL) captured with the CCD spectrometer. 3-d (intensity vs. wavelength vs. time) plots for a) raw data and b) background corrected data. And c), 2-d (intensity vs. wavelength) plot of summed net K signal.*

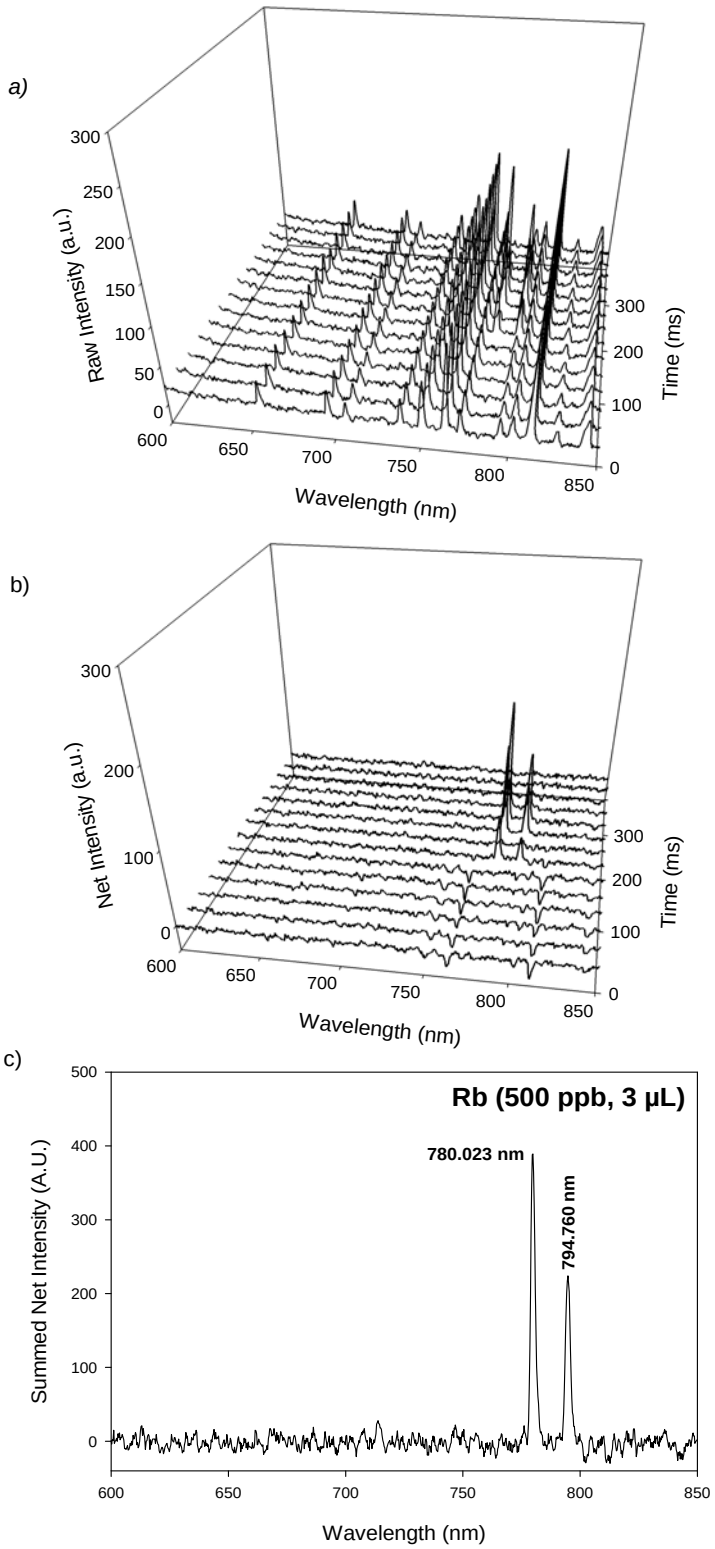

Figure 4.21: *Bluish colour MPD signal for Rb (500 ppb, 3 µL) captured with the CCD spectrometer. 3-d (intensity vs. wavelength vs. time) plots for a) raw data and b) background corrected data. And c), 2-d (intensity vs. wavelength) plot of summed net Rb signal.*

The present tubular geometry (or simply tubular) 30 mm IED MPD had estimated detection limits for 16 elements ranging from 5-310 pg (at mid-to-front observation location). How do these estimated detection limits compare with those of the most recent planar geometry (or simply planar) Ar/H_2 MPD?[7] Before a direct comparison can be made, there are a few main differences with the planar MPD and the tubular MPD that must be discussed. Firstly, the planar MPD does not have a limiting orifice. For instance, the outlet tube of the vapourization chamber of mini-ITV microsample introduction system had a 1.8 mm I.D.. This outlet was directly connected to the inlet of the planar MPD. Thus, there was no flow restriction between vapourization chamber outlet and MPD inlet. Furthermore, the outlet of the planar MPD was designed to be 7.1 mm I.D.. Thus, there was no flow restriction at the MPD outlet either.

For the tubular MPD there were some flow restrictions. For instance, the 1.8 mm (I.D.) outlet of the vapourization chamber was connected to a 0.84 mm (I.D.) of the syringe that formed the inlet to the MPD (and the grounded or front MPD electrode). Thus, a flow restriction was formed between the vapourization outlet and the inlet of the tubular MPD. The needle electrode that also served as the MPD outlet and as the HVac electrode (Fig. 2.1) had the same I.D. as the electrode that served as the inlet to the MPD. This symmetric, tubular MPD was used throughout.

For completeness and to reduce possible flow restriction effects placed by the electrode that served as the MPD outlet, the I.D. of this electrode was enlarged. This made the tubular MPD asymmetric. No statistically significant analytical results were obtained between the symmetric and the asymmetric geometries. For design simplicity, and as mentioned above, the symmetric tubular MPD was used throughout this thesis. In

this geometry, the 0.84 mm I.D. was the limiting orifice that provided a flow restriction. This limiting orifice speeds up the linear flowrate of the carrier gas from 160 to 650 cm/s. In other words, due to this restriction the linear flowrate of the carrier gas at the outlet of the vapourization chamber increased 4 times when the gas went through the front MPD electrode to become the microplasma gas.

Secondly, the total data acquisition time per spectral episode was also changed when comparing spectral data obtained between the planar geometry and the tubular geometry MPD. More specifically the time required transferring data between the CCD spectrometer and the controlling computer was 32 ms when using the planar MPD. By reducing software overhead on the computer that controlled the CCD spectrometer, this delay was reduced to 16 ms. This 16 ms reduced software delay was used for all data acquired when employing the tubular MPD. Since the same 15 ms integration time was used for both planar and tubular MPDs, the only difference was in the time delay that was required for data transfer. For example, 15 ms integration time plus 32 ms required for data transfer made the total time per spectral episode equal to 47 ms. The 47 ms per spectral episode was the total time per episode that was used for the planar MPD.[7] But when experiments began with the tubular MPD, the data transfer time delay was reduced to 16 ms. For the same 15 ms integration time, this made the total time per spectral episode equal to 31 ms. Doing a rough calculation and assuming that everything else is equal (e.g., MPD conditions, stability of the microplasma background emission, sample loss, capturing the mini-ITV transient signal at the exact same time, observation location, etc.), the CCD spectrometer will acquire ~2.5 times less signal for the tubular MPD as compared to the past planar MPD.

Table 4.3 shows the comparison of the estimated detection limits for the planar MPD versus tubular MPD. A few elements (e.g., Na, Li, K, Rb, Mg) had similar estimated detection limits, within experimental error. For both Ca and Sr, the detection limits are poorer. The larger improvements in estimated detection limits from 1.5-3.8 times were seen for Ag, Pb, Mn, Cu, Zn and Cd. The increase in power density was likely a main driving force in the improvement of analyte signal. Also, the added stability of the background emission may have contributed to a decrease in the noise.

Table 4.3: *Comparison of estimated detection limits with past planar Ar/H_2 MPD[7] and current tubular Ar/H_2 MPD.*

Element	Planar Ar/H_2 - 8 W Estimated D.L. (pg)	Ar/H_2 - 9.315 W Estimated D.L. (pg)	Ar/H_2 - 11.682 W Estimated D.L. (pg)	Planar to Tubular Improvement
Na	5	5	5	1.0
Cd	120	70	55	2.2
Li	5	15	5	1.0
Rb	100	120	85	1.2
Sr	120	600	195	0.6
Zn	250	125	95	2.6
Ca	15	235	40	0.4
Cu	130	35	60	3.7
K	40	35	35	1.1
Mg	30	90	35	0.9
Mn	50	25	35	2.0
Pb	650	170	195	3.8
Ag	30	20	30	1.5
Fe	-	275	40	-
Eu	-	1100	120	-
Ba	-	3500	310	-

When factoring in the linear flowrate and time delay differences between the planar and the tubular geometry MPDs, the estimated detection limits of the tubular for all of the elements could be further improved by about 2.5 times by either lowering the linear flowrate or speeding up the DAQ time or both.

4.32 Estimated Detection Limits with Monochromator

This next section will use the monochromator and PMT detector to obtain estimated detection limits of the same 16 elements (Table 4.3). The MPD power (Table 4.3) that worked best with the CCD spectrometer will be used. Since the PMT is a much faster detector, there will be no signal loss to data transfer. Improvements were expected due to the increased sensitivity of the PMT. Data were taken at the following settings: 100 Hz DAQ rate, 5 seconds per run (i.e., 500 data pts), PMT gain of -800 V and inverted 500-1000 nA/V gain on the amplifier with 3 Hz cut-off frequency filter. Microsamples of standard solutions were vapourized at the highest mini-ITV vapourization power (87.3 W). The entrance slit viewed ~3-5 mm from to the front electrode to the middle region of the MPD.

Comparative data between the polychromator with a CCD detector versus the monochromator with PMT detector are shown in Table 4.4. The PMT system (Fig. 2.9) had a minimum of 2.5 times improvement for all of elements tested, excluding Fe. As shown in the Stability section (Sec. 3.2), the 248.8 nm Fe line falls on the maximum of the H_2 hump (Fig. 2.6) and the instability at higher vapourization powers causes the background hump to increase with the introduction of the hot gas from the mini-ITV. Also, the voltage, current and frequency at high power bluish colour MPD would sometimes drift from one part of the day to the next. Iron is very sensitive to MPD power and this drift in MPD power may be the reason why Fe detection limits did not improve when using the PMT based system. The elements with spectral lines from 200-450 nm had the highest improvements (as high as 24 times improvement for Eu). The CCD has a UV sensitive coating to enhance it's spectral response from 200-380 nm, but the PMT

remains more responsive in this wavelength range. The estimated detection limits for the 16 elements obtained using the PMT system were 1-35 pg.

Table 4.4: *Comparison of estimated detection limits with the CCD spectrometer and the more sensitive monochromator PMT system.*

	Polychromator with CCD		Monochromator with PMT		
Element	9.32 W Estimated D.L. (pg)	11.7 W Estimated D.L. (pg)	9.32 W Estimated D.L. (pg)	11.7 W Estimated D.L. (pg)	PMT to CCD Improvement
Na	5	5	-	1	5.0
Cd	70	55	-	3	18.3
Li	15	5	-	2	2.5
Rb	120	85	-	30	2.8
Sr	600	195	-	15	13.0
Zn	125	95	-	4	23.8
Ca	235	40	-	5	8.0
Cu	35	60	3	-	11.7
K	35	35	-	6	5.8
Mg	90	35	-	2	17.5
Mn	25	35	4	-	6.3
Pb	170	195	20	-	8.5
Ag	20	30	2	-	10.0
Fe	275	40	-	35	1.1
Eu	1100	120	-	5	24.0
Ba	3500	310	-	25	12.4

4.4 Conclusions

There are multiple factors affecting analytical performance of the MPD such as observation location, the MPD power, IED, frequency, mode, etc. The optimal observation location was shown to change drastically in some cases and gradually in others, depending on the element tested (e.g., Ca, Li, Ag, Zn) and the operating conditions used. The Ca and Li gave most intense signals with a more power-dense MPD in the observation location study whereas Ag and Zn had maximum emissions when an

MPD with lower power density was used. There was usually no useful analytical information when the fibre optic cable was placed directly on the front or back electrodes due to lack of or to excess of residence time, respectively. The more "thermal" pinkish colour MPD led to the idea of using a bluish colour MPD with more power (on the edge of turnover point from bluish to pinkish mode of microplasma). The higher power bluish colour MPD, although slightly unstable due to increase in H_2 broadband emission in the 200-400 nm spectral range caused by the heat generated by mini-ITV, showed to have improved analytical performance for a variety of elements (up to 10 times as compared to medium power bluish MPD). It was concluded that more MPD power means better analytical performance for some elements like Ca, Ba, Eu, and Fe. But, the improvements in analytical performance were element dependent with some elements have better performance at lower MPD power levels. The CCD spectrometer showed estimated detection limits of 16 elements to be 5-310 pg. The more sensitive and faster response PMT showed the true potential of the MPD with estimated detection limits of the 16 elements to be 1-35 pg.

Chapter 5

Some Fundamentals of Microplasmas

5.0 Overview

Unlike the thermal ICP, the MPD is non-thermal (as operated here) and this is evident for the simple and obvious fact that the MPD requires no external cooling and the quartz tube does not melt nor does electrode material sputter. At higher MPD powers, the glue that fastens the electrodes into the quartz tubing begins to melt but this is for glues with fairly low melting points (~100 ºC). The ICP requires ~18 L/min of coolant gas and a water-cooled load coil in order to prevent melting the quartz torch and the copper induction coil. The lack of MPD thermal character (in comparison to the ICP) is clearly demonstrated in the spectra for microplasma background (Fig. 2.6) and analyte emissions (Figs. 4.6 - 4.21). For some elements the ICP would have thousands of lines from 200-850 nm but with the MPD, no more than 10 lines are populated for the elements tested thus far.[5-7]

There are a series of questions to be addressed in this chapter such as "If the MPDs are non-thermal, cold plasmas, then what is the excitation mechanism of the microplasma?"; "How hot does the microplasma get?"; "Does the temperature change with an increase in power?"; "Does the pinkish colour MPD have higher Ar excitation temperature since a pinkish colour MPD becomes physically hotter than a bluish colour MPD?"; and "What is the highest energy emission line that the MPD can excite?"

This chapter will focus on describing possible excitation mechanisms of the microplasma using ICP and other discharges[3, 37-42] as a guide and some recent plasma literature.[29, 35, 43-52] The differences in plasma modes i.e., pinkish (likely a γ mode) and bluish (likely a α mode) will be discussed. In the past, a weak Cd 214 nm signal was

observed in the spectrum from the CCD spectrometer.[7] There is a Cd (II) 214.438 line that has excitation energy of 14.7 eV. The 214 nm region will be scanned using the monochromator to determine whether it is the ion line or some other neighbouring atomic line. The excitation temperature (T_{exc}) of Ar for various IEDs, observation locations, modes of operation and power is calculated using a Boltzmann plot. These values for T_{exc} will be compared to other plasma characterization studies. Finally, atom-to-ion ratios will be compared for Ca and Sr to demonstrate the effect of power on the analyte atomic and ionic populations.

5.1 Microplasma Excitation Mechanism

Since an MPD is a non-thermal, non-equilibrium excitation source there has to be some other explanation for the microplasma excitation mechanism. Most measurements of plasma temperatures and other fundamental characteristics require the assumption that there is complete thermodynamic equilibrium (TE) within the plasma. Since the microplasma is not in a "closed" system, complete TE is impossible. Also, since various temperatures calculated for ICP using analytes and background features (e.g., Ar spectral lines) are different depending on the method used (i.e., calculated T_{exc} range from 2300 K to ~15 000 K). The large variation of T_{exc} shows an observation location dependence thus providing further evidence that TE cannot be assumed. Local thermodynamic equilibrium (LTE) is a deviation from TE that assumes a localized area of the plasma to be in thermal equilibrium. LTE assumption still is not completely valid and there are deviations from LTE but this assumption for the "plasma or plasma region is said to be close to LTE." In ICP literature, two main non-LTE excitation mechanisms include the

Penning Ionization Reaction and the Charge Transfer Reaction. Another likely excitation mechanism is electron-impact ionization.[3]

A brief overview of excitation mechanisms will be provided. It should be strongly emphasized that a brief review of the literature will be presented in the following section. And that, based on the review, a great deal of conjecture and speculation will be presented. From the review it can also be concluded that there is a relative lack (in relation to an ICP) of fundamental studies and such studies are required before any definitive conclusion on microplasma excitation mechanisms can be drawn. The following sections can be used to offer starting points.

5.1.1 Penning Ionization Reaction

The Penning Ionization reaction involves the transfer of high energy Ar metastable (Ar^m) to ionize analyte atoms (X). Until the electron number density was determined experimentally, the Penning ionization mechanism was thought to be the dominant mechanism for ICPs. More recently, a charge transfer reaction involving Ar^+ (a species known to be abundant in ICPs) is believed to be the reaction responsible for species excitation.[3]

5.1.2 Charge Transfer Reaction

The charge transfer reaction has a similar mechanism to the Penning ionization reaction but now with Ar^+ (not the metastable). As mentioned above, Ar^+ is known to exist in high concentrations.

$$Ar^+ + X \rightarrow Ar + X^+ \qquad \text{(Eq. 5.0)}$$

$$Ar^+ + X \rightarrow Ar + X^{+*} \qquad \text{(Eq. 5.1)}$$

The reverse reaction is not shown due to the high concentration of Ar^+. This mechanism is limited to the total available energy from Ar^+ (15.76 eV) and analyte emissions cannot occur above this energy (excitation + ionization energy). Thus far, no emissions have been observed with the MPDs that exceed the energy of Ar^+.[3]

5.1.3 Electron-Impact Ionization

Another process thought to be responsible for the excitation of Ar and analyte atoms is electron-impact ionization. This model suggests energy transfer due to collisions of electrons with other species in the plasma. In fact, this is how the ICP is initiated, with a seed of electrons.[3] When characterizing a He (or Ar) plasma probe for ambient mass spectrometry, Hieftje et al. determined that the dominant excitation mechanism for N_2 and N_2^+ species (because the air contains ~80% N_2) was not through electron-impact. They suggest that excited N_2 molecules come from recombination of N_2^+ with an electron.[28]

Some key mechanisms that may be responsible for species excitation in microplasmas have been outlined above. Admittedly, these possible mechanisms were gathered using the literature on ICPs [3, 37-42] and other types of plasmas [29, 35, 43-52] as a guide. But the question still remains: "what is the dominant excitation mechanism for the microplasmas used in this thesis?" To the author's knowledge, there is a relative lack of fundamental data and of excitation mechanisms as applied to microplasmas.[44, 47-49, 51] Furthermore, the few examples of fundamentals and excitation mechanisms for microplasmas were done for microplasmas different than the MPDs used in this thesis. This makes fundamental studies an interesting and potentially useful future research area. Some fundamental data on microplasmas are provided below.

5.1.4 Microplasma Modes

The excitation mechanism of the microplasma is influenced by its operating modes. For the MPD work, the modes were referred to as pinkish and bluish due to the colour of their MPD background emission observed visually. In the literature, there are two distinct modes observed as well but they are referred to as α and γ modes.[29-32] The α mode is sustained by bulk ionization and can only be maintained over a limited power range. There is a sharp transition from α to γ mode where the electron density reaches a critical concentration and plasma sheath breaks down.[31]

In the literature, both modes showed a dependence on gap distance, a conceptual equivalent to inter-electrode distance with the MPDs.[29-32] For the current experimental setup, the bluish MPD mode was not observed at shorter IEDs (i.e., 10 mm IED). Plasma power and frequency also influenced the mode of microplasma.[29-32] Also, the two modes are described to be different in size. It has been reported that the α mode produced a more diffuse microplasma and the γ mode produced a microplasma that was half the size of the α mode.[31] This was also visually observed with MPDs. The bluish mode produced a "diffuse" microplasma while the pinkish mode produced a thinner and "string-like" discharge.

5.2 Prominent Emission Lines of Analytes

The charge transfer reaction states that total energy for a transition has to be less than Ar^+ (15.76 eV).[39-42] Not surprisingly, analyte signals seen thus far with the MPD have all been less than 15.76 eV. Table 5.0 lists the 16 elements studied in the past chapter and their atomic or ionic emission wavelengths, and excitation and ionization energies. The total energy requirements of the 16 analytes range from 1.6-14.7 eV.[33,34]

The elements that were shown to be very sensitive to power, namely, Ca, Sr, Ba, and Eu all have either high energy ionic transitions as prominent lines. Iron is another element that is very sensitive to power. Iron has thousands of lines by ICP from 200-850 nm[33] and Fe also has the most complex MPD spectrum (of all elements tested by the MPD thus far to this date). In fact, the spectrum for Fe has many overlapping emission lines that can compete for available energy.

Table 5.0: *Physical properties of prominent emission lines populated with MPD.*[33, 34]
***Excitation potential + ionization potential for ion lines*

Element	Atom (I), Ion (II)	Wavelength (nm)	Excitation potential (eV)	Ionization potential (eV)
Rb	I	780.023	1.6	4.18
	I	794.760	1.6	
K	I	766.490	1.6	4.34
	I	769.896	1.6	
Cd	II	214.438	**14.7	8.99
	I	228.802	5.4	
	I	479.991	-	
	I	508.582	-	
Na	I	589.592	2.1	5.14
	I	589.995	2.1	
Zn	I	213.856	5.8	9.39
	I	472.216	6.6	
	I	481.053	6.6	
Mg	I	278.297	4.5	7.65
	I	280.976	4.4	
	I	383 cluster	5.9	
	I	518 cluster	5.1	
Li	I	610.364	3.9	5.39
	I	670.784	1.8	
Sr	II	407.771	**8.7	5.69
	II	421.552	**8.6	
	I	460.733	2.7	
Ca	II	393.529	**9.2	6.11
	II	397.371	**9.2	
	I	422.673	2.9	
Eu	I	381.967	-	5.67
	II	412.973	**8.6	
	II	420.504	**8.6	
Pb	II	220.351	**14.7	7.42
	I	283.306	4.4	
	I	363.958	4.4	
	I	368.347	4.3	
	I	405.783	4.4	
Ba	II	455.404	7.9	5.21
	II	493.409	7.7	
	I	553.555	2.2	
Mn	II	259 cluster	**12.2	7.43
	I	279/280 cluster	4.4	
	I	403 cluster	3.1	
Ag	I	328.068	3.8	7.58
	I	338.289	3.6	
Cu	I	324.754	3.8	7.73
Fe	I	248.327	4.9	7.87
	I	374.556	3.4	
	I	381.584	3.2	

The Cd (II) 214.438 nm has an excitation plus ionization potential of 14.7 eV (Table 5.0). A spectral line for Cd around 214 nm was observed here and in previous work done with Ar/H_2 planar MPD.[7] However, due to the poor resolution of the CCD spectrometer it was not possible to confirm if this spectral line was indeed the Cd (II) 214.438 nm (with a total energy requirement of 14.7 eV) or some other spectral line having a total energy requirement of less than 14.7 eV. The wavelength of this emission line will be confirmed by using a spectrometer with higher resolution than the CCD system, namely by using the scanning monochromator with the PMT detector (Fig. 2.9).[7]

Figure 5.0 shows a scan of the 214 nm region using the monochromator PMT system. For the data shown in Fig. 5.0a), a 200 μm entrance slit was used. This entrance slit width was used for all of the PMT data included in this thesis. The monochromator scans are from 214.1 to 214.9 nm at 0.1 nm increments, and at each location Cd (3 pg) is introduced into the MPD at a fixed vapourization power of 87.3 W. At this entrance slit width, it appears that two peaks may contribute to the shape of the curve (Fig. 5.0a). For the data shown in part b) of this figure, the entrance slit width was reduced to 100 μm and 214.4 to 214.7 nm was scanned at 0.02 nm increments with the Cd introduced at the same vapourization conditions. These data clearly show that only one peak contributes to the emission seen in this region. Surprisingly, they also demonstrate that the spectrometer needs to be calibrated (off by ~0.05 to 0.1 nm). For example, the location where the maximum net Cd signal was observed read ~214.53 nm on the monochromator dial instead of 214.438 nm. When referring to the NIST spectral online database,[33] there are no other Cd emission lines listed that appear in this region, reconfirming that the MPD

can excite up to 14.7 eV emission lines. The relatively low intensity of this Cd (II) 214.438 nm line (as compared to an ICP) is noteworthy.

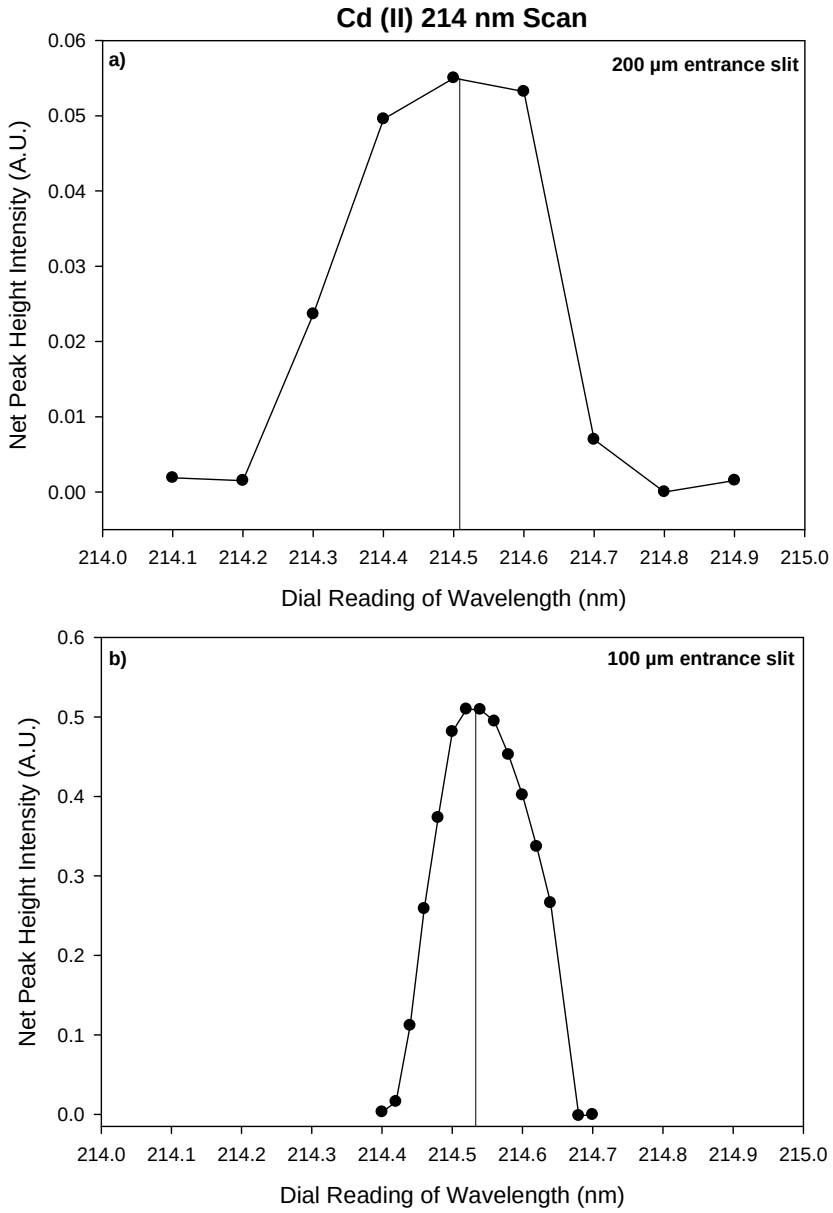

Figure 5.0: *Cd (II) study scanning 214 nm region using the monochromator with a) 200 µm entrance slit and b) 100 µm entrance slit. Cd (1 ppm, 3 µL) was introduced via mini-ITV at fixed vapourization power (87.3 W) for each wavelength tested.*

Since the beginning of the MPD work, the Pb (II) 220.351 nm line has not been observed by the CCD spectrometer. The last chapter clearly showed that the

monochromator PMT system is more sensitive in the UV region (200-380 nm). If the 220.351 nm line is populated and is not observed with the CCD spectrometer simply due to the low sensitivity of the CCD detector in this region, then the PMT-based system will detect emission from this line. In Fig. 5.1a), a mini-ITV coil blank at 87.3 W is shown. The mini-ITV has minimal to no effect at this particular region of the microplasma spectrum. Fig. 5.1b) and 5.1 c) show the raw Pb (II) 220.351 nm signal and the net signal, respectively. Once again, the MPD is confirmed to excite emission lines as high as 14.7 eV.

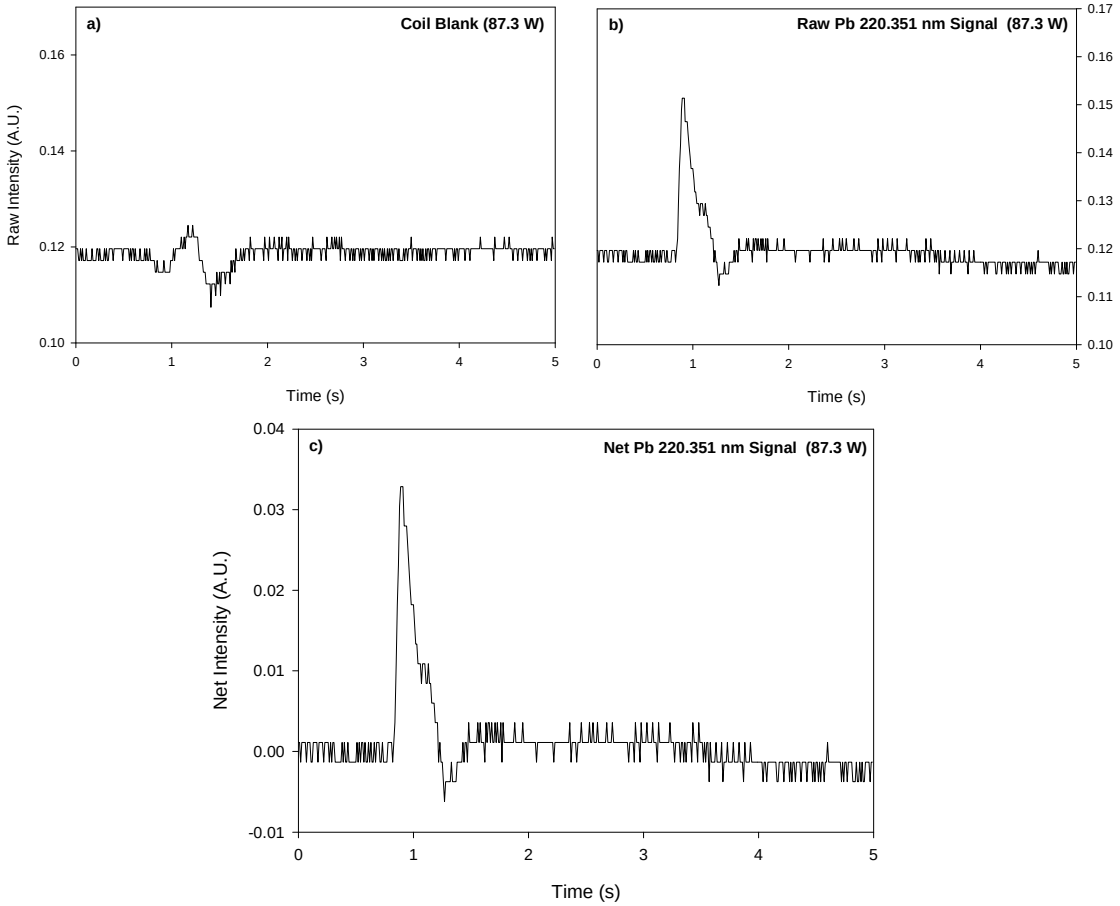

Figure 5.1: *Pb (II) 220.351 nm line with monochromator PMT system: a) coil blank, b) raw Pb signal and c) net Pb signal at high mini-ITV vapourization power (87.3 W).*

5.3 Excitation Temperature (T_{exc}) of the Microplasma Device (MPD)

The temperature of plasma is the average energies of components that make up the plasma (ions, electrons, radicals, and neutral atoms and molecules) and their degrees of freedom in terms of translational, vibrational, rotational, and electronic excitation energies. From this, it seems quite evident why plasma can exhibit multiple temperatures. The excitation temperature is one of them and it can be determined by using Ar or analyte emission lines and a Boltzmann plot. For a system in LTE, the population density of atomic and ionic species at a given temperature (T) is given in Equation 5.2:

$$n(p) = n \cdot \frac{g_p}{Z(T)} \cdot \exp\frac{(-E_p)}{kT} \qquad \text{(Equation 5.2)}$$

Where, n is concentration of neutral atom or ions
g_p is statistical weight for the particular transition
Z(T) is partition function of an atom or ion
E_p is excitation energy level p
k is Boltzmann constant
T is the excitation temperature.

The observed emission intensity I_{pq} (with an optically thin radiation source) is:

$$I_{pq} = \frac{(l/4\pi) \cdot n(p) \cdot A_{pq} \cdot hc}{\lambda_{pq}} \qquad \text{(Equation 5.3)}$$

Where: l = cell path length
A_{pq} = transition probability for spontaneous emission of a photon
h = Planck's constant
c = speed of light
λ_{pq} = wavelength of the emission line.

When Equations 5.2 and 5.3 are combined, Equation 5.4 is obtained:

$$I_{pq} = \left(\frac{1}{4\pi}\right) \cdot n \cdot \left[\frac{g_p}{Z(T)}\right] \cdot A_{pq} \cdot \left(\frac{hc}{\lambda_{pq}}\right) \exp\left(\frac{-E_p}{kT}\right) \qquad \text{(Equation 5.4)}$$

Expressed in logarithmic form, Equation 5.4 becomes Equation 5.5:

$$\ln\left(\frac{I_{pq}\lambda_{pq}}{g_p A_{pq}}\right) = \frac{-E_p}{kT} + \ln\left[\frac{nlhc}{4\pi Z(T)}\right] \qquad \text{(Equation 5.5)}$$

A plot of $\ln\left(\frac{I_{pq}\lambda_{pq}}{g_p A_{pq}}\right)$ versus E_p will be linear, with a slope of -1/kT.[3]

To get an indication of the T_{exc} of the MPD, Ar will be used as a thermometric species. There are 3 Ar lines used in applying Equation 5.5 and the wavelength, degeneracy, transition probability and upper energy level are listed in Table 5.1.

Table 5.1: *Ar lines used with wavelength, degeneracy, transition probability and upper energy level.*[36]

. Wavelength (nm)	g	A (s^{-1})	E_{upper} (cm^{-1})
763.51	5	24500000	106237.55
794.82	3	18600000	107131.71
826.44	3	15300000	107496.4

Using the information from Table 5.1 combined with microplasma background emission data (e.g., pinkish MPD background from 600-850 nm, Fig 5.2a) a Boltzmann plot is obtained as shown in Fig. 5.2b. The slope of the best-fit line is then used to determine T_{exc}. The calculated T_{exc} for the various IEDs and modes from the Observation Location Study are shown in Table 5.2. The T_{exc} ranges from 1574-2412 K, with the pinkish colour 50 mm IED MPD having the highest T_{exc}.

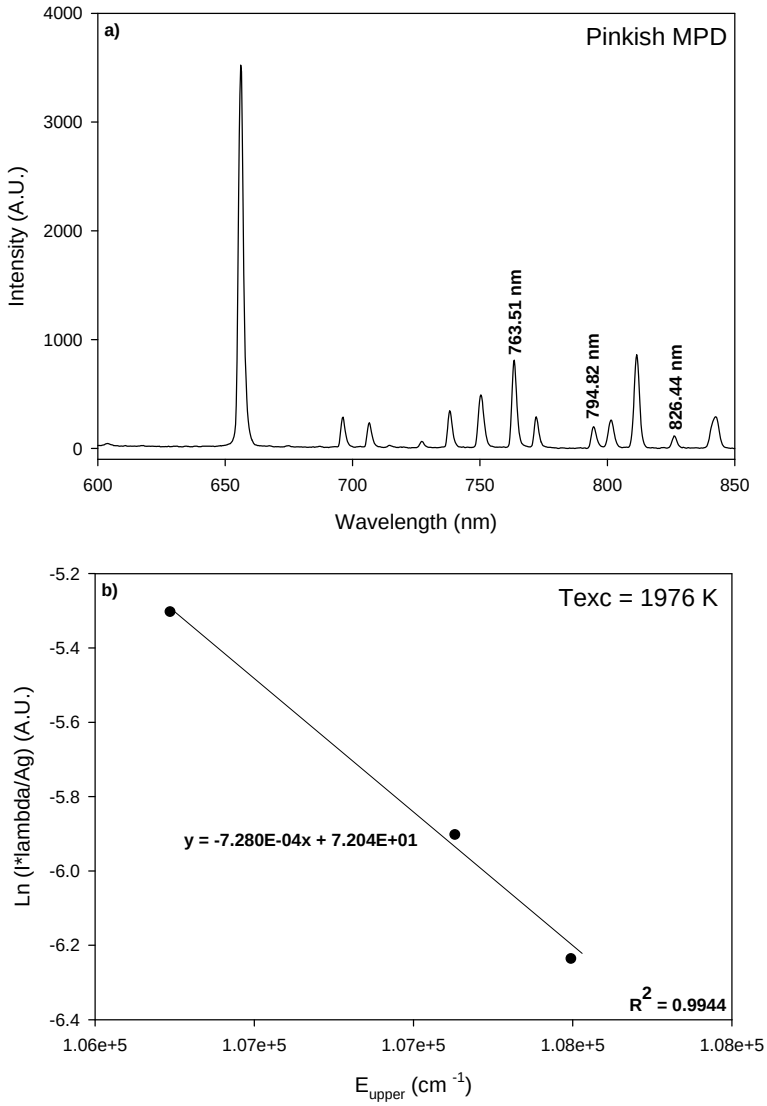

Figure 5.2: *Pinkish colour MPD background from 600-850 nm and the resulting Boltzmann plot using Ar as a thermometric species.*

Table 5.2: *Calculated excited temperatures using a Boltzmann plot for the various IEDs and modes tested in observation location study at mid-to-front (MTF) and middle observation locations.**due to distorted waveform*

IED	MPD Conditions					T_{exc} (K)	
(mm)	Voltage (V)	Current (A)	Frequency (kHz)	Power Density (W/mm3)	Mode	MTF	Middle
10	8.4	0.63	****670.0**	0.6738	Pinkish	1871	1894
30	8.1	1.10	64.1	0.3782	Bluish	1589	1614
30	8.4	1.35	****280.0**	0.4813	Pinkish	2005	2075
50	8.3	1.83	61.4	0.3868	Bluish	1574	1665
50	11.0	1.93	****300.0**	0.5406	Pinkish	2412	1992

The T_{exc} was also determined for the various powers tested in the 30 mm IED MPD power study (Table 5.3). The T_{exc} ranges from 1590-1976 K, with the pinkish colour MPD once again having the highest T_{exc}. The T_{exc} results for the bluish colour MPD are interesting since the highest MPD power density does not have the highest T_{exc} at either mid-to-front or middle observation locations.

Table 5.3: *Calculated excitation temperatures using a Boltzmann plot for the various powers tested in the 30 mm IED MPD power study at mid-to-front (MTF) and middle observation locations.***due to distorted waveform

MPD Conditions					T_{exc} (K)	
Voltage (V)	Current (A)	Frequency (kHz)	Power Density (W/mm^3)	Mode	Mid-to-Front	Middle
8.1	0.95	64	0.3261	Bluish	1655	1881
8.1	1.15	64	0.3947	Bluish	1643	1648
8.2	1.33	64	0.4621	Bluish	1674	1634
9.5	1.26	56.6	0.5072	Bluish	1590	1780
8.4	1.28	**298	0.4556	Pinkish	1915	1976

But how do these calculated T_{exc} compare to that of an ICP and other microplasmas? The range of excitation temperatures listed in Table 5.4 below is comparable to the range more recently reported for ICPs[53-57] and other plasma discharges.[27, 58-61]

Table 5.4: Excitation temperatures for an ICP using Ar lines and a Boltzmann plot.[3]

T_{exc} (K)	Method	Frequency (MHz)	Power (kW)	Observation Height (mm)
5000 - 7000	Ar Slope	5.4	6	0 - 12
4380	Ar Slope	50	0.27	0.5
7000	Ar Slope	27	1.5	15
7000	Ar Slope	27	1.5	15

The T_{exc} for an ICP is quite hot in comparison to the T_{exc} for an MPD which ranges from 1600-2400 K. As observed for ICPs and other plasma discharges, the T_{exc} of

various microplasmas also have a wide range of T_{exc}. For example, Hou[20] calculated T_{exc} of tubular MPD (<10 mm IED) to be 3000 K, using the two-line method. Hopwood and Iza,[35] determined T_{exc} for an Ar microwave–frequency microplasma that was 3500 K. Oliveria et al.[36] determined T_{exc} for a 50 W Ar/H_2 microplasma jet was 8000 K.

Although the T_{exc} for the MPD showed very little difference in the power and observation location study, determining T_{exc} using Ar as the thermometric species does not necessarily give an accurate picture of analyte excitation temperature. In the future, determination of T_{exc} using an analyte will give a better indication of the microplasma excitation energy. Due to the few spectral lines observed using the MPD for the elements tested and also due to the poorer resolution of the CCD spectrometer, no excitation temperatures were determined using analyte as the thermometric species.

5.4 Atom-to-Ion Ratio Using Ca and Sr

The difference in analyte emission intensities for the variety of MPD powers and power densities, HVac frequencies, IEDs and modes tested was an indication that energetics of the microplasma are not the same for all operating conditions. The atom-to-ion ratio (atom/ion) of Ca and Sr were noted to change depending on operating conditions and observation location. Figure 5.3 shows how the atomic emission line for Ca (422.67 nm) is more prominent at lower power density (Fig. 5.3a) and how the ionic emission line surpasses the atom line at higher power density.

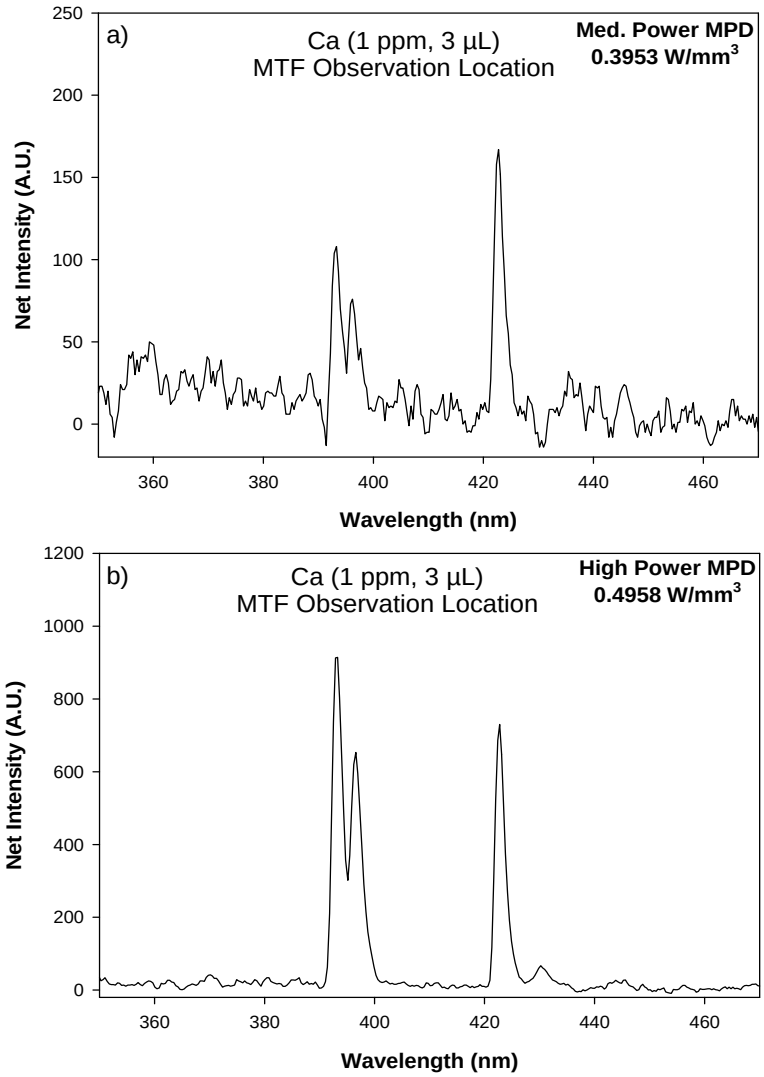

Figure 5.3: Main *atomic emission lines for Ca (1 ppm, 3 µL) for 30mm IED MPD at a) low power density (0.3953 W/mm^3) and b) high power density (0.4958 W/mm^3) for the mid-to-front observation location [393.37 nm (II), 396.85 nm (II) and 422.67nm (I)]. In a), low power MPD, the 422.67 nm line is prominent, that is, the atomic line. In contrast, as the power density increased the 393.37 nm ion line became the prominent emission line as shown in b).*

A similar change in atom/ion was observed with Sr signal from the planar geometry Ar/H_2 MPD and the current tubular geometry Ar/H_2 MPD (Fig. 5.4). The planar MPD has a lower power density and at the middle observation location the atom line (460.773 nm) is the more prominent line (Fig. 5.4a). As the power density was increased, the ion line (407.771 nm) became the most prominent line. Although the T_{exc}

data did not suggest any differences in energetics for the various power densities (for Ar lines), this change in atom/ion confirms that the energetics of the microplasma (for analyte) changes with increasing power density. The energetics of the microplasma are not just power density dependent but rather a contribution of the inter-dependent operating variables including HVac frequency, IED and observation location, to name a few.

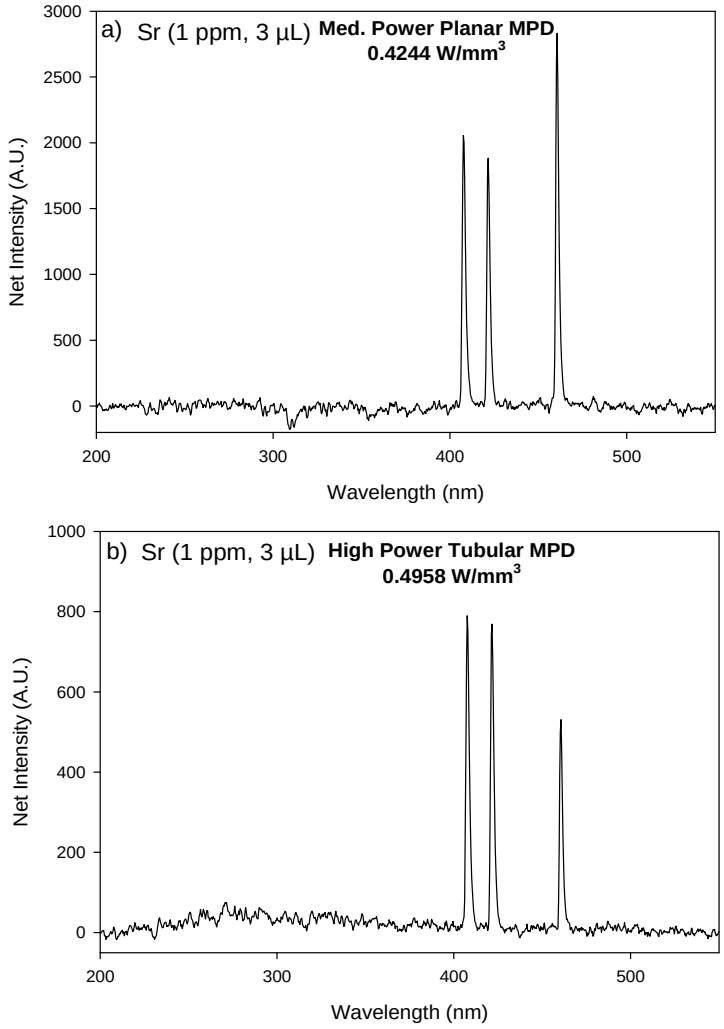

Figure 5.4: Main *atomic emission lines for Sr with a) medium power density (0.4244 W/mm^3) 12 mm IED bluish planar MPD and b) higher power density (0.4958 W/mm^3) 30 mm IED bluish tubular MPD. In a), medium power planar MPD, the 460.733 nm line is prominent, that is, the atomic line. In contrast, as the power density increased the 407.771 nm ion line became the prominent emission line as shown in b).*[7]

5.5 Conclusions

Non-thermal microplasma excitation mechanisms were reviewed and it was postulated the Penning ionization reaction, charge transfer reaction and electron-impact ionization mechanisms may be operative. Further fundamental studies are needed in order to draw any concrete conclusions on the actual excitation mechanism of the microplasma. The charge transfer reaction states that the total energy (excitation + ionization energy) of possible analyte emissions must be less than excitation energy of Ar (15.76 eV). To this date, it has been shown that the MPD has the ability to excite analytes with potentials from 1.6-14.7 eV for the 16 elements tested, which are less than 15.76 eV. The 14.7 eV ion line for Cd (214.438 nm) and Pb (220.351 nm) are the highest energy lines excited by the MPD. The bluish and pinkish modes observed for the MPD are similar to two modes described in the literature as α and γ modes.[29-32] In this thesis, the α mode MPD was more diffuse (as observed with the bluish colour MPD) and the γ mode MPD was smaller in diameter and more "string-like" (as observed with the pinkish colour MPD).

The excitation temperature (T_{exc}) of the MPD was determined using Ar as a thermometric species and was found to be 1600-2400 K depending on the microplasma power, the HVac frequency, the inter-electrode distance (IED) and operating mode. The change in atom/ion for Ca and Sr with increasing MPD power density demonstrates that the energetics of the microplasma change depending on the operating conditions.

In summary, in the future more fundamental studies (of the type described above and others) are needed to fully characterize microplasmas and to aid in understanding of their excitation mechanisms and their other fundamental characteristics.

Chapter 6

Conclusions and Future Work

6.0 Conclusions

Stability of the MPD improved drastically when planar geometry MPDs[5,7] were replaced by wall-stabilized tubular geometry MPDS (as described in this thesis). In fact, the He/H_2 planar MPD required that 100% of the analyte episodic spectra to be normalized.[5] The next generation Ar/H_2 planar MPD only required 30% of runs to be normalized.[7] Now with the tubular MPD, no normalization was required. The bluish colour microplasma proved to be more stable than the pinkish colour microplasma. As MPD power was increased within a fixed IED and frequency, the bluish mode MPD would eventually turn into the pinkish mode MPD when the dc power supply switched from current controlled to voltage controlled. The high power bluish MPD would become unstable when higher mini-ITV vapourization power was used (e.g., ~90 W), disturbing, primarily, the spectral region between 200-400 nm. In addition, with the pinkish colour MPD, the intensity of the more sensitive Hydrogen atomic and molecular lines increase due to an increase in temperature from mini-ITV.

The background emission stability and analytical performance of the MPD are influenced by a number of inter-dependent variables including nominal dc power (voltage, current); frequency; IED; electrode size, material, sharpness of tip; observation location, etc. The optimum observation location varied depending on these variables and on the analyte introduced into the MPD. The observation location results clearly show that where the microplasma is viewed is crucial. Observation locations close to the front or the back electrode did not contain any appreciable emissions for Ca, Li, Ag, and Zn.

Furthermore, varying MPD power, HVac frequency, IED, etc. causes the optimal observation location to change.

The MPD had 4-4.5% precision for 10 consecutive Ag (500 ppb, 3 μL) signals acquired with the single channel PMT based spectrometer. The multichannel CCD spectrometer had 17.5% precision for 25 consecutive Ag (500 ppb, 3 μL) runs. The limiting precision when using the CCD spectrometer was due to the "data transfer time delay" which was taking up to half of the total integration time (integration time + data transfer time). In essence, half of the useable analyte signal was being lost to the data transfer time.

The MPD power study confirmed that similar to the ICP, some elements/emission lines for the MPD require a hotter plasma or higher energy plasma for improved performance. From the 16 elements tested, Ca, Sr, Ba, Eu and Fe had maximum emissions from a higher power MPD. The CCD spectrometer showed estimated detection limits for the 16 elements of 5-310 pg. The more sensitive and faster response PMT showed the true potential of the MPD with estimated detection limits for the 16 elements of 1-35 pg.

The excitation mechanism for the microplasma was briefly examined and it was concluded that more scientific evidence is required to arrive at even an approximate excitation mechanism. The bluish and pinkish operating modes observed for the MPD appear to be similar to two distinct modes of plasma described in the literature as α and γ modes. The α mode microplasma was more diffuse (as observed with the bluish colour MPD) and the γ mode microplasma was smaller in diameter and more "string-like" (as observed with the pinkish colour MPD).

In general, total energy (excitation + ionization energy) of possible analytical emissions must be less than excitation energy of Ar^+ (15.76 eV). The MPD has shown the ability to excite lines ranging from 1.6-14.7 eV for the 16 elements tested. The 14.7 eV ion line for Cd (214.438 nm) and Pb (220.351 nm) are the highest energy lines excited by the MPD albeit at reduced sensitivities.

The excitation temperature (T_{exc}) of the MPD was determined using Ar as a thermometric species and it was found to be 1600-2400 K depending on MPD power, HVac frequency, inter-electrode distance (IED) and bluish colour or pinkish colour mode of microplasma operation. A change in atom/ion for Ca and Sr with increasing MPD power density was observed and it demonstrated that the microplasma energetics change as power changes.

In summary, MPDs show a very promising future as a reliable and sensitive analytical tool for trace analysis. MPDs have come a long way since the days when the lights had to be turned off in order to see if a microplasma was actually being formed or not. Now, MPDs have been shown to be interesting excitation and quite sensitive analytical emission sources.

6.1 Future Work

There are still many variables to be studied for even partial understanding of MPDs. These variables include geometry; electrode material and diameter, geometry and sharpness; nominal dc power (voltage and current); HVac frequency; IED; observation location; and plasma gas type. Also, other temperatures and characterization yardsticks should be determined to try and further understand excitation mechanisms and modes of operation of the microplasma.

Planar geometry, if made to have a more stable background emission can be comparable to the tubular MPD. The channel width can be made smaller to stabilize the microplasma (as seen with the wall-stabilized quartz tube) and the material can be changed to a higher temperature material if need be. A hybrid planar-tubular geometry or a tube in a plastic substrate with planar electrodes may gain the benefits of the two geometries. If tubular geometry MPD is continued to be studied then a smaller mini-ITV needs to be made in order to reduce the increase in linear flowrate.

The length study should be mapped out from the middle to front with more locations for 30 and 50 mm IED (4 observation locations x 0.6 mm = ~2.5 mm of total distance). The MPD power study showed that more MPD power can be beneficial for some elements and that the 50 mm IED bluish colour MPD showed some promising results for some elements. Finding a higher power bluish MPD with increased stability from 200-400 nm, would be beneficial. It is possible that shorter IED can increase the power density and increase the analytical response of some analytes, i.e., Ca. More IEDs, both shorter and longer than the ones tested in this thesis, should be studied in the future. Will longer MPDs cause other lines (atomic and/or ionic) to appear in the analyte spectra?

The MPDs are being developed for future field applications but the setup has yet to be brought out of the lab. The first step would be to try and analyze field samples (e.g., lake water) in the lab. Multi element solutions have been tested successfully with MPDs but only with six elements.[7] It will be interesting to see how MPDs operate with more complex samples. Although the emission spectra for the elements tested thus far are simple, overlapping analyte emissions may become a problem with "real" samples.

In this case, an array of spectrometers, e.g., 2-3 CCD spectrometers, each with shorter wavelength range, may be needed for improved resolution.

References

1. D.C. Harris, "Quantitative Chemical Analysis", 6th Edition, W.H. Freeman and Co., New York, New York, 2003.
2. V. Karanassios, "CHEM 323 lecture notes", University of Waterloo, Waterloo, Ontario, 2006.
3. A. Montaser, "Inductively Coupled Plasmas in Analytical Atomic Spectrometry", 2nd Edition, VCH Publishers, Inc., New York, New York (1992).
4. V. Karanassios, "Microplasmas for chemical analysis: analytical tools or research toys?", Spectrochemica Acta Part B., **59**, 909-928 (2004).
5. S. Weagant and V. Karanassios, "Helium-hydrogen microplasma device (MPD) on postage-stamp-size plastic-quartz chips", Anal. Bioanal. Chem., **395**, 577-589 (2009).
6. S. Weagant, "Further Development of Planar Micro Plasma Devices (MPDs) on Plastic for Atomic Emission Spectrometry", CHEM 392 Undergraduate Research Project for Fulfillment of Qualifying Master's Term , University of Waterloo, Waterloo, Ontario, Summer Term, 2008.
7. S. Weagant, V. Chen, and V. Karanassios, "Battery-operated, argon-hydrogen microplasma on hybrid, postage stamp-size plastic-quartz chips for elemental analysis of liquid microsamples", Anal. Bioanal. Chem., (2011) (Submitted).
8. H.S. Park, S.J. Kim, H.M. Joh, T.H. Cheung, S.H. Bae, and S.H. Leem, "Optical and electrical characterization of an atmospheric pressure microplasma jet with a capillary electrode", Phys. of Plasmas, **17**, 033502-033502(9), (2010).

9. J.Y. Kim, S-O Kim, Y. Wei, and J. Li, “A flexible cold microplasma jet using biocompatible dielectric tubes for cancer therapy”, Applied Phys. Letters, **96**, 203701-203701(2), (2010).

10. R. Junker, P.J.D. Manders, J. Walke, Y. Borisov, I. Braceras, and J.A. Jansen, “Loaded Microplasma-sprayed CaP-coated Implants in vivo”, J. Dent. Res., **89**, 1489-1493 (2010).

11. F.-C. Chang, C. Richmonds, and R. M. Sankaran, “Microplasma-assisted growth of colloidal Ag nanoparticles for point-of-use surface-enhanced Raman scattering applications”, J. Vac. Sci. Tecnol. A, **28** (4), in press, DOI: 10.1116/1.3428708 (2010).

12. D. Mariotti, A.Chandra Bose, and Kostya Ostrikov, “Atmospheric-microplasma-assisted nanofabrication: metal and metal-oxide nanostructures and nanoarchitectures”, IEEE Trans. Plasma Sci., **37**, 1027-1033 (2009).

13. R.S. Besser and P.J. Lindner, “Microplasma reforming of hydrocarbons of fuel cell power”, J. Power Sciences, in press, DOI: 10.1016/j.jpowsour.2010.11.135 (2011).

14. C. Meyer, S. Muller, E.L. Gurevich, and J. Franzke, “Dielectric barrier discharges in analytical chemistry”, Analyst, in press, DOI: 10.1039/c0an00994f (2011).

15. C. Meyer, R. Heming, E.L. Gurevich, U. Marggraf, M. Okruss, S. Florek, and J. Franzke, “Radiofrequency driven and low cost fabricated microhollow cathode discharge for gaseous atomic emission spectrometry”, J. Anal. At. Spectrom., **26**, 505-510 (2010).

16. A.R. Hoskinson, J. Hopwood, N.W. Bostrum, J.A. Crank, and C. Harrison, "Low-power microwave-generated helium microplasma for molecular and atomic spectrometry", J. Anal. At. Spectrom., in press, DOI: 10.1039/c0ja00239a (2011).

17. H.R. Badiei, "Further development, optimization, and characterization of in-torch vaporization-inductively coupled plasma (ITV-ICP) spectrometry", PhD Dissertation, University of Waterloo, Waterloo, Ontario (2004).

18. H.R. Badiei and V. Karanassios, "Direct elemental analysis of lead in micro-samples of human fingernails by rhenium-cup in-torch vaporization-inductively coupled plasma atomic emission spectrometry (ITV-ICP-AES)", J. Anal. At. Spectrom., **14**, 603–605 (1999).

19. A.T. Smith, "Further development of a miniature In-Torch Vaporization Microplasma Device (mini-ITV-MPD) and characterization using optical emission spectrometry and mass spectrometry", Master's Thesis, University of Waterloo, Waterloo, Ontario (2004).

20. D. Hou, "Further development and optimization of a miniature In-Torch Vaporization sample introduction system and micro plasma device (mini-ITV-MPD)", Master's Thesis, University of Waterloo, Waterloo, Ontario (2005).

21. J.W. Olesik, "Investigating the fate of individual sample droplets in inductively coupled plasmas", Appl. Spectrosc., **51**, 158A-175A (1997).

22. V. Karanassios, K. Johnson, and A.T. Smith, "Micromachined, planar-geometry, atmospheric-pressure, battery-operated microplasma devices (MPDs) on chips for analysis of microsamples of liquids, solids, or gases by optical-emission spectrometry", Anal. Bioanal. Chem., **388**, 1595-1604 (2007).

23. W.M.Vander Wilp, "A Portable, Battery Powered, Atomic Fluorescence-based Instrument for Mercury Determinations", Master's Thesis, University of Waterloo, Waterloo, Ontario (2002).

24. D.A. Skoog, F.J. Holler, and T.A. Nieman, "Principles of Instrumental Analysis", 5th Edition, Saunders College Publishing, Fort Worth, Texas (1998).

25. http://www.stellarnet-inc.com Stellarnet© website [accessed April, 2011].

26. T. Frentiu, D. Petreus, M. Senila, A.I. Mihaltan, E. Darvasi, M. Ponta, E. Plaian, and E.A. Cordos, "Low power capactively coupled plasma microtorch for simultaneous multielemental determination by atomic emission using microspectrometers", Microchemical Journal, **97**, 188-195 (2011).

27. A. Simon, S.D. Anghel, M. Papiu, and O. Dinu, "Physical and analytical characterisitics of an atmospheric pressure argon-helium radiofrequency capacitively coupled plasma", Spectrochimica Acta Part B, **65**, 272-278 (2010).

28. G. C.-Y. Chan, J.T. Shelly, A.U. Jackson, J.S. Wiley, C. Engelhard, R.G. Cooks, and G.M. Hieftje, "Spectroscopic plasma diagnostics on a low-temperature plasma probe for ambient mass spectrometry", J. Anal. At. Spectrom., in press, DOI: 10.1039/c0ja00230e (2011).

29. F. Iza, D.W. Liu, and M.G. Kong, "Electron avalanches and diffused γ-mode in radiofrequency capacitively coupled atmospheric-pressure microplasmas", Applied Phys. Lett., **95**, 031501-031503 (2009).

30. J. Laimer, H. Reicher, and H. Stori, "Atmospheric pressure plasma jet operated at narrow gap spacings", Vacuum, **84**, 104-107 (2010).

31. J. Laimer, A. Puchhammer, and H. Stori, “Plasma sheath dynamics in dielectric barrier-free atmospheric pressure radio-frequency glow discharges”, Plasma Process. Polym., **6**, 253-257 (2009).

32. D.W. Liu, F. Iza, and M.G. Kong, “Evolution of atmospheric-pressure RF plasmas as the excitation energy increases”, Plasma. Process. Polym., **6**, 446-450 (2009).

33. http://physics.nist.gov/PhysRefData/ASD/lines_form.html NIST Atomic Spectra Database Lines Data website [accessed May, 2011].

34. G.R. Harrison, “M.I.T. Wavelength Tables with intensities in arc, spark, or discharge tube”, The M.I.T. Press, Massachusetts, USA (1969).

35. F. Iza and A. Hopwood, “Rotational, vibrational, and excitation temperatures of a microwave-frequency microplasma”, IEEE Plasma Science, **32** (2), 498-504 (2004).

36. B.N. Sismanoglu, J. Amorim, J.A. Souza-Correa, C. Oliveira, and M.P. Gomes, “Optical emission spectroscopy diagnostics of an atmospheric pressure direct current microplasma jet”, Spectrochimica Acta Part B, **64**, 1287-1293 (2009).

37. J. A. C. Broekaert, “Analytical atomic spectrometry with flames and plasmas”, Wiley-VCH (2005).

38. S. A. Lehn and G. M. Hieftje, “Experimental evaluation of analyte excitation mechanisms in the inductively coupled plasma”, Spectrochim. Acta, Part B, **58**, 1821-1836 (2003).

39. G. C. Y. Chan and G. M. Hieftje, "Using matrix effects as a probe for the study of the charge-transfer mechanism in inductively coupled plasma-atomic emission spectrometry`, Spectrochim. Acta, Part B, **59**, 163-183 (2004).

40. G. C. Y. Chan and G. M. Hieftje, "Experimental evidence of state-selective charge transfer in inductively coupled plasma-atomic emission spectrometry", Spectrochim. Acta, Part B, **59**, 1007-1020 (2004).

41. J. W. Carnahan and G. M. Hieftje, "Helium-chlorine charge transfer: an explanation for chlorine emission behavior in helium discharges", Spectrochim. Acta, Part B, **47**, 731-739 (1992).

42. P. G. Brandl and G. M. Hieftje, "Charge transfer in analytical helium plasmas", Spectrochim. Acta, Part B, **49**, 105-115 (1994).

43. J. Tang, Y. Duan and W. Zhao, "Characterization and mechanism studies of dielectric barrier discharges generated at atmospheric pressure", Appl. Phys. Lett., **96**, 191503-101503(3), (2010).

44. F. Iza, G. J. Kim, S. M. Lee, J. K. Lee, J. L. Walsh, Y. T. Zhang, and M. G. Kong, "Microplasmas: Sources, particle kinetics, and biomedical applications", Plasma Process Polym., **5**, 322-344 (2008).

45. J. Benedikt, S. Hofmann, N. Knake, H. Böttner, R. Reuter, A. von Keudell, and V. Schulz-von der Gathen, "Phase resolved optical emission spectroscopy of coaxial microplasma jet operated with He and Ar", Eur. Phys. J. D: 60, 539-546 (2010).

46. Q-U-Ain, H. Störi and J. Laimer, "Non-equilibrium atmospheric pressure radio-frequency glow-like discharges", Surface Coatings Tech., in press, DOI: 10.1016/j.surfcoat.2011.03.130 (2011).

47. K. H. Becker, K. H. Schoenbach and J. G. Eden, "Microplasmas and applications", J. Phys. D: Appl. Phys., **39**, R55-R70 (2006).

48. S. G. Belostotsly, T. Ouk, V. M. Donnelly, D. J. Economou and N. Sadeghi, "Time- and space-resolved measurement of Ar($1s_5$) metastable density in a microplasma using diode laser absorption spectroscopy", J. Phys. D: Appl. Phys., **44**, 145202-145202(7), (2011).

49. B. Niermann, M. Boke, N. Sadeghi and J. Winter, "Space resolved density measurements in Argon and Helium metastable atoms in radio-frequency generated He-Ar micro-plasmas", Eur. Phys. J. D, **60**, 489-495 (2010).

50. D.-X. Liu, M.-Z. Rong, X.-H. Wang, F. Iza, M. G. Kong and P. Bruggeman, "Main species and physicochemical processes in cold atmospheric-pressure He+O_2 plasmas", Plasma Process. Polym., **7**, 846-856 (2010).

51. M. McKay, F. Iza and M. G. Kong, "Excitation frequency effects on atmospheric-pressure Helium RF microplasmas: plasma density, electron energy and plasma impedance", Eur. Phys. J. D., **60**, 497-503 (2010).

52. D. X. Liu, P. Bruggeman, F. Iza, M. Z. Rong and M. G. Kong, "Global model of low-temperature atmospheric-pressure He+H_2O plasmas", Plasma Sci. Tech., **19**, 025018-025018(22), (2010).

53. J. L. Walsh, F. Iza, N. B. Janson, V. J. Law and M. G. Kong, "Three distinct modes in a cold atmospheric pressure plasma jet", J. Phys. D: Appl. Phys., **43**, 075201-075201(14), (2010).

54. M, Grotti, C. Lagomarsino and J. M. Mermet, "Effect of operating conditions on excitation temperature and electron number density in axially-viewed ICP-OES with introduction of vapours or aerosols", J. Anal. Atom. Spectrom., **21**, 963-969 (1996).

55. M. Huang, S. A. Lehn, E. J. Andrews and G. M. Hieftje, "Comparison of electron temperatures, gas kinectic temperatures, and excitation temperatures in Ar ICPs operated at 27 and 450 MHz", Spectrochim. Acta, Part B, **52**, 173-1193 (1997).

56. S-H. Nam and Y. S. Kim, "Excitation temperature and electron number density measured for end-on-view Inductively Coupled Plasma discharge", Bull. Korean Chem. Soc., **22**, 827-832 (2001).

57. E. Tognoni, M. Hadilgo, A. Canals, G. Cristoferetti, S. Lagnaioli, S. Salvetti and V. Palleschi, "Combination of the ionic-to-atomic line intensity ratios from two test elements for the diagnostic of plasma temperature and electron density in Inductively Coupled Plasma Atomic Emission Spectrometry", Spectrochim. Acta,. Part B, **62**, 435-443 (2007).

58. Z. Cui, K. Kodama, H. Oyama and K. Kitagawa, "Two-dimensional observation of excited atoms and ions and excitation temperature in inductively coupled plasma using newly developed four channel spectro-video camera", J. of Visualization, **13**, 89-96 (2010).

59. H. Park and W. Choe, “Parametric study on excitation temperature and electron temperature in low pressure plasmas”, Current Applied Physics, **10**, 1456-1460 (2010).

60. B. Gielniak, T. Fiedler and J. A. C. Broekaert, “Study of a new direct current atmospheric pressure glow discharge in Helium”, Spectrochim. Acta, Part B, **66**, 21-27 (2011).

61. S. D. Anghel, A. Simon, A. I. Radu and I. J. Hidi, “Low power cross-flow atmospheric pressure Ar+He plasma jet”, Spectrochim. Acta, Part B, **65**, 265-271 (2010).